

DISCONTINUOUS GALERKIN FINITE ELEMENTS METHOD WITH
STRUCTURE PRESERVING TIME INTEGRATORS FOR GRADIENT FLOW
EQUATIONS

A THESIS SUBMITTED TO
THE GRADUATE SCHOOL OF APPLIED MATHEMATICS
OF
MIDDLE EAST TECHNICAL UNIVERSITY

BY

AYŞE SARIAYDIN FİLİBELİOĞLU

IN PARTIAL FULFILLMENT OF THE REQUIREMENTS
FOR
THE DEGREE OF DOCTOR OF PHILOSOPHY
IN
SCIENTIFIC COMPUTING

AUGUST 2015

Approval of the thesis:

**DISCONTINUOUS GALERKIN FINITE ELEMENTS METHOD WITH
STRUCTURE PRESERVING TIME INTEGRATORS FOR GRADIENT
FLOW EQUATIONS**

submitted by **AYŞE SARIAYDIN FİLİBELİOĞLU** in partial fulfillment of the requirements for the degree of **Doctor of Philosophy in Department of Scientific Computing, Middle East Technical University** by,

Prof. Dr. Bülent Karasözen
Director, Graduate School of **Applied Mathematics**

Assoc. Prof. Dr. Ömür Uğur
Head of Department, **Scientific Computing**

Prof. Dr. Bülent Karasözen
Supervisor, **Department of Mathematics & Institute of Applied
Mathematics, METU**

Examining Committee Members:

Assoc. Prof. Dr. Ömür Uğur
Institute of Applied Mathematics, METU

Prof. Dr. Bülent Karasözen
Department of Mathematics & Institute of Applied Mathematics,
METU

Assoc. Prof. Dr. Murat Manguoğlu
Department of Computer Engineering, METU

Assist. Prof. Dr. Enes Yılmaz
Department of Mathematics, Gazi University

Assist. Prof. Dr. Fikriye Nuray Yılmaz
Department of Mathematics, Gazi University

Date: _____

I hereby declare that all information in this document has been obtained and presented in accordance with academic rules and ethical conduct. I also declare that, as required by these rules and conduct, I have fully cited and referenced all material and results that are not original to this work.

Name, Last Name: AYŞE SARIAYDIN FİLİBELİOĞLU

Signature :

ABSTRACT

DISCONTINUOUS GALERKIN FINITE ELEMENTS METHOD WITH STRUCTURE PRESERVING TIME INTEGRATORS FOR GRADIENT FLOW EQUATIONS

Sarıaydın-Filibeliöđlu, Ayşe

PhD, Department of Scientific Computing

Supervisor : Prof. Dr. Bülent Karasözen

August 2015, 92 pages

Gradient flows are energy driven evolutionary equations such that the energy decreases along solutions. There have been surprisingly a large number of well-known partial differential equations (PDEs) which have the structure of a gradient flow in different research areas such as fluid dynamics, image processing, biology and material sciences. In this study, we focus on two systems which can be modeled by gradient flows; Allen-Cahn and Cahn-Hilliard equations. These equations model the phase separation in material science. Since an essential feature of the Allen-Cahn and Cahn-Hilliard equations is the energy decreasing property, it is important to design efficient and accurate numerical schemes that satisfy the corresponding energy decreasing property. We have used symmetric interior penalty Galerkin (SIPG) method to discretize the Allen-Cahn and Cahn-Hilliard equations in space. The resulting large system of ordinary differential equations (ODEs) as a gradient system are solved by the energy stable (energy decreasing) time integrators: implicit Euler and average vector field (AVF) methods. We have shown that implicit Euler and AVF time integrators coupled with SIPG method are unconditionally energy stable. Numerical results for both equations with polynomial and logarithmic energy functions, and constant and variable mobility functions illustrate the efficiency and accuracy of this approach.

Advective Allen-Cahn equation is the simplest model of surface tension in the droplet breakup phenomena. The small surface time scale and convective time scale lead to

unphysical oscillations in the solution. In contrast to the discretization of Allen-Cahn and Cahn-Hilliard equations using the method of lines, the advective Allen-Cahn equation is first discretized in time using implicit Euler method and the resulting sequence of semi-linear elliptic equations are solved with an adaptive algorithm. This corresponds to Rothe's method. As a remedy of unphysical oscillations, an adaptive version of SIPG method based on residual based a posteriori error estimate is applied. Numerical results for convection dominated Allen-Cahn equation show the performance of adaptive algorithm.

Keywords: gradient flow equations, discontinuous Galerkin finite elements method, structure preserving time integrators

ÖZ

GRADYAN DENKLEMLERİ İÇİN YAPI KORUYAN ZAMAN INTEGRATÖRLERİ İLE SÜREKSİZ SONLU ELEMANLAR YÖNTEMİ

Sarıaydın-Filibeliolu, Ayşe

Doktora, Bilimsel Hesaplama Bölümü

Tez Yöneticisi : Prof. Dr. Bülent Karasözen

Ağustos 2015, 92 sayfa

Gradyan akışlar bir enerji tarafından yönetilen ve enerjinin çözümler boyunca azaldığı sistemlerdir. Akışkanlar dinamiği, görüntü işleme, biyoloji ve malzeme bilimi gibi farklı araştırma alanlarında gradyan akış yapısına sahip şaşırtıcı şekilde pek çok kısmi türevli denklem bulunmaktadır. Bu tezde, gradyan akışlarla modellenen iki sistem üzerinde yoğunlaştık; Allen-Cahn ve Cahn-Hilliard denklemleri. Bu iki denklem malzeme biliminde faz ayrımını modellemektedir. Allen-Cahn ve Cahn-Hilliard denklemlerinin en önemli özelliği azalan enerji olduğu için, bu azalan enerji özelliğini sağlayan etkili ve doğru nümerik yöntemlerin geliştirilmesi önem kazanmaktadır. Allen-Cahn ve Cahn-Hilliard denklemlerinin uzaydaki ayrıklaştırılmasında simetrik kesintili Galerkin yöntemini kullandık. Ortaya çıkan büyük adi diferansiyel denklem sistemlerini gradyan sistem olarak yapı koruyan zaman integratörlerinden geriye doğru yapılan Euler yöntemi ve ortalama vektör alanı yöntemi ile çözdük. Geriye doğru yapılan Euler yöntemi ve ortalama vektör alanı yöntemlerinin simetrik kesintili Galerkin yöntemi ile bir araya geldiğinde şartsız olarak enerjiyi koruduğunu gösterdik. Her iki denklemin polinom ve logaritmik enerji fonksiyonları ve sabit ve değişken akışkanlık fonksiyonu ile elde edilen sayısal sonuçları bu yöntemin verimliliğini ve doğruluğunu göstermektedir.

Advektif Allen-Cahn denklemi damlacık ayrılması olayındaki yüzey geriliminin basit bir modelidir. Küçük zaman ölçeği ve konvektif zaman ölçeği bu denklemin çözümünde fiziksel olmayan dalgalanmalara sebep olmaktadır. Doğrular yöntemi kullanılarak

ayrıklaştırılan Allen-Cahn ve Cahn-Hilliard denklemlerinin aksine, advektif Allen-Cahn denklemini ilk önce geriye doğru yapılan Euler yöntemi ile zamanda ayrıklaştırılarak ortaya çıkan yarı liner elliptik denklemleri uyarlanabilir algoritmalarla çözüldü. Bu Rothe yöntemine karşılık gelmektedir. Fiziksel olmayan dalgalanmalara bir çare olarak çözüme bağlı hata kestiriciler üzerine kurulu simetrik kesintili Galerkin yönteminin uyarlanabilir biçimini kullandık. Konveksiyonun baskın olduğu Allen-Cahn denklemleri için verilen sayısal sonuçlar uyarlanabilir algoritmanın performansını göstermektedir.

Anahtar Kelimeler: gradyan denklemleri, sürekli olmayan Galerkin sonlu elemanlar yöntemi, yapı koruyan zaman integratörleri

To My Mom and Dad

ACKNOWLEDGMENTS

First of all, I would like to express my thankfulness to my supervisor Prof. Dr. Bülent Karasözen for his invaluable guidance, useful suggestions, kindness and patience throughout this thesis. I would have not been able to continue and succeed in completing my PhD studies without his unfailing support.

I acknowledge Dr. Murat Uzunca for discussions on discontinuous Galerkin methods and for his endless help throughout the difficulties I encountered in programing.

I also want to thank to my thesis defense committee members for their useful comments and discussions.

I am thankful to my ‘roomies’, Cansu Evcin, Meral Şimşek, Özge Tekin, Ahmet Sınak, Sinem Kozpınar, who shared all the stages of this thesis and provide me a joyful working atmosphere. I am also grateful to people of Institute of Applied Mathematics (IAM) for the pleasant and friendship environment.

A special thank to my love Semih Filibelioğlu, for always finding a way to make me smile and making my life joyful, colorful and livable.

Last but not the least important, I am deeply thankful to my parents Rukiye & Bahattin Sariaydın for being me all my life. I would not be able to succeed without them. They really deserve the dedication of this thesis. So glad I have you Mommy and Daddy.

TABLE OF CONTENTS

ABSTRACT	vii
ÖZ	ix
ACKNOWLEDGMENTS	xiii
TABLE OF CONTENTS	xv
LIST OF FIGURES	xix
LIST OF TABLES	xxiii
LIST OF ABBREVIATIONS	xxv
CHAPTERS	
1 INTRODUCTION	1
2 THE ALLEN-CAHN EQUATION	7
2.1 Interior Penalty Galerkin Method	11
2.2 SIPG Discretization of Allen-Cahn Equation	15
2.2.1 Semi-Discrete System in Matrix-Vector Form	16
2.3 Time Discretization by Backward Euler and AVF Method	17
2.3.1 Time Discretization by Backward Euler Method	17
2.3.2 Time Discretization by AVF Method	19
2.4 Energy Stability of Fully Discrete Scheme	22
2.4.1 Energy Stability of Fully Discrete Scheme with Backward Euler	22

2.4.2	Energy Stability of Fully Discrete Scheme with AVF Method	24
2.5	Time Adaptivity with Average Vector Field (AVF) Method and Ripening Time	25
2.6	Numerical Results	26
2.6.1	1D AC equation with constant mobility function and double-well potential	26
2.6.2	1D AC equation with constant mobility function and double-well potential	28
2.6.3	2D AC equation with constant mobility function and double-well potential	30
2.6.4	2D AC with constant mobility function and double-well potential	31
2.6.5	2D AC with constant mobility function and double-well potential	32
2.6.6	2D AC equation with constant mobility function and logarithmic free energy	32
2.6.7	2D AC with degenerate mobility function and logarithmic free energy	33
3	THE CAHN-HILLIARD EQUATION	39
3.1	SIPG Discretization of Cahn-Hilliard Equation	42
3.2	Fully Discrete System by Backward Euler and AVF Method	44
3.2.1	Fully Discrete System by Backward Euler	44
3.2.2	Fully Discrete System by Average Vector Field Method	45
3.3	Energy Stability	47
3.3.1	Energy Stability of Fully Discrete Scheme with Backward Euler	47
3.3.2	Energy Stability of Fully Discrete Scheme with AVF Method	48

3.4	Numerical Results	50
3.4.1	Constant mobility function and double-well potential under Neumann boundary condition	50
3.4.2	Degenerate mobility function and double-well potential under periodic boundary condition	51
3.4.3	Constant mobility function and double-well function under Neumann boundary condition: spinodal decomposition and nucleation	51
3.4.4	Constant mobility and logarithmic energy under Neumann Boundary Condition	53
3.4.5	Degenerate mobility and logarithmic energy under Neumann boundary condition	53
4	ADVECTIVE ALLEN-CAHN EQUATION	59
4.1	Time Discretization of Advective AC Equation	61
4.2	Full Discretization of Advective AC Equation	62
4.3	The adaptive algorithm	63
4.4	A posteriori error estimation	65
4.4.1	Proof of a Posteriori Error Bounds	65
4.5	Numerical Results	70
4.5.1	1D advective non-local AC equation	70
4.5.2	1D advective non-local AC equation: non-monotone initial condition	71
4.5.3	2D advective non-local AC equation: expanding flow	73
4.5.4	2D advective non-local AC equation: sheer flow	76
5	CONCLUSION	81
	REFERENCES	83

CURRICULUM VITAE 91

LIST OF FIGURES

Figure 2.1 Left: two neighbor elements sharing an edge, Right: an element adjacent to boundary of the domain	13
Figure 2.2 Time Adaptive strategy	27
Figure 2.3 Example 2.6.1: evolution of phase function and decay of the numerical energy with backward Euler	28
Figure 2.4 Example 2.6.1: decay of the numerical energy with backward Euler method and AVF method for different time steps: $\Delta t = 0.5$ (top left), $\Delta t = 0.25$ (top right), $\Delta t = 0.1$ (bottom left), $\Delta t = 0.01$ (bottom right) . .	29
Figure 2.5 Example 2.6.2: evolution of phase function and decay of the numerical energy with AVF method	29
Figure 2.6 Example 2.6.2: evolution of time step sizes	30
Figure 2.7 Example 2.6.3: evolution of phase function	31
Figure 2.8 Example 2.6.3: decay of numerical energy (left) and evolution of time steps (right)	32
Figure 2.9 Example 2.6.5: evolution of phase function	34
Figure 2.10 Example 2.6.5: decay of numerical energy	35
Figure 2.11 Example 2.6.6: evolution of phase function	35
Figure 2.12 Example 2.6.6: decay of numerical energy (left) and evolution of time steps (right)	36
Figure 2.13 Example 2.6.7: evolution of solutions	36
Figure 2.14 Example 2.6.7: decay of numerical energy (left) and evolution of time steps (right)	37
Figure 3.1 Example 3.4.3: Phase solution of 2D CH equation with constant mobility with $\Delta t = 1 \times 10^{-5}$ (spinodal decomposition)	52
Figure 3.2 Example 3.4.3: Energy decrease and mass conservation of 2D CH equation with constant mobility with $\Delta t = 1 \times 10^{-5}$ (spinodal decomposition)	53

Figure 3.3	Example 3.4.3: Phase solution of 2D CH equation with constant mobility with $\Delta t = 1 \times 10^{-5}$ (nucleation)	54
Figure 3.4	Example 3.4.3: Energy decrease and mass conservation of 2D CH equation with constant mobility with $\Delta t = 1 \times 10^{-5}$ (nucleation)	55
Figure 3.5	Example 3.4.4: Phase solution of 2D CH equation with constant mobility with $\Delta t = 1 \times 10^{-8}$	55
Figure 3.6	Example 3.4.4: Energy decrease and mass conservation of 2D CH equation with constant mobility with $\Delta t = 1 \times 10^{-8}$	56
Figure 3.7	Example 3.4.5: Phase solution of 2D CH equation with degenerate mobility with $\Delta t = 1 \times 10^{-7}$	56
Figure 3.8	Example 3.4.5: Energy decrease and mass conservation of 2D CH equation with degenerate mobility with $\Delta t = 1 \times 10^{-7}$	57
Figure 4.1	Adaptive algorithm chart on a single step $(t_{k-1}, t_k]$	63
Figure 4.2	Example 4.5.1: Solutions at initial and final times with $V_0 = 3$	71
Figure 4.3	Example 4.5.1: Solution profile (left) and mass error (right) with $V_0 = 3$	72
Figure 4.4	Example 4.5.1: Solutions with $V_0 = 10$	72
Figure 4.5	Example 4.5.1: Solution profile (left) and mass error (right) with $V_0 = 10$	73
Figure 4.6	Example 4.5.2: Solutions with non-monotone initial condition	74
Figure 4.7	Example 4.5.2: Solution profile (left) and mass error (right)	74
Figure 4.8	Example 4.5.3: Uniform solutions at initial and final times (top) for expanding flow and mass error plot (bottom)	75
Figure 4.9	Example 4.5.3: Adaptive mesh at final time $t = 0.06$ (left) and evolutions of DoFs (right) for expanding flow	76
Figure 4.10	Example 4.5.3: Uniform (left) and adaptive (right) solutions at final time $t = 0.06$ for expanding flow	76
Figure 4.11	Example 4.5.3: (Top) Uniform (left) and adaptive (right) solutions at final time $t = 0.06$, (Bottom) adaptive mesh (left) at final time $t = 0.06$ and evolution of DoFs (right) for expanding flow with square initial data	77
Figure 4.12	Example 4.5.4: Uniform solutions at initial and final times (top) and mass error plot (bottom) for sheer flow with $\epsilon = 0.01$	78

Figure 4.13 Example 4.5.4: Adaptive mesh at final time $t = 0.06$ (left) and evolution of DoFs (right) for shear flow with $\epsilon = 0.01$	78
Figure 4.14 Example 4.5.4: Uniform (left) and adaptive (right) solutions at final time $t = 0.06$ for shear flow with $\epsilon = 0.01$	79
Figure 4.15 Example 4.5.4: Adaptive mesh (left) and adaptive solution (right) at final time $t = 0.06$ for shear flow with $\epsilon = 0.001$	79

LIST OF TABLES

Table 2.1 Example 2.6.2: Convergence of the ripening time with the adaptive AVF method using linear (quadratic) polynomials.	30
Table 2.2 Example 2.6.3: Convergence of the ripening time with adaptive AVF method using linear (quadratic) polynomials	32
Table 2.3 Accuracy test for AC equation with constant mobility for backward Euler method and AVF method $\Delta t = 0.03\Delta x$, $\Delta x = \pi$	33
Table 3.1 Example 3.4.1: Accuracy test with constant mobility for backward Euler and AVF methods	50
Table 3.2 Example 3.4.2: Accuracy test with degenerate mobility for backward Euler and AVF methods	51

LIST OF ABBREVIATIONS

AC	Allen-Cahn
AVF	Average Vector Field
CH	Cahn-Hilliard
DG	Discontinuous Galerkin
DGFEM	Discontinuous Galerkin Finite Elements Method
DoF	Degree of freedom
FEM	Finite Elements Method
FVM	Finite Volume Method
IMEX	Implicit-explicit
IPDGFEM	Interior Penalty Discontinuous Galerkin Finite Elements Method
LDG	Local Discontinuous Galerkin
PDEs	Partial Differential Equations
SIPG	Symmetric interior penalty Galerkin

CHAPTER 1

INTRODUCTION

Gradient flows are evolutionary systems driven by the energy dissipation mechanism. A large number of well-known PDEs with a gradient flow structure occur in different research areas such as fluid dynamics, image processing, biology and material science [23, 32, 40, 58, 60]. In this thesis, we deal with two famous example from material science; Allen-Cahn (AC) and Cahn-Hilliard (CH) equations.

The AC equation was first introduced by Allen and Cahn [2] in 1979 as a simple model for phase separation in a binary alloy at a fixed temperature, and given by

$$\begin{aligned} u_t &= \mu(u) (\epsilon^2 \Delta u - f(u)) & \text{in } \Omega \times (0, T], \\ u(\mathbf{x}, 0) &= u_0 & \text{in } \Omega \times \{0\}. \end{aligned} \tag{1.1}$$

The CH equation was proposed by Cahn and Hilliard [16] in 1958 to describe the phase separation of a binary fluid mixture below a critical temperature, and given by

$$\begin{aligned} u_t &= \nabla \cdot [\mu(u) \nabla (f(u) - \epsilon^2 \Delta u)], & \text{in } \Omega \times (0, T], \\ u(\mathbf{x}, 0) &= u_0 & \text{in } \Omega \times \{0\}. \end{aligned} \tag{1.2}$$

Both equations are considered with periodic, Neumann, or Dirichlet boundary conditions. The function u represents the concentration of one of the components of the mixture with the values in the region $-1 < u < 1$ representing the mixture state and the end points correspond to pure states. Here, $\Omega \subset \mathbb{R}^d (d \leq 3)$ is a bounded domain, the parameter ϵ is a measure of interfacial layer representing the effective diffusivity, and $\mu(u)$ is the non-negative mobility function. There are two choices for mobility function; constant mobility and degenerate mobility. In many numerical studies constant mobility is used [3, 20, 22, 37, 39]. The degenerate or variable mobility is given as a non-negative quadratic function either as $\mu(u) = \beta u(1 - u)$ [40, 79] or $\mu(u) = \beta(1 - u^2)$ [9, 11, 40, 82], where β is a constant.

The phase separation is thoroughly explained by the difference in the concentration of mixture of a binary alloy in the time evolution of AC and CH equations. It starts

with cooling of a uniform mixture of a binary alloy under a critical temperature where the uniform mixture becomes unstable. After that, two phases with different concentrations develop immediately. If initially both components have roughly similar proportions, spinodal decomposition process takes place, where a mixture of two or more materials separates into distinct regions with different composition. On the other hand, if the amount of one component is higher, nuclei of the parameter component form and grow, and phase separation takes via a process called nucleation and growth. During the late stages of the time evolution, the structure becomes coarser, either by merging of particles or by the growth of bigger particles at the expenses of smaller ones, known as domain coarsening phenomena. The transition between these processes is known as metastability, representing the transition from unstable to stable state in a short time.

The AC and CH equations can be written as a gradient descent flow

$$u_t = -\mu(u) \frac{\delta \mathcal{E}(u)}{\delta u}, \quad (1.3)$$

with the Ginzburg-Landau free energy

$$\mathcal{E}(u) = \int_{\Omega} \left(\frac{\epsilon^2}{2} |\nabla u|^2 + F(u) \right) dx, \quad (1.4)$$

in L^2 space and H^{-1} Hilbert spaces, respectively. Here, $\delta \mathcal{E}(u)/\delta u$ denotes the variational derivative and $F(u)$ is the free energy function where $f(u) = F'(u)$. There are two common types of energy functions. One of these functions is the non-convex logarithmic energy function [12, 68]

$$F(u) = \frac{\theta}{2} [(1-u) \ln(1-u) + (1+u) \ln(1+u)] - \frac{\theta_c}{2} u^2, \quad (1.5)$$

which has different forms for CH equation (see [9, 11, 40, 79, 83]). The other one is the convex double-well energy function [32, 54, 55]

$$F(u) = \frac{(1-u^2)^2}{4}, \quad (1.6)$$

which is an approximation of the logarithmic energy function for temperatures θ close to θ_c . In most of the studies, AC and CH equations are considered with double-well energy function and constant mobility. In this thesis, we consider the double-well energy and logarithmic free energy with constant and degenerate mobility function for both equations.

The main characteristic of both equations is the energy decreasing property, i.e.,

$$\mathcal{E}(u(t_n)) \leq \mathcal{E}(u(t_m)), \quad \forall \quad t_n > t_m$$

which poses a challenge to construct an unconditionally energy stable numerical methods. Moreover, the inherent non-linearity in the equations, the presence of the small parameter ϵ in phase separation applications and the different time scales of the stages in the evolution of the concentration are other difficulties encountered in the numerical solution of AC and CH equations.

AC and CH equations are the most popular examples of gradient descent flow. In gradient flow problems, the construction of higher order methods with above energy decreasing property is one of the major topics. The conservation of other structural properties is also important. So, it is needed efficient and accurate numerical methods.

In the literature, many numerical methods have been developed with finite difference [18, 73], spectral elements [23], continuous finite element [55], and local discontinuous Galerkin (LDG) methods [31, 39] for space discretization of AC equation. Time integration is performed by implicit-explicit (IMEX) methods [69], standard integrators like Crank-Nicolson method [34] and linear multi-step integrators [33]. Recently high accurate time integrators like the spectral deferred correction methods [55] and exponential integrators [73] are applied. The CH equation is mostly considered with the constant mobility function and finite differences [23], finite elements [12] and spectral methods [20, 43] are used for space discretization whereas CH equation with degenerate mobility is discretized by continuous finite elements [9, 11, 12], by LDG method [82, 83] discontinuous Galerkin (DG) method with C^0 elements and with mixed finite elements [79], finite differences [51], NURSB [36] and by spectral methods [84]. Most of the time discretization methods for CH equation with degenerate mobility are based on the convex splitting of the energy function. Moreover splitting methods are used by adding stabilization terms to the energy function $F(u)$. A survey of time discretization techniques for CH equation can be found in [72].

Discontinuous Galerkin finite elements methods (DGFEMs) have become so popular since they exhibit attractive properties. They have higher accuracy and work better in complex geometries in contrast to continuous finite elements method (FEM). Furthermore, the discontinuous approximation spaces bring the flexibility of discontinuous Galerkin (DG) methods which allows to adapt the mesh and the polynomial degree of the basis function. By this way, the sharp layers and singularities can be detected easily. Another interesting feature of DG method is local mass conservation which makes them a good candidate to solve flow and transport problems. In addition, the boundary conditions can be imposed weakly different from continuous finite element method. In this thesis we discretize the AC equation and mass conservative CH equation in space with symmetric interior point discontinuous Galerkin (SIPG) method [4, 63].

The design of energy stable time discretization techniques is an important topic in the numerical solution of gradient flow equations. The small values of the diffusion parameter ϵ leads to stiff systems after spatial discretizations. In this case, implicit-explicit methods are developed since the explicit methods are not suitable for stiff systems and the fully implicit systems require solution of non-linear equations at each time step. In the semi-implicit schemes, the linear stiff part is treated implicitly and the non-linear part explicitly, so that at each time step a linear system of equations is solved. Implicit Euler method and average vector field (AVF) method are energy stable time discretization techniques which are robust with small ϵ . Implicit Euler method is the most popular energy stable method. It is strongly energy decreasing, i.e. the discrete energy decreases without any restriction on the step size Δt for very stiff gradient systems for very small ϵ [41]. The AVF method is the only second order implicit energy stable method [17, 41] and it preserves energy decreasing property for the gradient systems and for systems with Lyapunov functionals. The mid-point method corresponds

to AVF method for quadratics non-linearities. For gradient systems involving higher order polynomial or general nonlinear terms, the mid-point method is not energy stable [41]. There are also some higher order energy decreasing methods with orders ≥ 3 ; the discontinuous Galerkin-Petrov in time methods (with different trial and test functions) [66] and Gauss Radau IIA Runge-Kutta collocation methods [42]. However, they require coupled systems of equations at each time step which increase the computational cost.

The AC and CH equations are also investigated by an advection term to model surface tension in the droplet breakup phenomena [56, 57]. We consider the advective AC equation [57]

$$\begin{aligned} u_t + \nabla \cdot (u\mathbf{V}) &= \epsilon \Delta u - \frac{1}{\epsilon} f(u) \quad \text{in } \Omega \times (0, T], \\ \frac{\partial u}{\partial n} &= 0 \quad \text{in } \partial\Omega \times [0, T], \end{aligned} \tag{1.7}$$

with an appropriate initial condition and prescribed velocity field $\mathbf{V} = (V_1, V_2)^T$. In most studies, the velocity field is divergent free, for example when the AC equation with the incompressible Navier-Stokes equation is considered. Since we consider droplet breakup phenomena under compressible flow, the velocity field \mathbf{V} is not divergent free; it is expanding when $\nabla \cdot \mathbf{V} > 0$ or it is contracting when $\nabla \cdot \mathbf{V} < 0$.

The existing numerical studies for advective AC equation are especially on the behavior of solutions with respect to droplet breakup phenomena and analysis of the breakup condition (see [57] and references in it). On the other hand, the advective AC equation is known for its computational stiffness due to the small surface time scale and convective time scale. These two different time scales lead to sharp gradients and unphysical oscillations in the solution and require an adaptive algorithm. We utilize a space adaptive algorithm by first discretizing the advective AC equation in time using implicit Euler method and then solving the resulting sequence of semi-linear elliptic equations with an adaptive version of SIPG method using upwinding for the convective term. This is known as Rothe's method [26]. We also derive residual based a posteriori error estimate [74] which is based on the a posteriori error estimates for stationary non-linear diffusion-convection-reaction equations with divergent free velocity field.

The fully discretized systems of AC/advective AC and CH equations result in non-linear system of equations. We apply Newton's method to solve this non-linear system of equations and all linear system of equations arising from the applied Newton's method are solved by sparse direct solvers of MATLAB.

The goal of this thesis is to solve AC and CH equations in an accurate and efficient way using DG methods and structure preserving time integrators implicit Euler and AVF methods. We have derived unconditionally energy stable schemes coupling DG space discretization with implicit Euler and AVF methods which has not been applied to AC and CH equations with constant and degenerate mobility, polynomial and non-polynomial free energy functionals. We developed a residual based adaptive algorithm to resolve the dynamics of the advective AC equation with expanding and contracting

velocity fields. To the best of our knowledge, this is the first study combining adaptive algorithms with Rothe's method and non-divergent velocity field.

The thesis is organized as follows: in Chapter 2, we first construct discontinuous DGFEM based on the interior penalty method for the general Poisson problem. Then, we give SIPG discretization of AC equation for Dirichlet, Neumann and periodic boundary conditions. The large system of ordinary differential equations (ODEs) resulting from semidiscretization by the SIPG method are solved in with the implicit Euler method and AVF method, which corresponds to method of lines. The proof of the unconditionally energy stability of the fully discrete scheme is given. Also, a time adaptive algorithm is presented to resolve the multiple time dynamics of AC equation. Several numerical examples are given to demonstrate the applicability of the DGFEM discretization coupled with time integrators for the AC equation.

In Chapter 3, we give the SIPG method discretization of mass conservative CH equation for Dirichlet, Neumann and periodic boundary conditions and present the time discretization with the implicit Euler and AVF methods. The unconditionally energy stability of the fully discrete schemes is given. Numerical examples are presented to demonstrate the applicability of our method for the CH equation.

In chapter 4, we first discretize the advective AC equation in time by implicit Euler method and the resulting sequence of semi-linear elliptic equations are discretized by SIPG method. Then, we construct space adaptive algorithm for advective AC equation with non-divergent velocity field and residual based a posteriori error estimates are utilized. We highlight some examples that our adaptive algorithm is capturing the spatial layers in the solution of advective AC equation. Finally, we end up with a conclusion and future work in Chapter 5.

CHAPTER 2

THE ALLEN-CAHN EQUATION

The first occurrence of AC equation goes over the 1970s when Allen and Cahn introduced it to describe the motion of anti-phase boundaries in crystalline solids [2]. Recently, it has been widely used to model various phenomena in nature including biology, image processing, fluid flows, and material science. Actually, it is a basic model equation for the diffuse interface approach to study phase separation and inter-facial dynamics in material science. The generalized AC equation in a bounded domain $\Omega \subset \mathbb{R}^d (d \leq 3)$ is given by

$$\begin{aligned} u_t &= \mu(u) (\epsilon^2 \Delta u - f(u)) \quad \text{in } \Omega \times (0, T], \\ u(\mathbf{x}, 0) &= u_0 \quad \text{in } \Omega \times \{0\}, \end{aligned} \quad (2.1)$$

with suitable boundary conditions such as periodic boundary condition [18, 23], homogeneous Neumann boundary condition [22, 31, 35] or homogeneous Dirichlet boundary condition [33, 50]. In the above, u represents the phase state between materials, the parameter ϵ is known as the interaction length, capturing the dominating effect of the reaction kinetics and represents the effective diffusivity $f(u) = F'(u)$ is an energy function, and $\mu(u)$ is the non negative mobility function which describes the physics of phase separation.

It is well-known that the AC equation is a gradient flow with Liapunov energy functional in L^2

$$\mathcal{E}(u) = \int_{\Omega} \left(\frac{\epsilon^2}{2} |\nabla u|^2 + F(u) \right) dx, \quad (2.2)$$

with the convex double-well energy function [32, 54, 55]

$$F(u) = \frac{1}{4}(1 - u^2)^2, \quad (2.3)$$

or the non-convex logarithmic energy function [12, 68]

$$F(u) = \frac{\theta}{2} [(1 - u) \ln(1 - u) + (1 + u) \ln(1 + u)] - \frac{\theta_c}{2} u^2, \quad (2.4)$$

where θ is the absolute temperature, θ_c is the transition temperature with $\theta \leq \theta_c$. Note that the logarithmic free energy function is usually approximated by the double well energy function when θ is close to θ_c which has the advantage of being smooth.

If the double-well energy function (2.3) is taken into consideration, $f(u) = u^3 - u$ represents the bi-stable non-linearity. The bi-stability comes from checking the sign of $f(u)$ on various intervals at the equilibrium points $u = 0$, $u = 1$, and $u = -1$. It is easily seen that $u = 0$ is an unstable equilibrium, $u = 1$ and $u = -1$ are stable equilibrium which leads to new behavior. When we obtain solutions with $u \geq 0$, the state $u = -1$ is not relevant and traveling waves occur. However, if the solutions are between $u = -1$ and $u = 1$, we have a rather interesting competition between equal and opposite stable states. When the logarithmic free energy function (2.4) is considered $f(u) = \frac{\theta}{2} \ln\left(\frac{1+u}{1-u}\right) - \theta_c u$ in which the logarithmic terms describe the entropy of mixture. The AC equation is considered with the double-well potential and constant mobility in all numerical studies [33, 34, 35, 54, 55, 81]. In [68] it is introduced with degenerate mobility function and logarithmic free energy for the first time. The degenerate mobility function is introduced as $\mu(u) = \beta(1 - u^2)$, β is a constant, which is thermodynamically reasonable choice. The main property that a mobility function should have is that it is zero in the pure component, i.e, when $u = \pm 1$, and the mobility function should be positive for $|u| < 1$.

The mobility function $\mu(u)$, and both energy functionals (2.3) and (2.4) and their derivatives are Lipschitz continuous for $u_1, u_2 \in \mathbb{R}$ with the constraints $|u_{1,2}| \leq 1$ [75] :

$$\begin{aligned} |\mu(u_1) - \mu(u_2)| &\leq L_\mu |u_1 - u_2|, \\ |f(u_1) - f(u_2)| &\leq L_f |u_1 - u_2|, \\ |f'(u_1) - f'(u_2)| &\leq L_{f'} |u_1 - u_2|, \end{aligned} \tag{2.5}$$

with $L_\mu, L_f, L_{f'} \geq 0$ stand for the related Lipschitz constants.

The main characteristic of the AC equation is the energy decay property obtained by differentiating the energy functional (2.2) to get

$$\begin{aligned} \frac{d}{dt} \mathcal{E}(u) &= \int_{\Omega} (f(u)u_t + \epsilon^2 \nabla u \cdot \nabla u_t) d\mathbf{x} \\ &= \int_{\Omega} (f(u) - \epsilon^2 \Delta u) u_t d\mathbf{x} \\ &= - \int_{\Omega} (u_t)^2 d\mathbf{x} \end{aligned}$$

where we have used integration by parts and apply periodic boundary condition or homogenous Neumann boundary condition. Therefore, the total energy is decreasing in time, i.e.,

$$\mathcal{E}(u(t_n)) < \mathcal{E}(u(t_m)), \quad \forall t_n > t_m. \tag{2.6}$$

In addition to energy decreasing property, the other main characteristics of AC equation are

- No mass conservation:

$$\int_{\Omega} u(\mathbf{x}, t) dx \neq \int_{\Omega} u(\mathbf{x}, 0) dx.$$

- Phase separation:

When the time t is large enough, the solution $u(\mathbf{x}, t)$ shows the combination of intervals of $u(\mathbf{x}, t_0) = 1$ and $u(\mathbf{x}, t_0) = -1$ at the time $t = t_0$.

- Metastability phenomena:

In the time evolution of AC equation, the solution pass to stable state in a short period and transforms to another state dramatically.

The presence of the small inter-facial parameter ϵ in the equation and inherent non-linearity leads to the difficulties in the numerical solution of AC equation. To overcome these difficulties the spatial mesh size Δx and the time Δt has to be identified properly to have an accurate and efficient solution. In most of the studies, finite difference [18, 73], spectral elements [23], continuous finite element [55], LDG methods [31, 39] are used for space discretization of AC equation.

Designing energy stable time discretization methods which conserve the decay of discrete energy is also a significant topic in the numerical solution of AC equation. Most of the energy stable methods for AC equation have been developed with constant mobility function. It is observed that the small values of the diffusion parameter ϵ leads to stiff systems after spatial discretizations. In this case, IMEX methods are developed (see for example [69]), since the explicit methods are not suitable for stiff systems and the fully implicit systems require solution of non-linear equations at each time step. In the semi-implicit schemes, the linear stiff part is treated implicitly and the non-linear part explicitly, so that at each time step a linear system of equations is solved. Since the semi-implicit methods have time step restriction inherently, parametrized energy stable methods are developed like the IMEX methods [69], standard integrators like Crank-Nicolson method [34] and linear multi-step integrators [33]. Recently high accurate time integrators like the spectral deferred correction methods [55] and exponential integrators [73] are applied for solving the AC equation.

In this work, we use interior penalty discontinuous Galerkin finite elements method (IPDGFEM) for the space discretization [5, 63]. The DG methods were first introduced in 1973 by Reed and Hill [62] for the solution of steady-state neutron transport being a first-order hyperbolic problem. Then, Douglas, Dupont and Wheeler [27, 80], and Arnold [5] developed the DG methods for elliptic and parabolic problems. Afterward, the DG methods for elliptic problems were developed in [7, 13, 15, 61, 65] and for the ones with advection in [6, 14, 24, 38, 46].

In recent years, the DG methods have become so popular since they exhibit attractive properties of both classical finite elements method (FEM) and finite volume method (FVM). The combination of pros of both methods gives the DG methods flexibility, stability, conservation of local quantities, robustness and compactness properties. The discontinuity of the functions in DGFEM space along the inter-element boundaries

brings in the flexibility of DG methods. Then, one can construct unstructured meshes or hanging nodes to handle the complex geometries. In addition, different order basis functions on each element can be used with DG discretization. Hence, it allows to use in *hp*-methods [70] which arranges the mesh elements and also the order of polynomials on each element adaptively. The stabilization of DG methods are handled via the penalty term which penalizes the jumps of the solution on the element boundaries. Since the stability in DG methods are inherited by this way, there is no need to propose additional stabilization as in the classical FEMs. The DG methods locally conserve several physical quantities such as mass and energy, which plays an important role in the flow and transport problems. Moreover, the sharp gradients or the singularities in the mesh can be locally detected owing to the fully discontinuous polynomial representation of the solution. In addition to all, the (Dirichlet) boundary conditions in DG methods are imposed in a weak manner. In this way, one not only have a scheme which is robust on the boundary conditions but also do not need to construct finite element spaces with certain conditions on the boundary. Besides all the advantages, DG methods have some drawbacks. Compared to the continuous finite elements methods, DG methods produce systems with larger degrees of freedom and ill-conditioned matrices increasing linearly with the order of basis functions.

For time discretization, energy stable implicit Euler method and AVF method is used. Implicit Euler method is the most popular energy stable method. It is strongly energy decreasing, i.e. the discrete energy decreases without any restriction on the step size Δt for very stiff gradient systems for enough small ϵ [41]. The AVF method is the only second order implicit energy stable method [17, 41] and it preserves energy decreasing property for the gradient systems and for systems with Lyapunov functionals. The mid-point method corresponds to AVF method for quadratics non-linearities. For gradient systems involving higher order polynomial or general nonlinear terms, the mid-point method is not energy stable [41]. Higher order energy decreasing methods with orders ≥ 3 are the discontinuous Galerkin-Petrov in time methods (with different trial and test functions) [66] and Gauss Radau IIA Runge-Kutta collocation methods [42]. However, they require coupled systems of equations at each time step which increase the computational cost.

In this chapter, we first construct discontinuous Galerkin finite elements method based on the interior penalty method for the general Poisson problem in Section 2.1. Then, in Section 2.2, we give the SIPG discretization of AC equation for Dirichlet, Neumann and periodic boundary conditions. Section 2.3 presents the time discretization with the implicit Euler method and AVF method, where solution of the non-linear equations are described in detail. Unconditionally energy stability of the fully discrete scheme is given in Section 2.4. In Section 2.5, a time adaptive algorithm is presented. Lastly, several numerical examples are given Section 2.6 to demonstrate the applicability of the DGFEM discretization coupled with time integrators for the AC equation.

2.1 Interior Penalty Galerkin Method

In this section, the construction of interior penalty Galerkin (IPG) method [4, 63] applied to the general Poisson equation

$$\begin{aligned} -\epsilon \Delta u &= f && \text{in } \Omega, \\ u &= g_D && \text{on } \partial\Omega^D, \\ \epsilon \nabla u \cdot \mathbf{n} &= g_N && \text{on } \partial\Omega^N, \end{aligned} \quad (2.7)$$

with $\partial\Omega = \partial\Omega^D \cup \partial\Omega^N$ and $\partial\Omega^D \cap \partial\Omega^N = \emptyset$ is presented since the construction of interior penalty Galerkin methods concern with the diffusion part of the problem.

We first give some basic definitions used in the construction of IPG methods. On a polygonal domain in \mathbb{R}^d , for $1 < p < \infty$, the spaces $L^p(\Omega)$ are defined by

$$L^p(\Omega) = \{w \text{ Lebesgue measurable} : \|w\|_{L^p(\Omega)}^2 < \infty\},$$

with the norms

$$\begin{aligned} \|w\|_{L^p(\Omega)} &= \left(\int_{\Omega} |w(x)|^p dx \right)^{1/p}, && 1 \leq p < \infty \\ \|w\|_{L^\infty(\Omega)} &= \text{esssup}\{|w(x)| : x \in \Omega\}, && p = \infty \end{aligned}$$

Along this thesis, the $L^2(\Omega)$ space which is a Hilbert space given with the usual L^2 -inner product

$$(u, w)_\Omega = \int_{\Omega} u(x)w(x)dx, \quad \|w\|_{L^2(\Omega)} = \sqrt{(w, w)_\Omega}.$$

Let $\mathcal{D}(\Omega)$ denotes the subspace of the space C^∞ having compact support in Ω . For any multi-index $\gamma = (\gamma_1, \dots, \gamma_d) \in \mathbb{N}^d$ with $|\gamma| = \sum_{i=1}^d \gamma_i$, the distributional derivative $D^\gamma w$ is defined by

$$D^\alpha w(\psi) = (-1)^{|\gamma|} \int_{\Omega} w(x) \frac{\partial^{|\gamma|} \psi}{\partial x_1^{\gamma_1} \dots \partial x_d^{\gamma_d}}, \quad \forall \psi \in \mathcal{D}(\Omega).$$

Then, the Sobolev space $W^{(s,p)}$ is introduced as

$$W^{(s,p)}(\Omega) = \{w \in L^p(\Omega) : D^\gamma w \in L^p(\Omega), \forall 0 \leq |\gamma| \leq s\}.$$

Our main interest along this thesis is the Sobolev space given as $H^s(\Omega) = W^{(s,2)}(\Omega)$ for an integer s with the associated Sobolev norm

$$\|w\|_{H^s(\Omega)} = \left(\sum_{0 \leq |\gamma| \leq s} \|D^\gamma w\|_{L^2(\Omega)}^2 \right)^{1/2},$$

and the associated Sobolev seminorm

$$|w|_{H^s(\Omega)} = \|\nabla^s w\|_{L^2(\Omega)} = \left(\sum_{|\gamma|=s} \|D^\gamma w\|_{L^2(\Omega)}^2 \right)^{1/2}.$$

The Sobolev spaces with vanishing functions on the domain boundary are defined by

$$H_0^s(\Omega) = \{w \in H^s(\Omega) : w|_{\partial\Omega} = 0\},$$

and we have for $s = 1$

$$H^1(\Omega) = \{w \in L^2(\Omega) : \nabla w \in (L^2(\Omega))^d\},$$

Moreover, for a partition (most possibly triangles) \mathcal{T}_h of Ω the broken Sobolev spaces are defined by

$$H^s(\mathcal{T}_h) = \{w \in L^2(\Omega) : w|_E \in H^s(E), \forall E \in \mathcal{T}_h\},$$

with the associated broken Sobolev norm

$$\|w\|_{H^s(\mathcal{T}_h)} = \left(\sum_{E \in \mathcal{T}_h} \|w\|_{H^s(E)}^2 \right)^{1/2},$$

and the associated broken gradient semi-norm

$$|w|_{H^0(\mathcal{T}_h)} = \left(\sum_{E \in \mathcal{T}_h} \|\nabla w\|_{L^2(E)}^2 \right)^{1/2}.$$

Now, we are ready to construct the IPG method. Let $\{\mathcal{T}_h\}$ be a family of shape regular meshes with triangular elements, i.e., there exists a constant c_0 such that

$$\max_{E \in \mathcal{T}_h} \frac{h_E^2}{|E|} \leq c_0$$

where h_E is the diameter and $|E|$ is the area of E , and also the elements $E_i \in \mathcal{T}_h$ satisfies $\bar{\Omega} = \cup \bar{E}$ and $E_i \cap E_j = \emptyset$ for $E_i, E_j \in \mathcal{T}_h$. We split the set of all edges E_h into the set of interior edges E_h^0 , the set of Dirichlet boundary edges E_h^D and the set of Neumann boundary edges E_h^N , so that $E_h = E_h^\partial \cup E_h^0$ with $E_h^\partial = E_h^D \cup E_h^N$. Then, set the finite dimensional solution and test function space by

$$V_h = \{u \in L^2(\Omega) : u|_E \in \mathbb{P}^q(E), \forall E \in \mathcal{T}_h\} \not\subset H_0^1(\Omega),$$

where $\mathbb{P}^q(E)$ denotes the set of all polynomials on $E \in \mathcal{T}_h$ of degree at most q . Note that the space of solution and test functions are chosen to be the same since the boundary conditions in DG methods are imposed weakly. In contrast to continuous finite element method, discontinuous Galerkin methods are suitable to use non-conforming

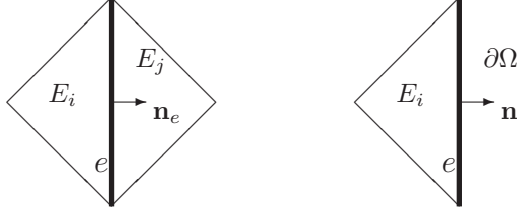


Figure 2.1: Left: two neighbor elements sharing an edge, Right: an element adjacent to boundary of the domain

spaces in which case the functions in $V_h \not\subset H_0^1$ are allowed to be discontinuous along the inter-element boundaries.

Because of the discontinuity of the functions in V_h along the inter element boundaries, there are two different traces from the neighboring elements sharing that edge. Accordingly, let us first give some notations before the construction of IPG methods. Let the edge e be a common edge for two elements E_i and E_j ($i < j$), (see Figure 2.1). Then for a scalar function u , there are two common traces of u along e , denoted by $u|_{E_i}$ from inside E_i and $u|_{E_j}$ from inside E_j . Then, the jump and average of u across the edge e are defined as

$$[u] = u|_{E_i} \mathbf{n}_e - u|_{E_j} \mathbf{n}_e, \quad \{u\} = \frac{1}{2}(u|_{E_i} + u|_{E_j}),$$

where \mathbf{n}_e is the unit normal to the edge e oriented from E_i to E_j . Similarly, we set the jump and average values of a vector field ∇u on e

$$[\nabla u] = \nabla u|_{E_i} \cdot \mathbf{n}_e - \nabla u|_{E_j} \cdot \mathbf{n}_e, \quad \{\nabla u\} = \frac{1}{2}(\nabla u|_{E_i} + \nabla u|_{E_j}),$$

Observe that $[u]$ is a vector for a scalar function u , while, $[\nabla u]$ is scalar for a vector field ∇u . On the other hand, for a boundary edge $e \subset E_i \cap \partial\Omega$, we set

$$[u] = u|_{E_i} \mathbf{n}, \quad \{u\} = u|_{E_i}, \quad [\nabla u] = \nabla u|_{E_i} \cdot \mathbf{n}, \quad \{\nabla u\} = \nabla|_{E_i}$$

where \mathbf{n} is the unit outward normal to the boundary at e .

Now, the IPG method discretization of the diffusion part of the problem is constructed. If we multiply the continuous equation (2.7) by a test function $v \in V_h$, integrate over Ω and split the integrals, we obtain

$$-\sum_{E \in \mathcal{T}_h} \int_E \epsilon \Delta u v dx = \sum_{E \in \mathcal{T}_h} \int_E f v dx$$

Applying the divergence theorem on every element integral gives

$$\sum_{E \in \mathcal{T}_h} \int_E \epsilon \nabla u \cdot \nabla v dx - \sum_{E \in \mathcal{T}_h} \int_{\partial E} \epsilon (\nabla u \cdot \mathbf{n}) v ds = \sum_{E \in \mathcal{T}_h} \int_K f v dx + \sum_{e \in E_h^N} \int_e g_N v ds$$

Using the jump definitions ($v \in V_h$ are element-wise discontinuous), we get

$$\sum_{E \in \mathcal{T}_h} \int_E \epsilon \nabla u \cdot \nabla v dx - \sum_{e \in E_h^0 \cup E_h^D} \int_e [\epsilon v \nabla u] ds = \sum_{E \in \mathcal{T}_h} \int_E f v dx + \sum_{e \in E_h^N} \int_e g_N v ds$$

It can be easily verified that $[\epsilon v \nabla u] = \{\epsilon \nabla u\} \cdot [v] + [\epsilon \nabla u] \cdot \{v\}$. Also, using the fact that $[\nabla u] = 0$ (u is assumed to be smooth enough so that ∇u is continuous), we get

$$\sum_{E \in \mathcal{T}_h} \int_E \epsilon \nabla u \cdot \nabla v dx - \sum_{e \in E_h^0 \cup E_h^D} \int_e \{\epsilon \nabla u\} \cdot [v] ds = \sum_{E \in \mathcal{T}_h} \int_E f v dx + \sum_{e \in E_h^N} \int_e g_N v ds$$

However, the left hand side is not coercive, even not symmetric. To handle this and to penalize the solutions, using the fact that $[u] = 0$ along the interior edges (u is assumed to be continuous), we reach at

$$\begin{aligned} \sum_{E \in \mathcal{T}_h} \int_E \epsilon \nabla u \cdot \nabla v dx - \sum_{e \in E_h^0 \cup E_h^D} \int_e \{\epsilon \nabla u\} \cdot [v] ds - \sum_{e \in E_h^0} \int_e \{\epsilon \nabla v\} \cdot [u] ds \\ + \sum_{e \in E_h^0} \frac{\sigma}{h_e} \int_e [u] \cdot [v] ds = \sum_{E \in \mathcal{T}_h} \int_E f v dx + \sum_{e \in E_h^N} \int_e g_N v ds \end{aligned}$$

where h_e denotes the length of the edge e and σ is called the penalty parameter. It should be sufficiently large to ensure the stability of the DG discretization with a lower bound depending only on the polynomial degree such that for 1D problems $\sigma = \frac{5}{2}(q+1)^2$ and $\sigma = 3q(q+1)$ for 2D problems.

Finally, by keeping unknown on the left hand side and imposing Dirichlet boundary condition on the right hand side, we add to the both sides the edge integrals on the Dirichlet boundary edges

$$\begin{aligned} \sum_{E \in \mathcal{T}_h} \int_E \epsilon \nabla u \cdot \nabla v dx - \sum_{e \in E_h^0 \cup E_h^D} \int_e \{\epsilon \nabla u\} \cdot [v] ds + \mathcal{K} \sum_{e \in E_h^0 \cup E_h^D} \int_e \{\epsilon \nabla v\} \cdot [u] ds \\ + \sum_{e \in E_h^0 \cup E_h^D} \frac{\sigma}{h_e} \int_e [u] \cdot [v] ds = \sum_{E \in \mathcal{T}_h} \int_E f v dx + \sum_{e \in E_h^D} \int_e g_D \left(\frac{\sigma}{h_e} v - \epsilon \nabla v \cdot \mathbf{n} \right) ds \\ + \sum_{e \in E_h^N} \int_e g_N v ds. \end{aligned}$$

which gives the IPG formulation. In this formulation, the parameter κ determines the type of the IPG method. It takes the values on $\mathcal{K} \in \{-1, 0, 1\}$ giving that

- $\mathcal{K} = -1$: symmetric interior penalty Galerkin (SIPG) method
- $\mathcal{K} = 0$: incomplete interior penalty Galerkin (IIPG) method
- $\mathcal{K} = 1$: non-symmetric interior penalty Galerkin (NIPG) method

In this thesis, symmetric interior penalty Galerkin (SIPG) method is considered.

2.2 SIPG Discretization of Allen-Cahn Equation

In this section, we describe the DG discretization based on SIPG method applied to the diffusion part of the AC equation (2.1) for Dirichlet, Neumann [63], and periodic boundary conditions [76]. Using the definitions and notations from the previous section, the solution of (2.1) reads as: for each $t \in (0, T]$ find $u_h(t) \in V_h$ such that

$$(\partial_t u_h, v_h)_\Omega + a_h(\kappa; u_h, v_h) + b_h(u_h, v_h)_\Omega = I_h(v_h), \quad \forall v_h \in V_h \quad (2.8)$$

where $b_h(u_h, v_h)_\Omega = (\mu(u)f(u), v)$ and the bilinear form is of the form $a_h(\kappa; u, v) = \tilde{a}_h(\kappa; u, v) + J_h^\partial(\kappa; u, v)$ with

$$\begin{aligned} \tilde{a}_h(\kappa; u_h, v_h) &= \sum_{E \in \mathcal{T}_h} \int_E \kappa \nabla u \cdot \nabla v - \sum_{e \in E_h^0} \int_e \{\kappa \nabla u\} \cdot [v] ds \\ &\quad - \sum_{e \in E_h^0} \int_e \{\kappa \nabla v\} \cdot [u] + \sum_{e \in E_h^0} \frac{\sigma \kappa}{h_e} \int_e [u] \cdot [v] ds. \end{aligned}$$

In the above formula, the mobility function $\mu(u)$ is computed explicitly as in form of the integral $\int_{E \in \mathcal{T}_h} \mu(u^n) d\Omega$, where u^n denotes the approximate solution at the previous time step n as for continuous finite elements in the Cahn-Hilliard equation [3, 4, 12]. In the DG discretized bilinear form (2.8) κ stands for $\kappa = \int_{E \in \mathcal{T}_h} \epsilon^2 \mu(u^n) d\Omega$. The bilinear form $\tilde{a}_h(\kappa; u_h, v_h)$ includes the face integrals only on the interior edges, the term $J_h^\partial(\kappa; u_h, v_h)$ includes the corresponding face integrals on the boundary edges and together with the right hand side $I_h(v_h)$. So, it changes depending on the boundary conditions. If Dirichlet boundary condition, $u = g_D$, is prescribed, we set

$$\begin{aligned} J_h^\partial(\kappa; u, v) &= - \sum_{e \in E_h^D} \int_e \{\kappa \nabla u\} \cdot [v] ds - \sum_{e \in E_h^D} \int_e \{\kappa \nabla v\} \cdot [u] \\ &\quad + \sum_{e \in E_h^D} \frac{\sigma \kappa}{h_e} \int_e [u] \cdot [v] ds, \\ I_h(v) &= \sum_{e \in E_h^D} \int_e \left(\frac{\sigma \kappa}{h_e} v - \kappa \nabla v \cdot \mathbf{n} \right) g_D ds. \end{aligned}$$

In the case of Neumann boundary condition, $\epsilon^2 \nabla u \cdot \mathbf{n} = g_N$, they become

$$J_h^\partial(\kappa; u, v) = 0, \quad I_h(v) = \sum_{e \in E_h^N} \int_e g_N v ds.$$

When periodic boundary condition is applied, the periodic edges are treated as unknown, in other words, as interior edges with appropriate definitions of the so-called

jump and average terms. In this case, the set of all edges E_h is splitted into the set E_h^0 of interior edges and the set E_h^{per} of periodic boundary edge-pairs. An individual element of the set E_h^{per} is of the form $\omega = \{E_l, E_m\}$ where $E_l \subset \partial K_l \cap \partial\Omega$, and $E_m \subset \partial K_m \cap \partial\Omega$ is the corresponding periodic edge-pair of E_l with $l > m$, and we associate with each ω a common normal vector \mathbf{n} that is outward unit normal to $E_l \subset \partial K_l \cap \partial\Omega$. Then, for each such ω , we define the jump and average operators

$$[u]_\omega = u|_{E_l} \mathbf{n} - u|_{E_m} \mathbf{n}, \quad \{u\}_\omega = \frac{1}{2}(u|_{E_l} + u|_{E_m}).$$

In this case, we have

$$\begin{aligned} J_h^\partial(\kappa; u, v) &= - \sum_{\omega \in E_h^{per}} \int_{\omega} \{\kappa \nabla u\}_\omega \cdot [v]_\omega ds - \sum_{\omega \in E_h^{per}} \int_{\omega} \{\kappa \nabla v\}_\omega \cdot [u]_\omega \\ &+ \sum_{\omega \in E_h^{per}} \frac{\sigma \kappa}{h_E} \int_{\omega} [u]_\omega \cdot [v]_\omega ds, \end{aligned}$$

and $I_h(v) = 0$.

2.2.1 Semi-Discrete System in Matrix-Vector Form

The approximate solution of the semi-problem (2.8) has the form

$$u_h(t) = \sum_{m=1}^N \sum_{j=1}^{n_q} \xi_j^m(t) \psi_j^m \quad (2.9)$$

where ψ_j^m are the basis functions of V_h and ξ_j^m are the unknown coefficients, n_q is local dimension with $n_q = q + 1$ for 1D problems, $n_q = \frac{(q+1)(q+2)}{2}$ for 2D problems, and N is the number of intervals for 1D problems or the number of triangular elements for 2D problems. In DG methods, the basis functions ψ_j^m 's are chosen in such a way that each piecewise basis polynomial has only one triangle as a support, i.e., on a specific triangle E_e , $e \in \{1, 2, \dots, N\}$, the basis polynomials ψ_j^e are zero outside E_e . This construction makes the stiffness matrix in DG methods block structure, each of which related to a triangle. The product $dof := N * n_q$ gives the degree of freedom in DG methods. Inserting the approximate solution u_h in (2.8) and choosing the test functions as $v_h = \psi_j^m$, $j = 1, 2, \dots, n_q$, $m = 1, 2, \dots, N$, the semi-discrete system (2.8) in matrix vector form is given by

$$M \xi_t + A \xi + r(\xi) = L, \quad (2.10)$$

where $\xi \in \mathbb{R}^{dof}$ is the vector of unknown coefficients ξ_j^m 's, $M \in \mathbb{R}^{dof \times dof}$ is the mass matrix, $A \in \mathbb{R}^{dof \times dof}$ is the stiffness matrix corresponding to the bilinear form $a_h(\kappa; u_h, v_h)$, $r \in \mathbb{R}^{dof}$ is the vector function of ξ related to the non-linear form

$r_h(u_h, v_h)$ and $L \in \mathbb{R}^{dof}$ is the load vector related to the linear term $I_h(v_h)$. The explicit definitions are given by

$$M = \begin{bmatrix} M_{11} & M_{12} & \cdots & M_{1,N} \\ M_{21} & M_{22} & & \vdots \\ \vdots & & \ddots & \\ M_{N,1} & \cdots & & M_{N,N} \end{bmatrix}, \quad A = \begin{bmatrix} A_{11} & A_{12} & \cdots & A_{1,N} \\ A_{21} & A_{22} & & \vdots \\ \vdots & & \ddots & \\ A_{N,1} & \cdots & & A_{N,N} \end{bmatrix}$$

$$\xi = \begin{bmatrix} \xi_1 \\ \xi_2 \\ \vdots \\ \xi_N \end{bmatrix}, \quad r(\xi) = \begin{bmatrix} \mathbf{r}_1 \\ \mathbf{r}_2 \\ \vdots \\ \mathbf{r}_N \end{bmatrix}, \quad \mathbf{L} = \begin{bmatrix} \mathbf{L}_1 \\ \mathbf{L}_2 \\ \vdots \\ \mathbf{L}_N \end{bmatrix}$$

where all the block matrices have dimension n_q :

$$M_{ji} = \begin{bmatrix} (\phi_1^i, \phi_1^j) & (\phi_2^i, \phi_1^j) & \cdots & (\phi_{n_q}^i, \phi_1^j) \\ (\phi_1^i, \phi_2^j) & (\phi_2^i, \phi_2^j) & & \vdots \\ \vdots & & \ddots & \\ (\phi_1^i, \phi_{n_q}^j) & \cdots & & (\phi_{n_q}^i, \phi_{n_q}^j) \end{bmatrix},$$

$$A_{ji} = \begin{bmatrix} a_h(\kappa; \phi_1^i, \phi_1^j) & a_h(\kappa; \phi_2^i, \phi_1^j) & \cdots & a_h(\kappa; \phi_{n_q}^i, \phi_1^j) \\ a_h(\kappa; \phi_1^i, \phi_2^j) & a_h(\kappa; \phi_2^i, \phi_2^j) & & \vdots \\ \vdots & & \ddots & \\ a_h(\kappa; \phi_1^i, \phi_{n_q}^j) & \cdots & & a_h(\kappa; \phi_{n_q}^i, \phi_{n_q}^j) \end{bmatrix},$$

$$\xi_i = \begin{bmatrix} \xi_1^i \\ \xi_2^i \\ \vdots \\ \xi_{n_q}^i \end{bmatrix}, \quad \mathbf{r}_i = \begin{bmatrix} r_h(u_h, \phi_1^i) \\ r_h(u_h, \phi_2^i) \\ \vdots \\ r_h(u_h, \phi_{n_q}^i) \end{bmatrix}, \quad \mathbf{L}_i = \begin{bmatrix} I_h(\phi_1^i) \\ I_h(\phi_2^i) \\ \vdots \\ I_h(\phi_{n_q}^i) \end{bmatrix}.$$

2.3 Time Discretization by Backward Euler and AVF Method

In this section, the fully discrete formulation of AC equation (2.1) in matrix–vector notation is given by using the backward Euler method and AVF method time integrators through the semi–discrete formulation (2.10).

2.3.1 Time Discretization by Backward Euler Method

We consider the semi–linear system of ordinary differential equations

$$M\xi_t + A\xi + r(\xi) = L, \quad (2.11)$$

for the ordered unknown coefficient vector

$$\xi = (\xi_1^1, \dots, \xi_{n_q}^1, \xi_1^2, \dots, \xi_{n_q}^2, \dots, \xi_1^N, \dots, \xi_{n_q}^N)^T.$$

Let consider the uniform partition $0 = t_0 < t_1 < \dots < t_J = T$ of the time interval $[0, T]$ with the uniform time step-size $\Delta t = t_k - t_{k-1}$, $k = 1, 2, \dots, J$. For $t = 0$, let $u_h(0) \in V_h$ be the projection (orthogonal L^2 -projection) of the initial condition u_0 onto V_h , and let ξ_0 be the corresponding coefficient vector (ordered) satisfying (2.9). Then, the backward Euler method applied to the semi linear system (2.11) reads as: for $n = 0, 1, \dots, J - 1$, solve

$$\begin{aligned} \frac{M\xi_{n+1} - M\xi_n}{\Delta t} + A\xi_{n+1} + r(\xi_{n+1}) &= L_{n+1}, \\ (M + \Delta t A)\xi_{n+1} + \Delta t r(\xi_{n+1}) - \Delta t L_{n+1} &= M\xi_n, \end{aligned}$$

which is the fully discretized system that we will solve for ξ_{n+1} . We solve this non-linear system of equations using Newton's method in Algorithm 1. From the algebraic point of view, Newton's method corresponds to solving the non-linear equations

$$R(\xi_{n+1}) = (M + \Delta t A)\xi_{n+1} + \Delta t r(\xi_{n+1}) - \Delta t L_{n+1} - M\xi_n. \quad (2.12)$$

Algorithm 1 Newton's Method

given initial guess ξ^0
for $k = 0, 1, 2, \dots$ **do**
 solve $\frac{\partial R}{\partial \xi_{n+1}} s^k = -R$
 update solution $\xi^{k+1} = \xi^k + s^k$

end for

Starting with an initial guess $\xi_{n+1}^{(0)}$, the k -th Newton iteration to solve the non-linear equation (2.12) for the unknown vector ξ_{n+1} reads as

$$J_S^{(k)} = -R(\xi_{n+1}^{(k)}), \quad \xi_{n+1}^{(k+1)} = \xi_{n+1}^{(k)} + s^{(k)}, \quad k = 0, 1, \dots \quad (2.13)$$

until a user defined tolerance is satisfied. In (2.13), J stands for the Jacobian matrix of $R(\xi_{n+1})$, whose entries are the partial derivatives with respect to ξ_{n+1}

$$J_{ij} = \frac{\partial R_i}{\partial (\xi_{n+1})_j}, \quad i, j = 1, 2, \dots, n_q \times N$$

at the current iteration. It is easy to differentiate the linear terms, to differentiate the nonlinear term using the expansion $u_h = \sum_{k=1}^{n_q \times N} \xi_k \psi^k$ ordered version of (2.9), we obtain

$$\begin{aligned} H(\xi) &= \frac{\partial r_i(\xi)}{\partial \xi_j} = \frac{\partial}{\partial \xi_j} (\mu(u_h^n) f(u_h), \psi^i), \quad i, j = 1, 2, \dots, N \\ &= \mu(u_h^n) \int_{\Omega} f'(u_h) \psi^j \psi^i dx \end{aligned}$$

where $f(u)$ is the double well potential or the logarithmic function in our model. We finally reach

$$J = (M + \Delta t A) + \Delta t H(\xi_{n+1}). \quad (2.14)$$

Note that the Jacobian matrix H is in the form of

$$H(\xi) = \begin{bmatrix} \frac{\partial \mathbf{r}_1(\xi)}{\partial \xi_1} & \frac{\partial \mathbf{r}_1(\xi)}{\partial \xi_2} & \dots & \frac{\partial \mathbf{r}_1(\xi)}{\partial \xi_N} \\ \vdots & & \ddots & \vdots \\ \frac{\partial \mathbf{r}_N(\xi)}{\partial \xi_1} & \frac{\partial \mathbf{r}_N(\xi)}{\partial \xi_2} & \dots & \frac{\partial \mathbf{r}_N(\xi)}{\partial \xi_N} \end{bmatrix}.$$

2.3.2 Time Discretization by AVF Method

The semi-discretized AVF equation is a gradient system

$$\dot{u} = -\nabla \mathcal{E}(u)$$

evolving into a state of minimal energy. Gradient systems are characterized by the monotonically energy decreasing property of the potential

$$\mathcal{E}(u(t)) \leq \mathcal{E}(u(s)), \quad \text{for } t > s.$$

In the numerical approximation of the gradient systems, it is desirable to preserve the energy decreasing property monotonically

$$\mathcal{E}(u(t_n)) \leq \mathcal{E}(u(t_{n-1})), \quad \text{for } n = 1, 2, \dots$$

The average vector field (AVF) method

$$u_n = u_{n-1} - \Delta t \int_0^1 \nabla \mathcal{E}(\tau u_n + (1 - \tau)u_{n-1}) d\tau$$

possesses the energy decreasing property without restriction to step sizes Δt . It is a modification of the implicit mid-point rule. In [25, 41] higher order variants of the AVF methods for Hamiltonian and Poisson systems with Gauss-Legendre collocation points are given. As Gauss-Legendre Runge-Kutta methods, the AVF method, and higher order versions do not have damping property for very stiff systems, whereas for discontinuous Galerkin-Petrov methods and Radua II Runge-Kutta methods, the energy decreases monotonically without restriction to the step size Δt and the Lipschitz constant for $\nabla \mathcal{E}(y)$. But they require solution of coupled system of equations, which increases the computation cost for 2 and 3 dimensional AC equations, where efficient solution techniques are required [30]. The AVF method can be regarded as an efficient integrator for the AC equation, i.e. the integrals by the DG semi-discretized can be computed with the desired accuracy at low cost.

The AVF method is equivalent to the Petrov-Galerkin discontinuous Galerkin in time, when the trial functions are piecewise linear and the test functions are piecewise constant, which are given by

$$u_n = u_{n-1} - \int_{t_{n-1}}^{t_n} \nabla \mathcal{E}(\Delta t^{-1}(t - t_{n-1})u_n + \Delta t^{-1}(t_n - t)u_{n-1}) dt. \quad (2.15)$$

With the time parametrization $t(\tau) = t_{n-1} + (t_n - t_{n-1})\tau$ and using the change of variable formulation

$$\int_{t_{n-1}}^{t_n} g(t)dt = \int_0^1 g(t(\tau))\frac{dt(\tau)}{d\tau}d\tau,$$

we obtain for the integral term in (2.15)

$$\begin{aligned} u_n &= u_{n-1} - \int_{t_{n-1}}^{t_n} \nabla \mathcal{E}(\Delta t^{-1}(t - t_{n-1})u_n + \Delta t^{-1}(t_n - t)u_{n-1})dt \\ &= u_{n-1} - \Delta t \int_0^1 \nabla \mathcal{E}(\tau u_n + (1 - \tau)u_{n-1})d\tau \end{aligned}$$

which is the AVF method on the interval $[t_{n-1}, t_n]$.

The semi-linear system of ordinary differential equations as a gradient system

$$M\xi_t = -\nabla \mathcal{E}(\xi) = A\xi + r(\xi) - L \quad (2.16)$$

for the ordered unknown coefficient vector

$$\xi = (\xi_1^1, \dots, \xi_{n_q}^1, \xi_1^2, \dots, \xi_{n_q}^2, \dots, \xi_1^N, \dots, \xi_{n_q}^N)^T,$$

same order for the basis functions. Let consider the same time interval partition in the previous section. Then, for $t = 0$, let $u_h(0) \in V_h$ be the projection (orthogonal L^2 -projection) of the initial condition u_0 onto V_h , and let ξ_0 be the corresponding coefficient vector (ordered) satisfying (2.9). Then, the AVF method applied to the gradient system (2.16) reads as: for $n = 0, 1, \dots, J - 1$, solve

$$\begin{aligned} \frac{M\xi_{n+1} - M\xi_n}{\Delta t} &= - \int_0^1 \nabla \mathcal{E}(\tau \xi_{n+1} + (1 - \tau)\xi_n)d\tau \\ M\xi_{n+1} &= M\xi_n + \Delta t \underbrace{\int_0^1 [L - A(\tau \xi_{n+1} + (1 - \tau)\xi_n)] d\tau}_{\text{linear}} \\ &\quad + \Delta t \underbrace{\int_0^1 r(\tau \xi_{n+1} + (1 - \tau)\xi_n)d\tau}_{\text{non-linear}} \end{aligned}$$

After a simple calculation for the linear part, we get

$$\begin{aligned} M\xi_{n+1} &= M\xi_n + \Delta t L + \frac{\Delta t}{2}(A\xi_n + A\xi_{n+1}) \\ &\quad + \Delta t \int_0^1 r(\tau \xi_{n+1} + (1 - \tau)\xi_n)d\tau \end{aligned} \quad (2.17)$$

which is the fully discretized system that we will solve for ξ_{n+1} . We solve this non-linear system of equations using Newton's method in Algorithm 1. Newton's method for (2.17) corresponds to solving the non-linear equations

$$\begin{aligned}
R(\xi_{n+1}) &= M\xi_{n+1} - \Delta t L - M\xi_n + \frac{\Delta t}{2}(A\xi_n + A\xi_{n+1}) \\
&+ \Delta t \int_0^1 r(\tau\xi_{n+1} + (1-\tau)\xi_n) d\tau \\
&= 0.
\end{aligned} \tag{2.18}$$

Starting with an initial guess $\xi_{n+1}^{(0)}$, the k -th Newton iteration to solve the non-linear equation (2.18) for the unknown vector ξ_{n+1} reads as

$$J_s^{(k)} = -R(\xi_{n+1}^{(k)}), \quad \xi_{n+1}^{(k+1)} = \xi_{n+1}^{(k)} + s^{(k)}, \quad k = 0, 1, \dots \tag{2.19}$$

until a user defined tolerance is satisfied. In (2.19), J stands for the Jacobian matrix of $R(\xi_{n+1})$, whose entries are the partial derivatives

$$J_{ij} = \frac{\partial R_i}{\partial (\xi_{n+1})_j}, \quad i, j = 1, 2, \dots, n_q \times N$$

at the current iteration. It is easy to differentiate the linear terms in (2.18)

$$\frac{\partial}{\partial (\xi_{n+1})_j} (M\xi_{n+1} - M\xi_n - \Delta t L + \frac{\Delta t}{2}(A\xi_n + A\xi_{n+1}))_i = M_{ij} + \frac{\Delta t}{2} A_{ij}.$$

We apply the chain rule to differentiate the non-linear term,

$$\frac{\partial}{\partial (\xi_{n+1})_j} \Delta t \int_0^1 r_i(\tau\xi_{n+1} + (1-\tau)\xi_n) d\tau = \Delta t \int_0^1 \tau \frac{\partial r_i}{\partial (\xi_{n+1})_j} (\tau\xi_{n+1} + (1-\tau)\xi_n) d\tau$$

where, using the expansion $u_h = \sum_{k=1}^{n_q \times N} \xi_k \varphi^k$, ordered version of (2.9),

$$\begin{aligned}
\frac{\partial r_i(\xi)}{\partial \xi_j} &= \frac{\partial}{\partial \xi_j} (\mu(u_h^n) f(u_h), \varphi^i)_\Omega, \quad i, j = 1, 2, \dots, n_q \times N \\
&= \mu(u_h^n) \int_\Omega f' \left(\sum_{j=1}^{n_q \times N} \xi_j \varphi^j \right) \varphi^j \varphi^i dx
\end{aligned} \tag{2.20}$$

We obtain finally

$$J = M + \frac{\Delta t}{2} A + \Delta t \int_0^1 \tau J_r(\tau\xi_{n+1}^{(k+1)} + (1-\tau)\xi_n) d\tau. \tag{2.21}$$

where $J_r(\tau\xi_{n+1}^{(k+1)} + (1-\tau)\xi_n)$ is the differential matrix, whose entries are given in (2.20), at $\tau\xi_{n+1}^{(k+1)} + (1-\tau)\xi_n$. At each Newton iteration, we approximate the integral term in (2.21) using the fourth order Gaussian quadrature rule.

2.4 Energy Stability of Fully Discrete Scheme

It is generally accepted that the fully discrete energy stable schemes should preserve the discrete energy dissipation as their continuous parts, which leads to qualitatively better approximations. The continuous (in time) energy of the semi-discrete AC equation is given as [31] :

$$\begin{aligned} \mathcal{E}^h(u) &= \frac{\epsilon^2}{2} \|\nabla u\|_{L^2(\mathcal{T}_h)}^2 + (F(u), 1)_\Omega \\ &+ \sum_{E \in E_h^0} \left(-(\{\epsilon^2 \partial_n u\}, [u])_E + \frac{\sigma \epsilon^2}{2h_e} ([u], [u])_E \right). \end{aligned} \quad (2.22)$$

On the other hand, the discrete DG counterpart of the continuous energy (2.22) at a time $t^n = n\Delta t$ reads as

$$\begin{aligned} \mathcal{E}_{DG}^h(u^n) &= \frac{\epsilon^2}{2} \|\nabla u^n\|_{L^2(\tau_h)}^2 + (F(u^n), 1)_\Omega \\ &+ \sum_{E \in E_h^0} \left(-(\{\epsilon^2 \partial_n u^n\}, [u^n])_E + \frac{\sigma \epsilon^2}{2h_E} ([u^n], [u^n])_E \right). \end{aligned} \quad (2.23)$$

In this section, we show that backward Euler and AVF methods applied to the semi-discrete system (2.8) are energy stable through the discrete energy (2.23).

2.4.1 Energy Stability of Fully Discrete Scheme with Backward Euler

When the backward Euler method applied to the semi-discrete system (2.8), the SIPG discretized fully discrete scheme is given by

$$\frac{1}{\Delta t} (u^{n+1} - u^n, q)_\Omega + a_h(\mu(u^n)\epsilon^2; u^{n+1}, q) + b_h(u^{n+1}, q)_\Omega = 0, \quad \forall q \in V_h, \quad (2.24)$$

where the bilinear form $a_h(\epsilon; u, v)$ is given by

$$\begin{aligned} a_h(\mu(u^n)\epsilon^2; u, v) &= \sum_{E \in \tau_h} \int_E \mu(u^n)\epsilon^2 \nabla u \cdot \nabla v dx - \sum_{e \in E_h^0} \int_e \{\mu(u^n)\epsilon^2 \nabla u\} [v] ds \\ &- \sum_{e \in E_h^0} \int_e \{\mu(u^n)\epsilon^2 \nabla v\} [u] ds + \sum_{e \in E_h^0} \frac{\sigma \mu(u^n)\epsilon^2}{h_e} \int_e [u][v] ds, \\ b_h(u, q) &= \sum_{E \in \tau_h} \int_E \mu(u^n) f(u) q dx. \end{aligned}$$

Taking $q = u^{n+1} - u^n$ in (2.24), we obtain

$$\begin{aligned} \frac{1}{\Delta t}(u^{n+1} - u^n, u^{n+1} - u^n)_\Omega &+ \mu(u^n)a_h(\epsilon^2; u^{n+1}, u^{n+1} - u^n) \\ &+ \mu(u^n)(f(u^{n+1}), u^{n+1} - u^n)_\Omega \\ &= 0. \end{aligned}$$

By using the identity $(a, a - b)_\Omega = \frac{1}{2}(a^2 - b^2 + (a - b)^2, 1)_\Omega$ and the bilinearity of a_h , we get

$$\begin{aligned} &(u^{n+1} - u^n, u^{n+1} - u^n)_\Omega + \mu(u^n)(f(u^{n+1}), u^{n+1} - u^n)_\Omega \\ &+ \mu(u^n)\frac{1}{2}a_h(\epsilon^2; u^{n+1}, u^{n+1}) - \mu(u^n)\frac{1}{2}a_h(\epsilon^2; u^n, u^n) \\ &+ \mu(u^n)\frac{1}{2}a_h(\epsilon^2; u^{n+1} - u^n, u^{n+1} - u^n) = 0. \end{aligned} \quad (2.25)$$

Expanding the term $F(u^n)$ around u^{n+1} , and neglecting the higher order terms, we obtain

$$\begin{aligned} F(u^n) &= F(u^{n+1}) - F'(u^{n+1})(u^{n+1} - u^n) \\ F(u^n) &\approx F(u^{n+1}) - f(u^{n+1})(u^{n+1} - u^n) \\ (f(u^{n+1}), u^{n+1} - u^n)_\Omega &\approx (F(u^{n+1}), 1)_\Omega - (F(u^n), 1)_\Omega. \end{aligned} \quad (2.26)$$

Note that the bilinear form $a_h(\epsilon^2; u^{n+1}, u^{n+1})$ satisfies

$$\begin{aligned} a_h(\epsilon^2; u^{n+1}, u^{n+1}) &= \frac{\epsilon^2}{2}\|\nabla u^{n+1}\|_{L^2(\Omega)}^2 - \sum_{e \in E_h^0} \int_e \{\epsilon^2 \nabla u^{n+1}\} [u^{n+1}] ds \\ &+ \sum_{e \in E_h^0} \frac{\sigma \epsilon^2}{2h_2} \|[u^{n+1}]\|_{L^2(E)}^2 \\ &\geq 0 \end{aligned} \quad (2.27)$$

since all the terms in ((2.27)) are non-negative (see [63, Sec. 2.7.1] for positivity of edge integral term). Similarly, we have $a_h(\epsilon^2; u^{n+1} - u^n, u^{n+1} - u^n) \geq 0$. Using these identities, and substituting the last equation in (2.26) into (2.25), we obtain

$$\begin{aligned} 0 &\geq -\left(\frac{1}{\Delta t \mu(u^n)}\|u^{n+1} - u^n\|_{L^2(\Omega)}^2 + \frac{1}{2}a_h(\epsilon^2; u^{n+1} - u^n, u^{n+1} - u^n)\right) \\ &\approx (F(u^{n+1}), 1)_\Omega + \frac{1}{2}a_h(\epsilon^2; u^{n+1}, u^{n+1}) - \left((F(u^n), 1)_\Omega + \frac{1}{2}a_h(\epsilon^2; u^n, u^n)\right) \\ &= \mathcal{E}(u^{n+1}) - \mathcal{E}(u^n) \end{aligned}$$

which implies that $\mathcal{E}(u^{n+1}) \leq \mathcal{E}(u^n)$. Hence, the backward Euler method is unconditionally energy stable.

2.4.2 Energy Stability of Fully Discrete Scheme with AVF Method

Time discretization of semi-discrete system (2.8) by the AVF methods, leads to

$$\begin{aligned} \frac{1}{\Delta t}(u_h^{n+1} - u_h^n, v_h)_\Omega + \mu(u_h^n) \frac{1}{2} a_h(\epsilon^2; u_h^{n+1} + u_h^n, v_h) \\ + \mu(u_h^n) \int_0^1 (f(\tau u_h^{n+1} + (1-\tau)u_h^n), v_h)_\Omega d\tau = 0, \quad \forall v_h \in V_h \end{aligned}$$

Taking $v_h = u_h^{n+1} - u_h^n$, we obtain

$$\begin{aligned} \frac{1}{\Delta t}(u_h^{n+1} - u_h^n, u_h^{n+1} - u_h^n)_\Omega + \mu(u_h^n) \frac{1}{2} a_h(\epsilon^2; u_h^{n+1} + u_h^n, u_h^{n+1} - u_h^n) \\ + \mu(u_h^n) \int_0^1 (f(\tau u_h^{n+1} + (1-\tau)u_h^n), u_h^{n+1} - u_h^n)_\Omega d\tau \\ = 0. \end{aligned}$$

By using the identity $(a+b, a-b)_\Omega = (a^2 - b^2, 1)_\Omega$ and the bilinearity of a_h , we get

$$\begin{aligned} \frac{1}{\Delta t}(u_h^{n+1} - u_h^n, u_h^{n+1} - u_h^n)_\Omega + \mu(u_h^n) \int_0^1 (f(\tau u_h^{n+1} + (1-\tau)u_h^n), u_h^{n+1} - u_h^n)_\Omega d\tau \\ + \mu(u_h^n) \frac{1}{2} a_h(\epsilon^2; u_h^{n+1}, u_h^{n+1}) - \mu(u_h^n) \frac{1}{2} a_h(\epsilon^2; u_h^n, u_h^n) \\ = 0. \end{aligned} \tag{2.28}$$

Taylor expansions of F around u_h^n and u_h^{n+1} leads to

$$\begin{aligned} F(u_h^n) &\approx F(\tau u_h^{n+1} + (1-\tau)u_h^n) - f(\tau u_h^{n+1} + (1-\tau)u_h^n)(\tau(u_h^{n+1} - u_h^n)), \\ F(u_h^{n+1}) &\approx F(\tau u_h^{n+1} + (1-\tau)u_h^n) + f(\tau u_h^{n+1} + (1-\tau)u_h^n)(1-\tau)(u_h^{n+1} - u_h^n). \end{aligned}$$

Subtracting $F(u_h^n)$ from $F(u_h^{n+1})$ and ignoring higher order terms including the derivatives of f , we obtain

$$\begin{aligned} F(u_h^{n+1}) - F(u_h^n) &\approx f(\tau u_h^{n+1} + (1-\tau)u_h^n)(u_h^{n+1} - u_h^n) \\ (F(u_h^{n+1}), 1)_\Omega - (F(u_h^n), 1)_\Omega &\approx (f(\tau u_h^{n+1} + (1-\tau)u_h^n), u_h^{n+1} - u_h^n)_\Omega \tag{2.29} \\ \int_0^1 ((F(u_h^{n+1}), 1)_\Omega - (F(u_h^n), 1)_\Omega) d\tau &\approx \int_0^1 (f(\tau u_h^{n+1} + (1-\tau)u_h^n), u_h^{n+1} - u_h^n)_\Omega d\tau \\ (F(u_h^{n+1}), 1)_\Omega - (F(u_h^n), 1)_\Omega &\approx \int_0^1 (f(\tau u_h^{n+1} + (1-\tau)u_h^n), u_h^{n+1} - u_h^n)_\Omega d\tau \end{aligned}$$

We note that the bilinear form $a_h(\epsilon^2; u^{n+1}, u^{n+1})$ satisfies

$$\begin{aligned} a_h(\epsilon^2; u^{n+1}, u^{n+1}) &= \epsilon^2 \|\nabla u^{n+1}\|_{L^2(\Omega)}^2 - 2 \sum_{E \in E_h^0} \int_E \{\epsilon^2 \nabla u^{n+1}\} [u^{n+1}] ds \\ &+ \sum_{E \in E_h^0} \frac{\sigma \epsilon^2}{h_E} \|[u^{n+1}]\|_{L^2(E)}^2 \geq 0. \end{aligned} \quad (2.30)$$

Similar to previous case all the terms in (2.30) are non-negative (see [63, Sec. 2.7.1] for positivity of edge integral term). Then, we have $a_h(\epsilon^2; u^{n+1}, u^{n+1}) \geq 0$ and similarly $a_h(\epsilon^2; u^n, u^n) \geq 0$. Using these identities and substituting the last equation in (2.29) into (2.28) we obtain

$$\begin{aligned} \underbrace{-\frac{1}{\Delta t} \|u_h^{n+1} - u_h^n\|_{L^2(\Omega)}}_{\leq 0} &\approx \mu(u_h^n) \left((F(u_h^{n+1}), 1)_\Omega + \frac{1}{2} a_h(\epsilon^2; u_h^{n+1}, u_h^{n+1}) \right) \\ &- \mu(u_h^n) \left((F(u_h^n), 1)_\Omega + \frac{1}{2} a_h(\epsilon^2; u_h^n, u_h^n) \right), \\ \underbrace{-\frac{1}{\Delta t \mu(u_h^n)} \|u_h^{n+1} - u_h^n\|_{L^2(\Omega)}}_{\leq 0} &\approx (F(u_h^{n+1}), 1)_\Omega + \frac{1}{2} a_h(\epsilon^2; u_h^{n+1}, u_h^{n+1}) \\ &- (F(u_h^n), 1)_\Omega + \frac{1}{2} a_h(\epsilon^2; u_h^n, u_h^n), \\ &= \mathcal{E}(u_h^{n+1}) - \mathcal{E}(u_h^n), \end{aligned}$$

which implies that $\mathcal{E}(u_h^{n+1}) \leq \mathcal{E}(u_h^n)$, i.e., AVF discretized scheme is energy stable through the discrete energy (2.23).

2.5 Time Adaptivity with Average Vector Field (AVF) Method and Ripening Time

The solution of AC equation includes transition layers between stable equilibriums. The initial dynamics require small time steps as the transition layers are formed. Then, the metastable state is formed and during the metastable state, the dynamics changes not much, larger time steps are required. Moreover, these transition layers changes rapidly by crossing the zero axis with the time scale of evolution. At the moment where the solution crosses the zero axis, it takes its minimum or maximum value and this time is named as ripening time. To determine the ripening time arising from rapid changes in the solution, and steep gradients in transition layers the uniform time steps are inefficient as shown in [23, 81]. We use adaptive time stepping to resolve the multiple time dynamics of the AC equation. The time adaptivity is required a local error estimator. In our time adaptive algorithm (2.2), for local error estimation two discrete solutions u_τ, \hat{u}_τ of order $p+1$ and p are computed in parallel such that

$$u_\tau(\tau) = u(\tau) + O(\tau^{p+2}), \quad \hat{u}_\tau(\tau) = u(\tau) + O(\tau^{p+1}),$$

where τ denotes the time step Δt . Then

$$\hat{\epsilon}_\tau = \|u_\tau(\tau) - \hat{u}_\tau\| = C\tau^{p+1} \quad (2.31)$$

is an estimator of the actual $\hat{\epsilon}_\tau$ of \hat{u}_τ measured in an Euclidean norm [26]. In the next step, we search for the optimal step size τ^* satisfying $\hat{\epsilon}_{\tau^*} \leq \delta_{TOL}$, where δ_{TOL} denotes a user specified tolerance. By insertion of both τ and τ^* into (2.31), the estimation formula

$$\tau^* = \sqrt[p+1]{\frac{\rho\delta_{TOL}}{\hat{\epsilon}_\tau}}\tau$$

is obtained with a safety factor $\rho \approx 0.9$. Then, it is checked for $\hat{\epsilon}_{\tau^*} \leq \delta_{TOL}$. If it is satisfied, we accept the current time step τ^* and use in the next step; or else the current time step is rejected and the present step is repeated with the time step τ^* . In the successful case, the more accurate value $u_\tau(\tau)$ will be used to start the next step.

In our time adaptive algorithm, the backward Euler method and AVF method are chosen which are order of p and $p + 1$, respectively. When we let $\delta_{TOL} \rightarrow 0$ the ripening time estimates converge which matches the convergence of our solution to an accurate value. Moreover, it is expected that the required number of time steps follow $\frac{M(\delta_{TOL}/10)}{M(\delta_{TOL})} = \sqrt[p+1]{10}$, where p is the order of the method, and in our case $p = 1$. The decrease of δ_{TOL} by a factor of 10 leads to error $\epsilon_{old} = C\tau^{p+1}$. The new error will be $\epsilon_{new} = C(\nu\tau)^{p+1} = \nu^{p+1}C\tau^{p+1} = \nu^{p+1}\delta_{old}$ where ν is a constant. Therefore the time step size should be reduced by a factor $\sqrt[p+1]{10}$ to reduce the local error by a factor 10. The findings of this numerical method are presented in the following section.

2.6 Numerical Results

In this section, we give several numerical examples demonstrating the accuracy and stability of our numerical approach. In all numerical experiments, we have used linear elements for the space discretization. Only for the ripening time calculations, linear and quadratic elements are used for comparison.

2.6.1 1D AC equation with constant mobility function and double-well potential

We first consider 1D AC equation with constant mobility $\mu(u) = 1$, homogeneous Neumann boundary conditions in the domain $(x, t) \in [-1, 1] \times [0, 80]$ and with the initial condition [18]

$$u(x, 0) = 0.53x + 0.47 \sin(-1.5\pi x).$$

The diffusion constant $\epsilon^2 = 0.01$ is taken as in [18] where Fourier spectral elements method and Strang splitting method are used for space and time discretization respectively with mesh sizes $\Delta x = \Delta t = 0.02$. The time discretization is performed by backward Euler method and the mesh sizes are taken as $\Delta x = \Delta t = 0.01$. In Figure 2.3, the evolution of phase function and energy are given. The solutions of AC

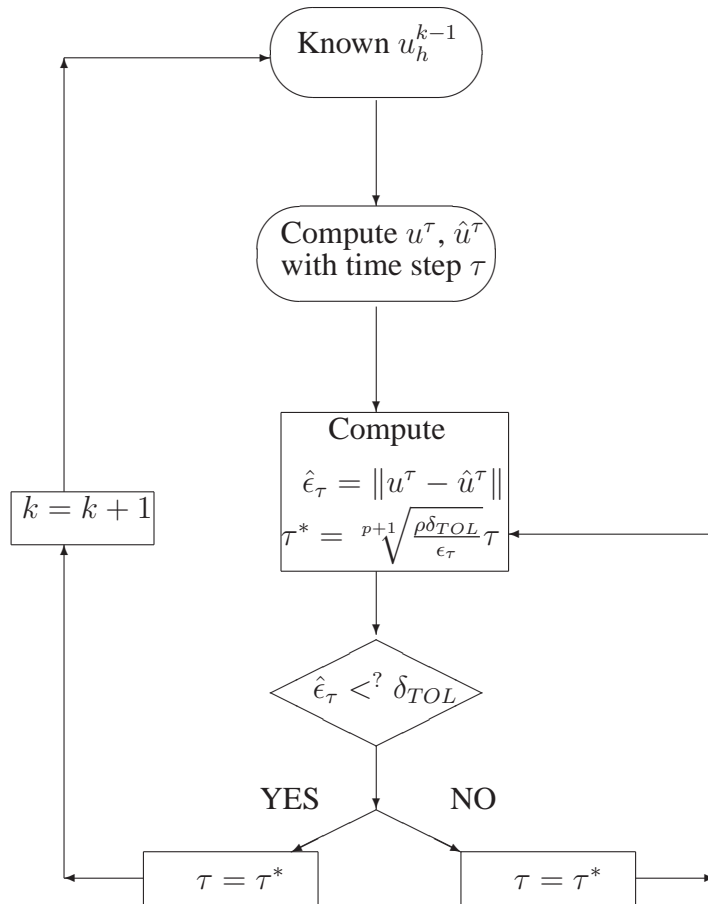


Figure 2.2: Time Adaptive strategy

equation move from one equilibrium to the other one, which is known as phase separation. The interfaces between two stable equilibria move over exponentially long times between the region, which is known as metastability phenomenon. The right plot in Figure 2.3 shows the phase separation and metastable state clearly. The state of phase function is reflected in monotonically decreasing numerical energy for both time discretization techniques. We have proven that backward Euler and AVF methods are unconditionally energy stable. Figure 2.4 shows the energy decrease for different time step sizes for both methods. It is clearly seen that both time integrators are energy stable independent of time step size.

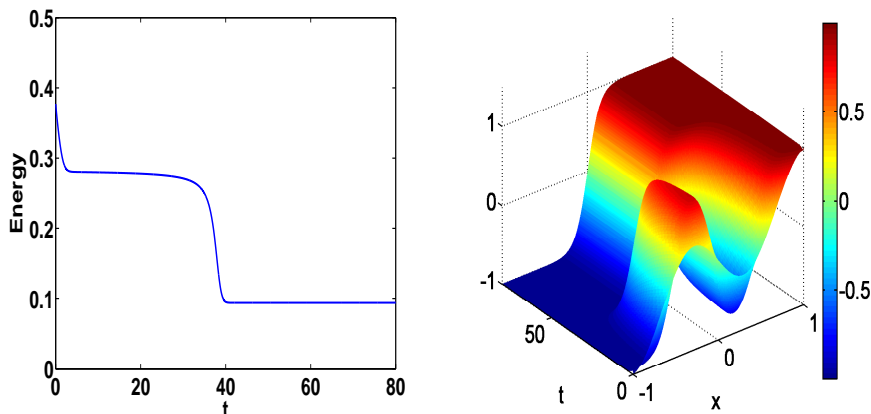


Figure 2.3: Example 2.6.1: evolution of phase function and decay of the numerical energy with backward Euler

2.6.2 1D AC equation with constant mobility function and double-well potential

We consider the 1D AC problem with constant mobility $\mu(u) = 1$, periodic boundary conditions and initial condition with diffusion constant $\epsilon = 0.12$ [81] in the domain $(x, t) \in [0, 2\pi] \times [0, 600]$

$$u(x, 0) = 0.8 + \sin(x).$$

Computations are done with the step sizes $\Delta x = \pi/50$ and $\Delta t = 0.01$ by AVF method. The same problem was solved in [81] again using Fourier spectral space discretization with the mesh size $\Delta x = \pi/64$ and with adaptive time integration using Backward Differential formula (BDF3)- Adams-Bashfort method (AB-3).

We see in Figure 2.5 the fast dynamics from the initial condition to the metastable state, where two transition layers are formed. Also, the numerical energy is decreasing monotonically.

For this problem, we also compute the ripening time given in Table 2.1. The calculations are done with linear and quadratic polynomials in space. The time adaptive algorithm is applied with initial time step size $\tau = 0.05$ and $\delta_{TOL} = 1e - 04$. We see that our solution converges to $T_r = 546.5$ as we expect. Also, the ratio of $M(\delta_{TOL})$ converges to $\sqrt[2]{10} = 3.1622$ which shows the reliability of our adaptive algorithm. In

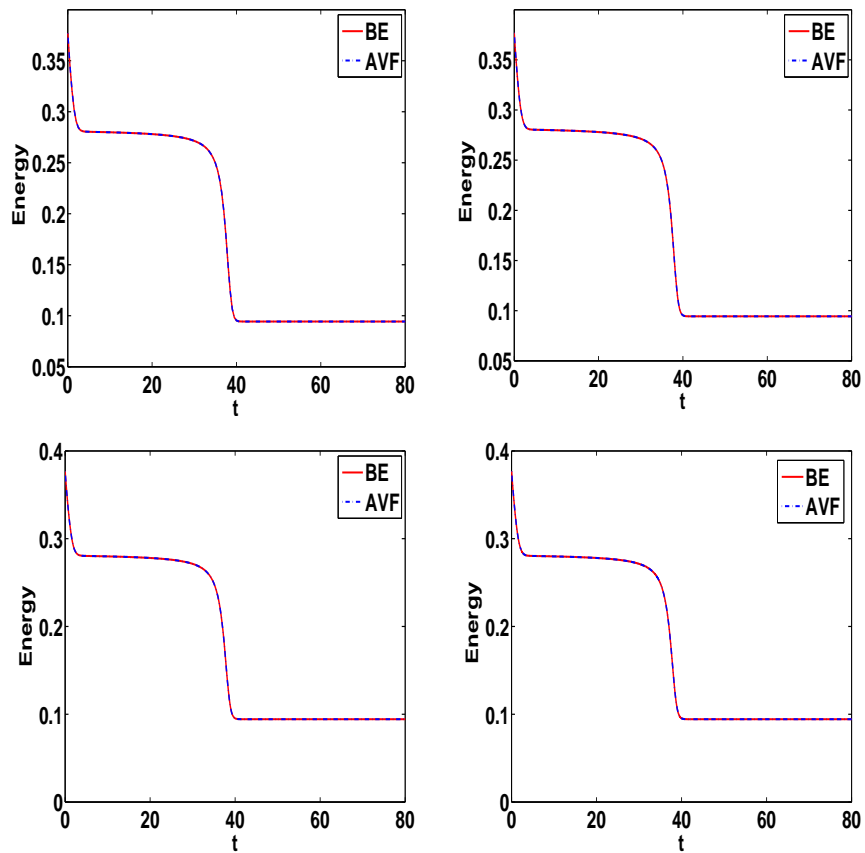


Figure 2.4: Example 2.6.1: decay of the numerical energy with backward Euler method and AVF method for different time steps: $\Delta t = 0.5$ (top left), $\Delta t = 0.25$ (top right), $\Delta t = 0.1$ (bottom left), $\Delta t = 0.01$ (bottom right)

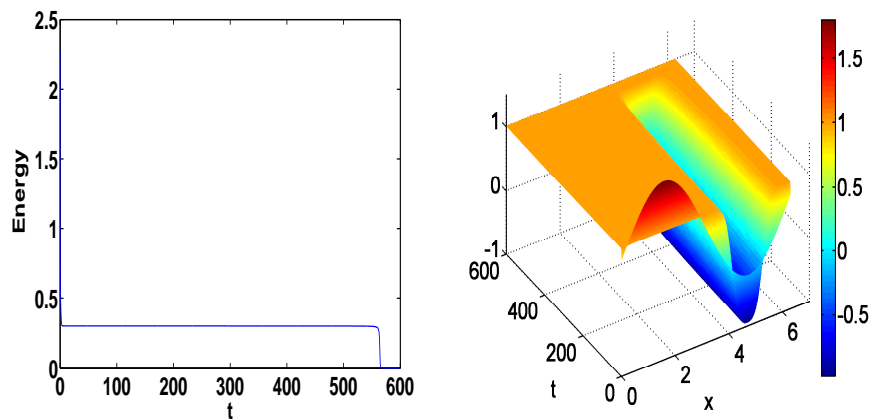


Figure 2.5: Example 2.6.2: evolution of phase function and decay of the numerical energy with AVF method

Figure 2.6, the time step size evolution is presented. We see rapid growth initially and step by step decline since the metastable state is finished.

Table 2.1: Example 2.6.2: Convergence of the ripening time with the adaptive AVF method using linear (quadratic) polynomials.

δ_{TOL}	Ripening Time	# Time Steps	$M(\delta_{TOL}^n)/M(\delta_{TOL}^{n-1})$
1e-04	549.52 (539.71)	480 (480)	3.02 (3.02)
1e-05	554.46 (544.54)	1515 (1515)	3.12 (3.16)
1e-06	555.99 (546.05)	4792 (4790)	3.16 (3.16)
1e-07	556.47 (546.52)	15153 (15152)	3.16 (3.16)

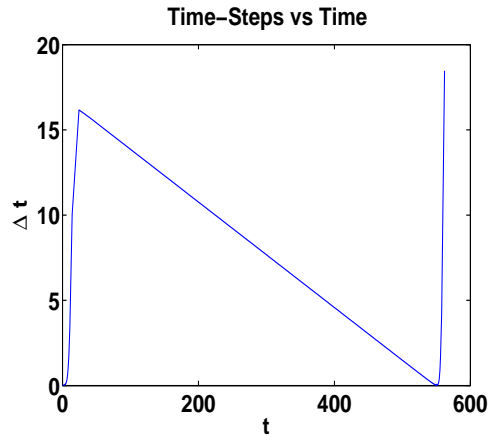


Figure 2.6: Example 2.6.2: evolution of time step sizes

2.6.3 2D AC equation with constant mobility function and double-well potential

2D AC equation with constant mobility $\mu(u) = 1$ under periodic boundary conditions and initial condition for the diffusion constant $\epsilon = 0.18$ in [81] in the domain $(x, y, t) \in [0, 2\pi]^2 \times [0, 33]$ is given as:

$$u(x, y, 0) = 2e^{\sin(x)+\sin(y)-2} + 2.2e^{-\sin(x)-\sin(y)-2} + 1.$$

We have taken as mesh size $\Delta x = \Delta y = \pi/8$ after three refinement steps in order to obtain accurate solutions. The solutions with contour plots are obtained for uniform time integration by average vector field (AVF) method with the step size $\Delta t = 0.01$. The evolution of phase solution at different time steps are shown in Figure 2.7. It is observed that the smaller region is annihilated prior to the larger region. Both reach the stable state of $u = -1$ at the end as we expect.

The ripening time for different tolerances with linear and quadratic polynomials is given in Table 2.2. The time adaptive algorithm is applied with initial time step size $\tau = 0.05$ and $\delta_{TOL} = 1e - 04$. We observe that the ripening time converges by decreasing tolerance and the ratio is close to the theoretical one $\sqrt[2]{10}$. The numerical energy is also decreasing for the adaptive time stepping in Figure 2.8 (left) and until formation of metastable state around $t = 30$, the small time steps are required. Afterward, time steps are increased 2.8 (right).

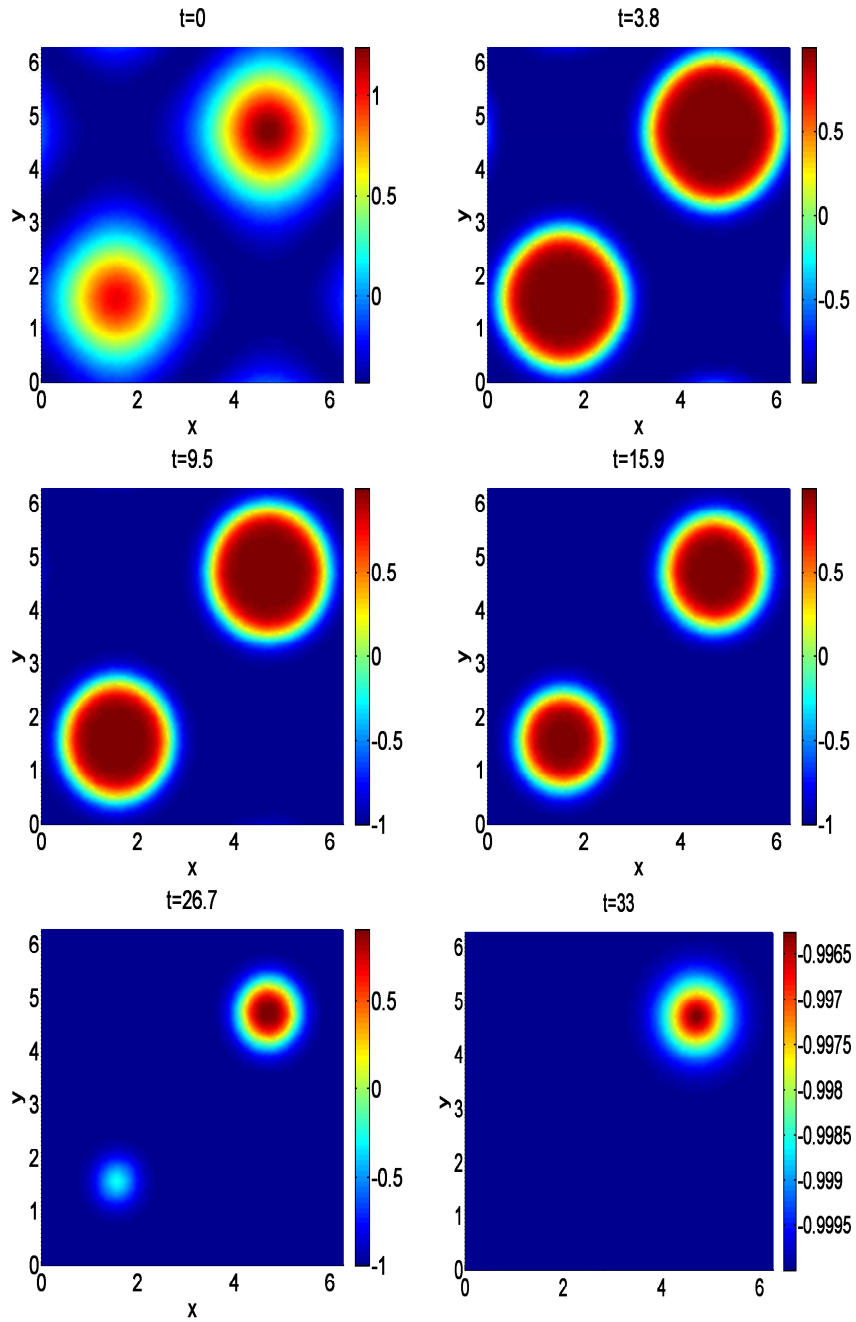


Figure 2.7: Example 2.6.3: evolution of phase function

2.6.4 2D AC with constant mobility function and double-well potential

We consider 2D AC equation with constant mobility $\mu(u) = 1$ under periodic boundary condition for diffusion constant $\epsilon = 0.1$ [39] in the domain $\Omega = [0, 2\pi] \times [0, 2\pi]$ for $0 < t < 0.5$

$$u_t - \epsilon^2 \Delta u + f(u) = g(x, y, t),$$

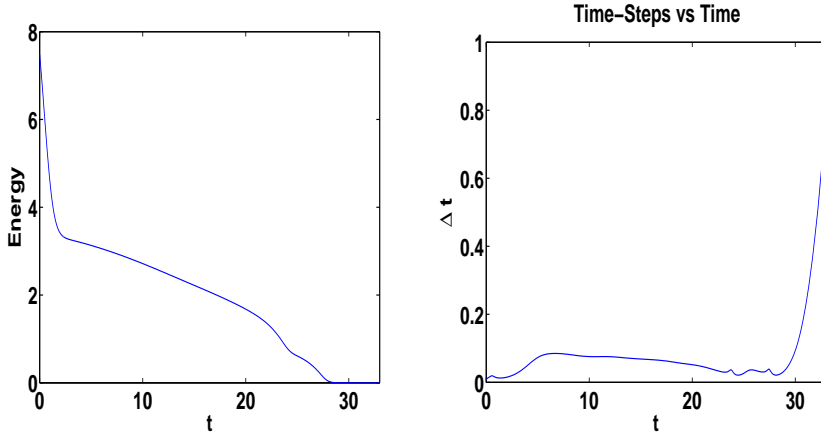


Figure 2.8: Example 2.6.3: decay of numerical energy (left) and evolution of time steps (right)

Table 2.2: Example 2.6.3: Convergence of the ripening time with adaptive AVF method using linear (quadratic) polynomials

δ_{TOL}	Ripening Time	# Time Steps	$M(\delta_{TOL}^n)/M(\delta_{TOL}^{n-1})$
1e-03	27.20 (30.10)	209 (216)	3.12 (3.13)
1e-04	27.33 (30.24)	668 (692)	3.20 (3.20)
1e-05	27.37 (30.25)	2121 (2197)	3.18 (3.17)
1e-06	27.37 (30.27)	6707 (6956)	3.16 (3.17)

with the exact solution $u(x, y, t) = e^{-2\epsilon^2 t} \sin(x) \sin(y)$. The source function g is computed from the left hand side using the exact solution. The initial condition is taken to be consistent with the exact solution. We present the L^2 error and the numerical order of accuracy for both time integrators in Table 2.3 at time $T = 0.5$. We can see that both methods with \mathbb{P}^k elements have the $(k + 1)$ -th order of accuracy.

2.6.5 2D AC with constant mobility function and double-well potential

We consider 2D AC equation with constant mobility $\mu(u) = 1$ under homogenous Dirichlet boundary condition [33] with diffusion constant $\epsilon = 0.01$ in the domain $\Omega = [0, 2\pi] \times [0, 2\pi]$ for $0 < t < 120$. We have taken the mesh size as $\Delta x = \Delta y = \pi/8$, and uniform time step $\Delta t = 0.1$ for AVF method. The initial condition is randomly distributed from -0.01 to 0.01 to each grid point. In Figure 2.9, the corresponding solution contours are plotted, the numerical energy is decreasing again monotonically.

2.6.6 2D AC equation with constant mobility function and logarithmic free energy

We consider the 2D AC equation with constant mobility $\mu(u) = 2$ [68] and diffusion constant is $\epsilon = 0.04$ subject to periodic boundary condition in the domain $\Omega = [0, 2\pi] \times$

Table 2.3: Accuracy test for AC equation with constant mobility for backward Euler method and AVF method $\Delta t = 0.03\Delta x$, $\Delta x = \pi$

	Mesh Size (Dof)	Backward Euler		Average Vector Field	
		L^2 -Error	Order	L^2 -Error	Order
\mathbb{P}^1	h(24)	1.605e+000	-	1.605e+000	-
	h/2(96)	4.595e-001	1.80	4.595e-001	1.80
	h/4(384)	1.225e-001	1.91	1.225e-001	1.91
	h/8(1536)	3.142e-002	1.96	3.115e-002	1.98
\mathbb{P}^2	h(48)	4.179e-001	-	4.179e-001	-
	h/2(192)	1.027e-001	2.02	1.027e-001	2.02
	h/4(768)	1.399e-002	2.88	1.400e-002	2.88
	h/8(3072)	2.300e-003	2.60	2.308e-003	2.60

$[0, 2\pi]$ for $0 < t < 10$. The logarithmic function $f(u) = \frac{\theta}{2} \ln\left(\frac{1+u}{1-u}\right) - \theta_c u$ is given. The initial condition is $u_0(x, 0) = 0.05(2 \times rand - 1)$ where 'rand' means a number in $[0, 1]$.

The spatial mesh size is taken as $\Delta x = \Delta y = \pi/8$. The snapshots of phase evolution is obtained with time adaptive algorithm for parameter values $\theta = 0.15, \theta_c = 0.30$ with time adaptive scheme. The initial time step size is $\tau = 0.05$ and $\delta_{TOL} = 4e - 03$. In Figure 2.11, the corresponding solution contours and numerical energy are plotted. It is clearly seen that the time adaptive solutions are in good agreement with the reference solutions in [68]. Figure 2.12 shows the progressively increase of time step based on the energy evolution of the solution. When the coarsening becomes dominant (for example $t > 1$), the time steps become larger which shows that time adaptivity works well.

2.6.7 2D AC with degenerate mobility function and logarithmic free energy

We consider the 2D AC equation with mobility function $\mu(u) = 2(1 - u^2)$ [68] with the diffusion constant $\epsilon = 0.04$ in the domain $\Omega = [0, 2\pi] \times [0, 2\pi]$ for $0 < t < 10$. The initial condition is $u_0(x, 0) = 0.05(2 \times rand - 1)$ where 'rand' means a number in $[0, 1]$.

The phase evolution is obtained for parameter values $\theta = 0.50, \theta_c = 0.95$ with time adaptive algorithm where the initial time step size is $\tau = 0.05$ and $\delta_{TOL} = 1e - 04$. In Figure 2.13, the corresponding solution contours are plotted, and the numerical energy decrease is seen clearly with time step evolution in Figure 2.14.

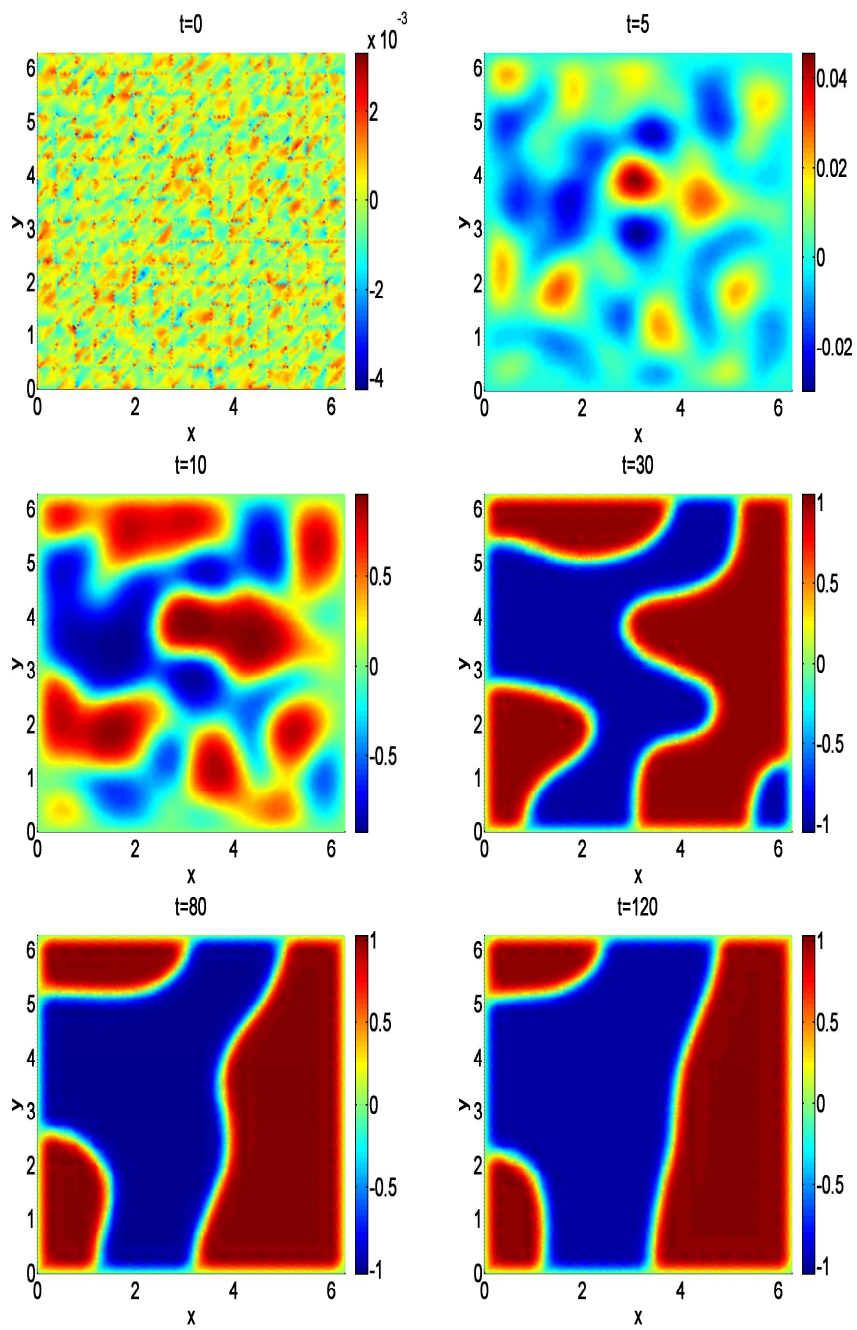


Figure 2.9: Example 2.6.5: evolution of phase function

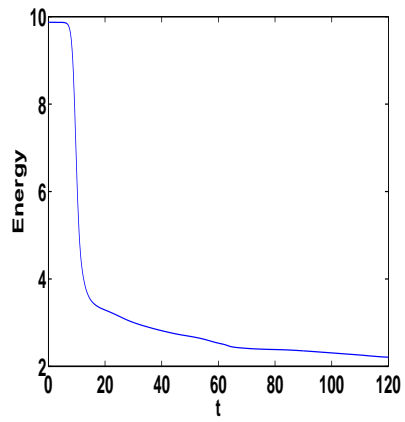


Figure 2.10: Example 2.6.5: decay of numerical energy

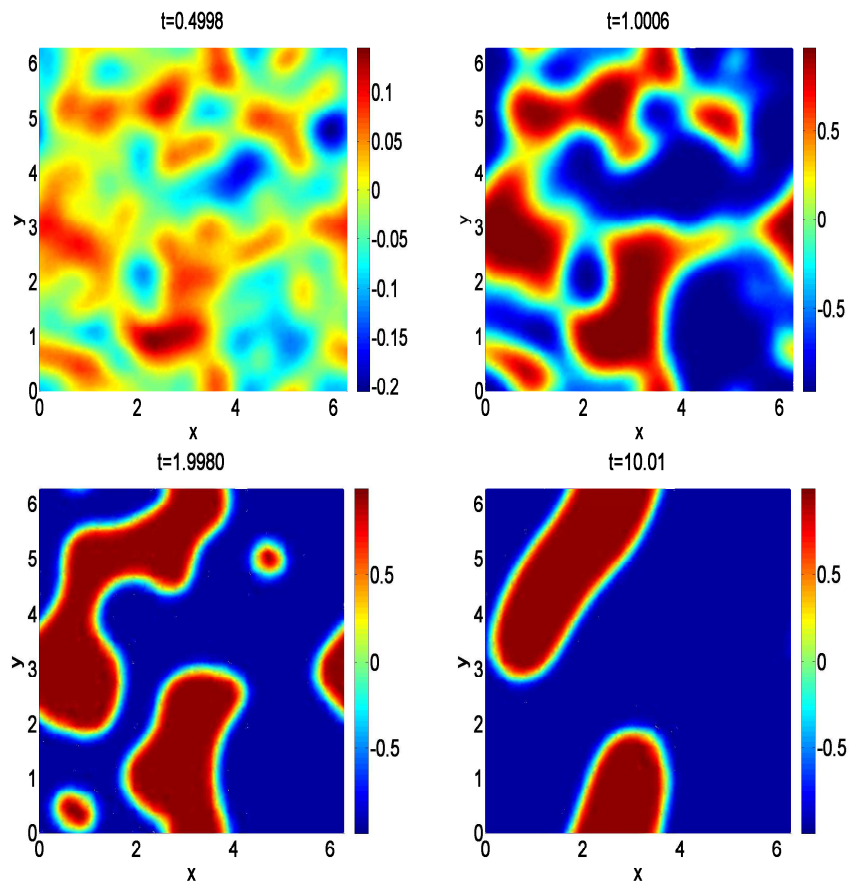


Figure 2.11: Example 2.6.6: evolution of phase function

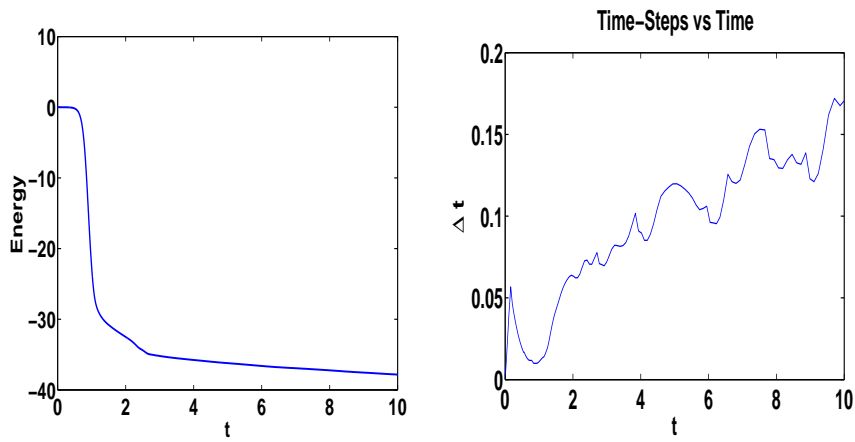


Figure 2.12: Example 2.6.6: decay of numerical energy (left) and evolution of time steps (right)

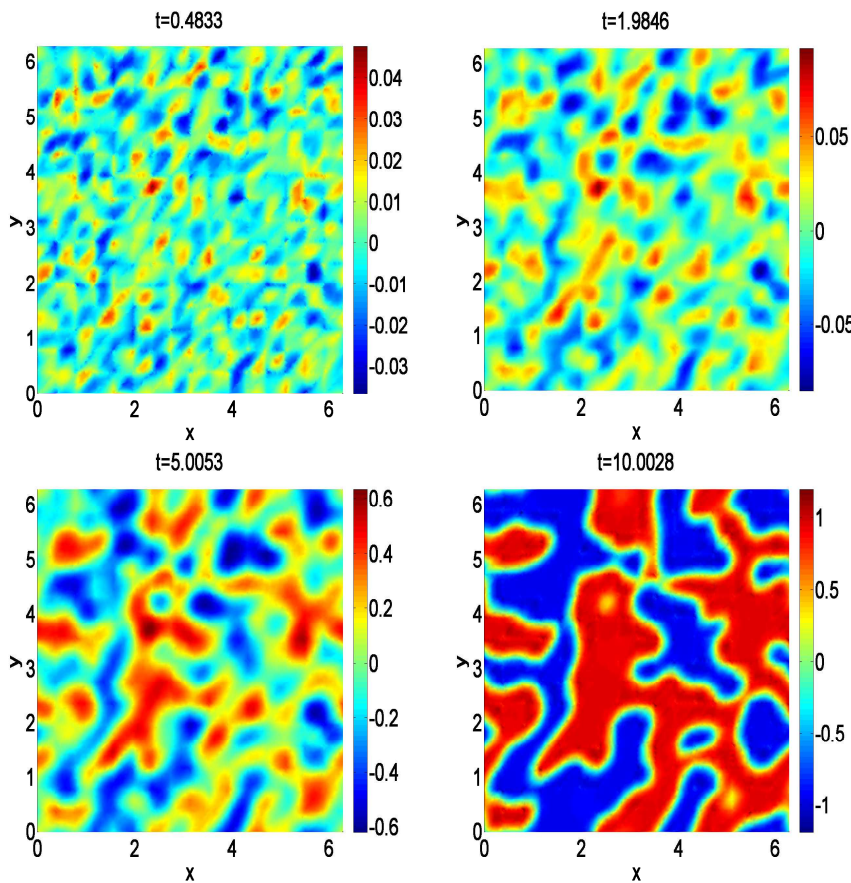


Figure 2.13: Example 2.6.7: evolution of solutions

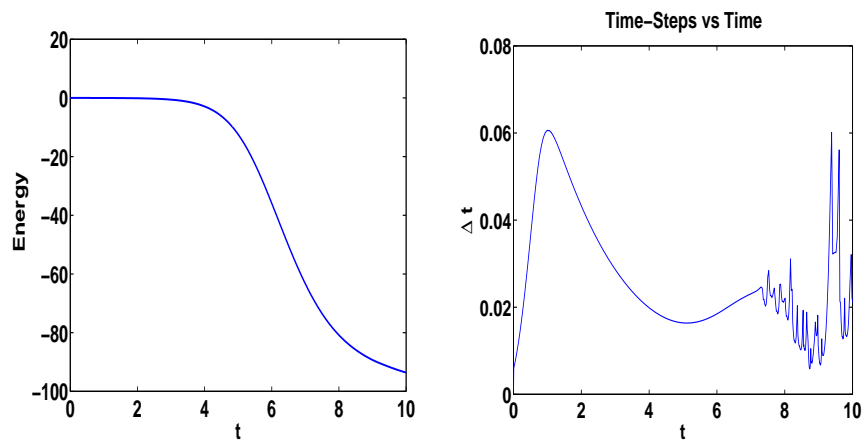


Figure 2.14: Example 2.6.7: decay of numerical energy (left) and evolution of time steps (right)

CHAPTER 3

THE CAHN-HILLIARD EQUATION

The CH equation is the most known model of phase separation. It was originally introduced by Cahn and Hilliard to describe the phase separation and coarsening phenomena in a binary alloy [16]. It is also used as diffuse interface model problem from different application areas, such as, image processing, planet formation and cancer growth. The fourth order CH equation in a bounded domain $\Omega \subset \mathbb{R}^d (d \leq 3)$ is given by,

$$\begin{aligned} u_t &= \nabla \cdot [\mu(u)\nabla(f(u) - \epsilon^2\Delta u)] + g(x, t), \quad \text{in } \Omega \times (0, T], \\ u(\mathbf{x}, 0) &= u_0 \quad \text{in } \Omega \times \{0\}, \end{aligned} \quad (3.1)$$

or, equivalently, the CH system [40, 71, 82]

$$\begin{aligned} u_t &= \nabla \cdot [\mu(u)\nabla w] + g(x, t), \quad \text{in } \Omega \times (0, T], \\ w &= -\epsilon^2\Delta u + f(u), \quad \text{in } \Omega \times (0, T], \\ u(\mathbf{x}, 0) &= u_0 \quad \text{in } \Omega \times \{0\}, \end{aligned} \quad (3.2)$$

with the suitable boundary conditions such as periodic boundary condition ([40]) and homogenous Neumann ([11, 48]) or Dirichlet boundary condition ([53]). In the CH equation u represents a relative concentration of one component in the binary mixture, the parameter ϵ is related to the width of inter-facial layer, $\mu(u)$ is the non negative mobility function, w is the chemical potential and $f(u) = F'(u)$ is the homogenous free energy in the Ginzburg-Landau energy functional in H^{-1}

$$\mathcal{E}(u) = \int_{\Omega} \left(\frac{\epsilon^2}{2} |\nabla u|^2 + F(u) \right) dx. \quad (3.3)$$

In the literature, the free energy function $F(u)$ is modeled in two different ways for CH equation. The first one is a combination of logarithmic terms stated as logarithmic free energy function and resulting in different forms in the literature

- [9, 11, 83]

$$F(u) = \frac{\theta_c}{2}(1 - u^2) + \frac{\theta}{2} [(1 + u) \ln(1 + u) + (1 - u) \ln(1 - u)], \quad (3.4)$$

- [12]

$$F(u) = \frac{\theta}{2} [(1 + u) \ln(1 + u) + (1 - u) \ln(1 - u)] - \frac{\theta_c}{2} u^2, \quad (3.5)$$

- [40, 79]

$$F(u) = \frac{\theta}{2} [u \ln u + (1 - u) \ln(1 - u)] - \frac{\theta_c}{2} u^2, \quad (3.6)$$

where θ is the absolute temperature θ_c is the transition temperature with $0 < \theta \leq \theta_c$. Note that the logarithmic free energy function is a non-convex function. The second one is the convex double well energy function

$$F(u) = \frac{(1 - u^2)^2}{4}, \quad (3.7)$$

which is the approximation of logarithmic free energy (3.4),(3.5),(3.6) in case the absolute temperature θ is close to transition temperature θ_c . It is easy to see that double-well energy function will favor two phases with densities $u = \pm 1$. The linear term in double well potential is responsible for the interesting dynamics including the instability of constant solutions near $u = 0$ and the nonlinear term is the one which mainly stabilizes the flow. In logarithmic free energy function, the logarithmic terms describe the entropy of mixture and the condition $\theta < \theta_c$ ensures that $F(u)$ has indeed double well form. Both logarithmic free energy functions (3.4), (3.5), (3.6) and double energy function (3.7) satisfy the monotonicity and Lipschitz continuity conditions for $u_1, u_2 \in \mathbb{R}$ with the constraints $|u_{1,2}| \leq 1$ [75]

$$\begin{aligned} (f(u_1) - f(u_2))(u_1 - u_2) &\geq -C_1(u_1 - u_2)^2, \\ |f(u_1) - f(u_2)| &\leq L_f |u_1 - u_2|, \\ |f'(u_1) - f'(u_2)| &\leq L_{f'} |u_1 - u_2|, \end{aligned} \quad (3.8)$$

for $C_1, L_f, L_{f'} \geq 0$ stand for the related Lipschitz constants.

The mobility function $\mu(u)$ can be constant or degenerate. In most of the studies on the CH equation mobility function $\mu(u)$ is assumed to be constant. However, the original derivation of CH equation includes degenerate mobility. Although the CH equation has been intensively studied, little mathematical analysis has been done for degenerate mobility. The CH equation with degenerate mobility was introduced in [28] and existence of the solutions are given. The commonly adapted versions of the degenerate mobility function are $\mu(u) = \beta u(1 - u)$ [40, 79] and $\mu(u) = \beta(1 - u^2)$ [9, 11, 40, 82]. The first representation of mobility function reduces the long range diffusion throughout bulk regions. This is a good choice when fluid flows with immiscible components are studied. The second representation is the most common one and thermodynamically reasonable choice as well as the first representation. By these representations the diffusion process is restricted to the interface zone, i.e. it is

zero in the pure component (i.e., when $u = \pm 1$) and the mobility function should be positive for $|u| < 1$.

The CH model (3.1) has two important global properties. In contrast to AC equation, CH equation has mass conservation property, i.e., the total amount of phase in the region Ω is always equal to the given original amount :

$$\begin{aligned} \frac{d}{dt} \int_{\Omega} u(t) dx &= \int_{\Omega} u_t dx = \int_{\Omega} \nabla \cdot (\mu(u) \nabla w) dx \\ &= \int_{\partial\Omega} \mu(u) \nabla w \cdot \mathbf{n} dS = 0, \end{aligned} \quad (3.9)$$

where the no flux boundary condition (or periodic boundary condition) is applied [20, 40, 82].

CH equation has the dissipation of energy property similar to AC equation. Since the CH equation is a gradient flow of energy functional, the total energy is always non increasing, that is,

$$\begin{aligned} \frac{d}{dt} \mathcal{E}(u(t)) &= \mathcal{E}'(u)(u_t) = \int_{\Omega} f(u) u_t + \epsilon^2 \nabla u u_t = \int_{\Omega} w u_t \\ &= \int_{\Omega} w \nabla \cdot (\mu(u) \nabla w) = - \int_{\Omega} \mu(u) |\nabla w|^2 d\Omega. \end{aligned} \quad (3.10)$$

In the numerical solution of CH equation three main challenges appear; the non-linearity in the system coming from energy function, the presence of the parameter ϵ in the equations (usually small in phase separation applications) and the different time scales of each of the stages in the evolution of the concentration. Then, an efficient numerical resolution of the problem requires proper relation of numerical scales, that is, the spatial mesh size Δx and the time step size Δt .

It is also desirable to develop numerical schemes which are energy decreasing and mass conservative from numerical point of view. Energy stability implies that the total energy of the fully discretized CH equation dissipates in time analogously to the continuous energy (3.3). The schemes that preserve the discrete versions of the continuous energy lead to approximate solutions, which behave qualitatively similar to the continuous ones. Explicit methods are not suitable for time discretization of the CH equation because they are not energy stable and require very small time steps because of stability restrictions. Also the semi-discretization of the CH equation in space leads to stiff systems for small values of the diffusion parameter ϵ . Explicit methods will work with severe restriction on time steps, which increase the computational cost enormously. In the literature, mostly the CH equation with the constant mobility function is studied using finite differences [23], finite elements [12] and spectral methods [20, 43] for space discretization. Energy stable time discretization methods are based on the convex splitting of the energy functional. Alternatively, splitting methods are

used by adding stabilization terms to the energy functional $F(u)$. A recent survey of different space and time discretizations for the CH is given in [72]. CH equation with degenerate mobility is discretized by continuous finite elements [9, 11, 12], local discontinuous Galerkin method [82, 83], discontinuous Galerkin method with C^0 elements, with mixed finite elements [79], finite differences [51], NURSB [36] and by spectral methods [84].

In this chapter, we use the mass conservative SIPG method [5, 63] for the space discretization. Since the DG method is based on the set of piecewise polynomials that are fully discontinuous at the interfaces, the DGFEM approximation allows to capture the sharp gradients or singularities that affect the numerical solution locally. Furthermore, CH equation describes a gradient flow in H^{-1} and the semi-discretized form of it (3.1) leads to a gradient system of ordinary differential equations. Then, we again need energy stable time integrators. It is well known that the first order backward Euler method is energy stable, i.e., the discrete energy decreases without any restriction for the step size Δt for very stiff gradient systems with $\epsilon \rightarrow 0$ [41]. The discontinuous Galerkin-Petrov in time methods (with different trial and test functions) [66] and Gauss Radau IIA Runge-Kutta collocation methods [42] are the most known higher order energy decreasing methods with orders ≥ 3 . The only second order implicit energy stable method is the average vector field (AVF) method [17, 41] preserving energy decreasing property for the gradient systems and for systems with Lyapunov functions.

The reminder of this chapter is organized as follows: we first construct the SIPG discretization of CH equation with degenerate mobility for Dirichlet, Neumann and periodic boundary conditions in Section 3.1. In Section 3.2, time discretization with backward Euler and AVF method is given. Then, energy stability of both methods is proven in Section 3.3. We give several numerical examples in Section 3.4 to demonstrate the performance of the SIPG discretization coupled with structure preserving time integrators.

3.1 SIPG Discretization of Cahn-Hilliard Equation

In this section, we briefly describe the SIPG method discretization, applied to the diffusion part of the CH equation (3.2) for Dirichlet, Neumann and periodic boundary conditions. Using the definitions and notations from the previous chapter, the solution of (3.2) reads as: find $u_h(t), w_h(t) \in V_h$ such that for almost every $t \in (0, T]$ and for all $v \in V_h$,

$$\begin{aligned} (\partial_t u_h, v_h)_\Omega + a_h(\bar{\mu}; w_h, v_h) &= I_h(\bar{\mu}; v_h), \\ (w_h, v_h)_\Omega - (f(u_h), v_h)_\Omega &= a_h(\epsilon^2; u_h, v_h) + I_h(\epsilon^2; v_h). \end{aligned} \tag{3.11}$$

The bilinear terms in the last two argument is of the form $a_h(\kappa; w, v) = \tilde{a}_h(\kappa; w, v) + J_{1h}^\partial(\kappa; w, v)$ such that

$$\begin{aligned} \tilde{a}_h(\kappa; w, v) = & \sum_{E \in \mathcal{T}_h} \int_E \kappa \nabla w \cdot \nabla v - \sum_{e \in E_h^0} \int_e \{\kappa \nabla w\} \cdot [v] ds \\ & - \sum_{e \in E_h^0} \int_e \{\kappa \nabla v\} \cdot [w] + \sum_{e \in E_h^0} \frac{\sigma \kappa}{h_e} \int_e [w] \cdot [v] ds, \end{aligned} \quad (3.12)$$

where the mobility function $\mu(u)$ is computed explicitly as in form of the integral $\int_K \mu(u^n) d\Omega$, where u^n denotes the approximate solution at the previous time step n as for continuous finite elements in [9, 11]. In the DG discretized bilinear form (3.12) κ stands for $\bar{\mu} = \int_K \mu(u^n) d\Omega$ or for ϵ^2 . The the bilinear form $\tilde{a}_h(\kappa; u_h, v_h)$ includes the face integrals only on the interior edges, whereas the term $J_h^\partial(\kappa; u_h, v_h)$ includes the corresponding face integrals on the boundary edges and together with the right hand side $I_h(\kappa; v_h)$. So, it changes depending on the boundary conditions. If Dirichlet boundary condition, $u = w = g_D$, is prescribed, we set

$$\begin{aligned} J_h^\partial(\kappa; u, v) &= - \sum_{e \in E_h^D} \int_e \{\kappa \nabla u\} \cdot [v] ds - \sum_{e \in E_h^D} \int_e \{\kappa \nabla v\} \cdot [u] \\ &+ \sum_{e \in E_h^D} \frac{\sigma \kappa}{h_e} \int_e [u] \cdot [v] ds, \\ I_h(\kappa; v) &= \sum_{e \in E_h^D} \int_e \left(\frac{\sigma \kappa}{h_e} v - \kappa \nabla v \cdot \mathbf{n} \right) g_D ds. \end{aligned}$$

In the case of Neumann boundary condition, $\frac{\partial u}{\partial \mathbf{n}} = \mu(u) \frac{\partial w}{\partial \mathbf{n}} = g_N$, they become

$$J_h^\partial(\kappa; u, v) = 0, \quad I_h(\kappa; v) = \sum_{e \in E_h^N} \int_e g_N v ds.$$

When periodic boundary condition is applied, we have

$$\begin{aligned} J_h^\partial(\kappa; u, v) &= - \sum_{\omega \in E_h^{per}} \int_\omega \{\kappa \nabla u\}_\omega \cdot [v]_\omega ds - \sum_{\omega \in E_h^{per}} \int_\omega \{\kappa \nabla v\}_\omega \cdot [u]_\omega \\ &+ \sum_{\omega \in E_h^{per}} \frac{\sigma \kappa}{h_E} \int_\omega [u]_\omega \cdot [v]_\omega ds, \end{aligned}$$

and $I_h(v) = 0$.

The semi-discrete solutions $u_h(t)$ and $w_h(t)$ of the system (3.11) satisfy

$$u_h(t) = \sum_{m=1}^N \sum_{j=1}^{n_q} \xi_j^m(t) \varphi_j^m, \quad w_h(t) = \sum_{m=1}^N \sum_{j=1}^{n_q} \zeta_j^m(t) \varphi_j^m, \quad (3.13)$$

where φ_j^m are the basis functions spanning the space V_h , ξ_j^m and ζ_j^m are the unknown coefficients, n_q is the local dimension, and N is the number of triangular elements. By substituting the identities in (3.13) into the system (3.11) and choosing $v = \varphi_i^k$, $i = 1, \dots, n_q$, $k = 1, \dots, N$, we obtain the semi-linear systems of ordinary differential equations

$$\begin{aligned} M\xi_t + A_\mu\zeta &= L_1, \\ A_\epsilon\xi + r(\xi) - M\zeta &= L_2, \end{aligned} \quad (3.14)$$

for the ordered unknown coefficient vectors and the basis functions

$$\begin{aligned} \xi &= (\xi_1^1, \dots, \xi_{n_q}^1, \xi_1^2, \dots, \xi_{n_q}^2, \dots, \xi_1^N, \dots, \xi_{n_q}^N)^T, \\ \zeta &= (\zeta_1^1, \dots, \zeta_{n_q}^1, \zeta_1^2, \dots, \zeta_{n_q}^2, \dots, \zeta_1^N, \dots, \zeta_{n_q}^N)^T, \\ \varphi &= (\varphi_1^1, \dots, \varphi_{n_q}^1, \varphi_1^2, \dots, \varphi_{n_q}^2, \dots, \varphi_1^N, \dots, \varphi_{n_q}^N)^T. \end{aligned}$$

In (3.14), M denotes the mass matrix with the entries $M_{ij} = (\varphi^j, \varphi^i)_\Omega$, $1 \leq i, j \leq n_q \times N$, A_μ and A_ϵ are the stiffness matrices with the entries $(A_\mu)_{ij} = a_h(\mu(u_h); \varphi^j, \varphi^i)$ and $(A_\epsilon)_{ij} = a_h(\epsilon^2; \varphi^j, \varphi^i)$, $1 \leq i, j \leq n_q \times N$, and b is the non-linear vector of unknown coefficient vector ξ with the entries $b_i(\xi) = (\psi'(u_h), \varphi^i)_\Omega$, $1 \leq i \leq n_q \times N$, and L_1 and L_2 are the load vector i -th component of which corresponding to the right hand side linear form $I_h(\varphi^i)$, $1 \leq i \leq n_q \times N$ such that a detailed description of each term is given in previous section.

3.2 Fully Discrete System by Backward Euler and AVF Method

In this section, we give the fully discrete formulations of the CH system (3.2) in matrix-vector notations by using the backward Euler and AVF time integrators through the semi-discrete formulation (3.11).

In the sequel, we consider the uniform partition $0 = t_0 < t_1 < \dots < t_J = T$ of the time interval $[0, T]$ with the uniform time step-size $\Delta t = t_k - t_{k-1}$, $k = 1, 2, \dots, J$. Moreover, for $t = 0$, we let $u_h(0), w_h(0) \in V_h$ be the projections (orthogonal L^2 -projections) of the initial condition u_0, w_0 onto V_h , and we let $\eta_0 = (\xi_0, \zeta_0)^T$ be the corresponding coefficient vector (ordered) satisfying (3.13). At a specific time $t = t_n$, we denote the coefficient vector of the solutions $(u_h(t_n), w_h(t_n))^T$ by $\eta_n = (\xi_n, \zeta_n)^T$, as well.

3.2.1 Fully Discrete System by Backward Euler

Backward Euler discretization of the semi-linear system (3.14) reads as: for $n = 0, 1, \dots, J - 1$, solve for ξ_{n+1} and ζ_{n+1} the system

$$\begin{bmatrix} M & \Delta t A_\mu \\ A_\epsilon & -M \end{bmatrix} \begin{bmatrix} \xi_{n+1} \\ \zeta_{n+1} \end{bmatrix} + \begin{bmatrix} -\Delta t (L_1)_{n+1} \\ r(\xi_{n+1}) - (L_2)_{n+1} \end{bmatrix} = \begin{bmatrix} M\xi_n \\ 0 \end{bmatrix} \quad (3.15)$$

which leads to the residual function $R(\eta) = (R_1(\eta), R_2(\eta))^T$ with

$$\begin{aligned} R_1(\eta_{n+1}) &= M\xi_{n+1} - M\xi_n + \Delta t A_\mu \zeta_{n+1} - \Delta t (L_1)_{n+1}, \\ R_2(\eta_{n+1}) &= A_\epsilon \xi_{n+1} + r(\xi_{n+1}) - M\zeta_{n+1} - \Delta t (L_2)_{n+1}. \end{aligned} \quad (3.16)$$

We solve the non-linear system of equations (3.16) using the Newton's method in Algorithm 1 in Chapter 2: starting with an initial guess $\eta_{n+1}^{(0)} = (\xi_{n+1}^{(0)}, \zeta_{n+1}^{(0)})^T$, the k -th Newton iteration to solve the nonlinear system of equations (3.16) for the unknown vector $\eta_{n+1} = (\xi_{n+1}, \zeta_{n+1})^T$ reads as

$$J_S^{(k)} = -R(\eta_{n+1}^{(k)}), \quad \eta_{n+1}^{(k+1)} = \eta_{n+1}^{(k)} + s^{(k)}, \quad k = 0, 1, \dots \quad (3.17)$$

until a user defined tolerance is satisfied. In (3.17), $s = (s_1, s_2)^T$ is the increment, and J stands for the Jacobian matrix of $R(\eta_{n+1})$, whose entries are the partial derivatives with respect to ξ_{n+1} and ζ_{n+1}

$$J_{ij} = \left[\frac{\partial R_i(\xi_{n+1}, \zeta_{n+1})}{\partial (\xi_{n+1})_j} \quad \frac{\partial R_i(\xi_{n+1}, \zeta_{n+1})}{\partial (\zeta_{n+1})_j} \right], \quad i, j = 1, 2, \dots, n_q \times N$$

at the current iteration. It is easy to differentiate the linear terms in (3.16), to differentiate the nonlinear term using the expansion $u_h = \sum_{k=1}^{n_q \times N} \xi_k \varphi^k$, ordered version of (3.13), we obtain

$$\frac{\partial b_i(\xi)}{\partial \xi_j} = \frac{\partial}{\partial \xi_j} (f(u_h), \varphi^i)_\Omega = \int_\Omega f'(u_h) \varphi^j \varphi^i dx \quad (3.18)$$

such that $f(u)$ may be double well potential or logarithmic function. Hence, we obtain for the Jacobian matrix J

$$J = \begin{pmatrix} M & \Delta t A_\mu \\ A_\epsilon + J_r & -M \end{pmatrix} \quad (3.19)$$

where J_r is the Jacobian matrix of the nonlinear form $r(\xi)$ w.r.t. ξ at $\xi = \xi_{n+1}$.

3.2.2 Fully Discrete System by Average Vector Field Method

Firstly, we rearrange the semi linear system (3.14) for $\eta = (\xi, \zeta)$:

$$\begin{bmatrix} M & 0 \\ 0 & 0 \end{bmatrix} \eta_t = - \begin{bmatrix} 0 & A_\mu \\ A_\epsilon & -M \end{bmatrix} \eta + \begin{bmatrix} L_1 \\ L_2 - r(\eta) \end{bmatrix} \quad (3.20)$$

and then applying AVF method to the gradient system (3.20) reads as: for $n = 0, 1, \dots, J-1$, solve

$$\begin{aligned} \begin{bmatrix} M & 0 \\ 0 & 0 \end{bmatrix} \frac{\eta_{n+1} - \eta_n}{\Delta t} &= - \begin{bmatrix} 0 & A_\mu \\ A_\epsilon & -M \end{bmatrix} \int_0^1 (\tau \eta_{n+1} + (1 - \tau) \eta_n) d\tau \\ &+ \begin{bmatrix} \int_0^1 L_1 d\tau \\ L_2 - \int_0^1 (r(\tau \xi_{n+1} + (1 - \tau) \xi_n)) d\tau \end{bmatrix}. \end{aligned} \quad (3.21)$$

After a simple calculation for the linear terms, we get

$$\begin{aligned} \begin{bmatrix} M & 0 \\ 0 & 0 \end{bmatrix} \frac{\eta_{n+1} - \eta_n}{\Delta t} &= - \begin{bmatrix} 0 & A_\mu \\ A_\epsilon & -M \end{bmatrix} \frac{\eta_{n+1} + \eta_n}{2} \\ &+ \begin{bmatrix} \frac{1}{2}((L_1)_{n+1} + (L_1)_n) \\ \frac{1}{2}((L_2)_{n+1} + (L_2)_n - \int_0^1 r(\tau\xi_{n+1} + (1-\tau)\xi_n)d\tau) \end{bmatrix} \end{aligned} \quad (3.22)$$

which is the fully discretized system that we will solve for $\eta_{n+1} = (\xi_{n+1}, \zeta_{n+1})$. We solve this nonlinear system of equations using Newton's method in Algorithm 1 in Chapter 2. From the algebraic point of view, Newton's method for (3.22) corresponds to solving the nonlinear system of equations

$$\begin{aligned} R_1(\xi_{n+1}, \zeta_{n+1}) &= M(\xi_{n+1} - \xi_n) + \frac{\Delta t}{2} A_\mu(\zeta_{n+1} + \zeta_n) \\ &- \frac{\Delta t}{2} ((L_1)_{n+1} + L_1)_n, \end{aligned} \quad (3.23)$$

$$\begin{aligned} R_2(\xi_{n+1}, \zeta_{n+1}) &= \frac{1}{2} A_\epsilon(\xi_{n+1} + \xi_n) - \frac{1}{2} M(\zeta_{n+1} + \zeta_n) \\ &+ \int_0^1 r(\tau\xi_{n+1} + (1-\tau)\xi_n) - \frac{1}{2} ((L_2)_{n+1} + L_2)_n, \end{aligned} \quad (3.24)$$

or equivalently,

$$R(\eta_{n+1}) = \begin{bmatrix} M(\xi_{n+1} - \xi_n) + \frac{\Delta t}{2} A_\mu(\zeta_{n+1} + \zeta_n) - \frac{\Delta t}{2} ((L_1)_{n+1} + (L_1)_n) \\ \frac{1}{2} A_\epsilon(\xi_{n+1} + \xi_n) - \frac{1}{2} M(\zeta_{n+1} + \zeta_n) \\ + \int_0^1 r(\tau\xi_{n+1} + (1-\tau)\xi_n) - \frac{\Delta t}{2} ((L_2)_{n+1} + (L_2)_n) \end{bmatrix} \quad (3.25)$$

where $\eta_{n+1} = (\xi_{n+1}, \zeta_{n+1})$. Starting with an initial guess $\eta_{n+1}^{(0)} = (\xi_{n+1}^{(0)}, \zeta_{n+1}^{(0)})$, the k -th Newton iteration to solve the nonlinear equation (3.23) for the unknown vector η_{n+1} reads as

$$J_S^{(k)} = -R(\eta_{n+1}^{(k)}), \quad \eta_{n+1}^{(k+1)} = \eta_{n+1}^{(k)} + s^{(k)}, \quad k = 0, 1, \dots \quad (3.26)$$

until a user defined tolerance is satisfied. In (3.26), $s = (s_1, s_2)^T$ is the increment, J stands for the Jacobian matrix of $R(\eta_{n+1})$, whose entries are the partial derivatives with respect to ξ_{n+1} and ζ_{n+1}

$$J_{ij} = \left[\frac{\partial R_i(\xi_{n+1}, \zeta_{n+1})}{\partial (\xi_{n+1})_j}, \frac{\partial R_i(\xi_{n+1}, \zeta_{n+1})}{\partial (\zeta_{n+1})_j} \right], \quad i, j = 1, 2, \dots, n_q \times N$$

at the current iteration. It is easy to differentiate the linear terms in (3.23)

$$\begin{aligned} \frac{\partial R_1(\eta_{n+1})_i}{\partial (\xi_{n+1})_j} &= M_{ij}, \\ \frac{\partial R_1(\eta_{n+1})_i}{\partial (\zeta_{n+1})_j} &= \frac{\Delta t}{2} (A_\mu)_{ij}, \\ \frac{\partial R_2(\eta_{n+1})_i}{\partial (\xi_{n+1})_j} &= \frac{1}{2} (A_\epsilon)_{ij} + \frac{\partial r_i}{\partial (\xi_{n+1})_j}(\xi_{n+1}), \\ \frac{\partial R_2(\eta_{n+1})_i}{\partial (\xi_{n+1})_j} &= -\frac{1}{2} M_{ij}. \end{aligned} \quad (3.27)$$

To differentiate the nonlinear term using the expansion $u_h = \sum_{k=1}^{n_q \times N} \xi_k \varphi^k$, ordered version of (3.13), we obtain

$$\begin{aligned} \frac{\partial r_i(\xi)}{\partial \xi_j} &= \frac{\partial}{\partial \xi_j} (f(u_h), \varphi^i)_\Omega, \quad i, j = 1, 2, \dots, n_q \times N \\ &= \int_\Omega f'(u_h) \varphi^j \varphi^i dx \end{aligned} \quad (3.28)$$

where $f(u)$ is logarithmic free energy or double-well potential in our model. Hence, we obtain for the Jacobien matrix J that

$$J = \begin{pmatrix} M & \frac{\Delta t}{2} A_\mu \\ \frac{1}{2} A_\epsilon + J_r & -\frac{1}{2} M \end{pmatrix} \quad (3.29)$$

where $J_r(\xi_{n+1}^{(k+1)})$ is the differential matrix whose entries given in (3.28).

3.3 Energy Stability

In this section, we show that the backward Euler and AVF methods applied to the semi-discrete system (3.11) are energy stable through the discrete energy

$$\begin{aligned} \mathcal{E}_{DG}^h(u^n) &= \frac{\epsilon^2}{2} \|\nabla u^n\|_{L^2(\mathcal{T}_h)}^2 + (F(u^n), 1)_\Omega \\ &+ \sum_{E \in E_h^0} \left(-(\{\epsilon^2 \partial_n u^n\}, [u^n])_E + \frac{\sigma \epsilon^2}{2h_E} ([u^n], [u^n])_E \right) \end{aligned} \quad (3.30)$$

which is the discrete DG counterpart of the continuous energy [31]

$$\begin{aligned} \mathcal{E}^h(u) &= \frac{\epsilon^2}{2} \|\nabla u\|_{L^2(\mathcal{T}_h)}^2 + \sum_{E \in E_h^0} \left(-(\{\epsilon^2 \partial_n u\}, [u])_E + \frac{\sigma \epsilon^2}{2h_e} ([u], [u])_E \right) \\ &+ (F(u), 1)_\Omega \end{aligned} \quad (3.31)$$

at a time $t^n = n\Delta t$.

3.3.1 Energy Stability of Fully Discrete Scheme with Backward Euler

The backward Euler discretized scheme of the semi-discrete system (3.11) is given by

$$\begin{aligned} (u^{n+1} - u^n, q)_\Omega + \Delta t a_h(\mu(u^n); w^{n+1}, q) &= 0, \quad \forall q \in V_h, \\ (w^{n+1}, \phi)_\Omega - (f(u^{n+1}), \phi)_\Omega &= a_h(\epsilon^2; u^{n+1}, \phi), \quad \forall \phi \in V_h. \end{aligned} \quad (3.32)$$

Taking $q = w^{n+1}$ and $\phi = u^{n+1} - u^n$ in (3.32), we obtain

$$\begin{aligned} (u^{n+1} - u^n, w^{n+1})_\Omega + \Delta t a_h(\mu(u^n); w^{n+1}, w^{n+1}) &= 0, \\ (w^{n+1}, u^{n+1} - u^n)_\Omega - (f(u^{n+1}), u^{n+1} - u^n)_\Omega &= a_h(\epsilon^2; u^{n+1}, u^{n+1} - u^n). \end{aligned}$$

Using the identity $(a, a - b)_\Omega = \frac{1}{2}(a^2 - b^2 + (a - b)^2, 1)_\Omega$ and the bilinearity of a_h in the last two arguments, we obtain

$$(u^{n+1} - u^n, w^{n+1})_\Omega + \Delta t a_h(\mu(u^n); w^{n+1}, w^{n+1}) = 0, \quad (3.33)$$

$$\begin{aligned} (w^{n+1}, u^{n+1} - u^n)_\Omega - (f(u^{n+1}), u^{n+1} - u^n)_\Omega &= \frac{1}{2} a_h(\epsilon^2; u^{n+1}, u^{n+1}) \\ &\quad - \frac{1}{2} a_h(\epsilon^2; u^n, u^n) \\ &\quad + \frac{1}{2} a_h(\epsilon^2; u^{n+1} - u^n, u^{n+1} - u^n). \end{aligned} \quad (3.34)$$

Expanding $F(u^{n+1})$ and neglecting higher order terms, we get

$$\begin{aligned} F(u^n) &\approx F(u^{n+1}) - f(u^{n+1})(u^{n+1} - u^n), \\ (f(u^{n+1}), u^{n+1} - u^n)_\Omega &\approx (F(u^{n+1}), 1)_\Omega - (F(u^n), 1)_\Omega. \end{aligned} \quad (3.35)$$

We note that the bilinear form $a_h(\mu(u^n); w^{n+1}, w^{n+1})$ satisfies

$$\begin{aligned} a_h(\mu(u^n); w^{n+1}, w^{n+1}) &= \mu(u^n) \|\nabla w^{n+1}\|_{L^2(\Omega)}^2 - 2 \sum_{E \in E_h^0} \int_E \{\mu(u^n) \nabla w^{n+1}\} [w^{n+1}] ds, \\ &\quad + \sum_{E \in E_h^0} \frac{\sigma \mu(u^n)}{h_E} \|[w^{n+1}]\|_{L^2(E)}^2 \geq 0. \end{aligned} \quad (3.36)$$

Since all the terms in (3.36) are non-negative (see [63, Sec. 2.7.1] for positivity of edge integral term), we have $a_h(\mu; w^{n+1}, w^{n+1}) \geq 0$. Similarly, we have $a_h(\epsilon^2; u^{n+1} - u^n, u^{n+1} - u^n) \geq 0$. Using these identities, subtracting (3.33) from (3.34) and substituting (3.35), we obtain

$$\begin{aligned} -\Delta t a_h(\mu(u^n); w^{n+1}, w^{n+1}) &\approx (F(u^{n+1}), 1)_\Omega + \frac{1}{2} a_h(\epsilon^2; u^{n+1}, u^{n+1}) \\ &\quad - \left((F(u^n), 1)_\Omega + \frac{1}{2} a_h(\epsilon^2; u^n, u^n) \right) \\ &\leq 0 \end{aligned}$$

which implies that $\mathcal{E}_{DG}^h(u^{n+1}) \leq \mathcal{E}_{DG}^h(u^n)$. Hence, the backward Euler discretized scheme is energy stable through the discrete energy (3.30).

3.3.2 Energy Stability of Fully Discrete Scheme with AVF Method

Applying the AVF to the semi-discrete system (3.11), the fully discrete system reads as

$$\begin{aligned} (u^{n+1} - u^n, q)_\Omega + \frac{\Delta t}{2} a_h(\mu(u^n); w^{n+1} + w^n, q) &= 0, \quad \forall q \in V_h, \\ \left(\frac{w^{n+1} + w^n}{2}, \phi \right)_\Omega - \int_0^1 (f(\tau u^{n+1} + (1 - \tau)u^n), \phi)_\Omega d\tau &= \frac{1}{2} a_h(\epsilon^2; u^{n+1} + u^n, \phi), \quad \forall \phi \in V_h, \end{aligned} \quad (3.37)$$

Taking $q = (w^{n+1} + w^n)/2$ and $\phi = u^{n+1} - u^n$ in (3.37), we obtain

$$\begin{aligned} \left(u^{n+1} - u^n, \frac{w^{n+1} + w^n}{2} \right)_{\Omega} + \frac{\Delta t}{4} a_h(\mu(u^n); w^{n+1} + w^n, w^{n+1} + w^n) &= 0, \\ \left(\frac{w^{n+1} + w^n}{2}, u^{n+1} - u^n \right)_{\Omega} - \int_0^1 (f(\tau u^{n+1} + (1-\tau)u^n), u^{n+1} - u^n)_{\Omega} d\tau &= \\ & \frac{1}{2} a_h(\epsilon^2; u^{n+1} + u^n, u^{n+1} - u^n). \end{aligned}$$

By using the identity $(a + b, a - b)_{\Omega} = (a^2 - b^2, 1)_{\Omega}$ and the bilinearity of a_h in the last two arguments, we get

$$\left(u^{n+1} - u^n, \frac{w^{n+1} + w^n}{2} \right)_{\Omega} + \frac{\Delta t}{4} a_h(\mu(u^n); w^{n+1} + w^n, w^{n+1} + w^n) = 0, \quad (3.38)$$

$$\begin{aligned} \left(\frac{w^{n+1} + w^n}{2}, u^{n+1} - u^n \right)_{\Omega} - \int_0^1 (f(\tau u^{n+1} + (1-\tau)u^n), u^{n+1} - u^n)_{\Omega} d\tau &= \\ \frac{1}{2} a_h(\epsilon^2; u^{n+1}, u^{n+1}) - \frac{1}{2} a_h(\epsilon^2; u^n, u^n). \end{aligned} \quad (3.39)$$

Expanding the terms $F(u^n)$ and $F(u^{n+1})$, and neglecting the higher order terms, we obtain

$$\begin{aligned} F(u^n) &\approx F(\tau u^{n+1} + (1-\tau)u^n) - f(\tau u^{n+1} + (1-\tau)u^n)(\tau(u^{n+1} - u^n)), \\ F(u^{n+1}) &\approx F(\tau u^{n+1} + (1-\tau)u^n) + f(\tau u^{n+1} + (1-\tau)u^n)(1-\tau)(u^{n+1} - u^n). \end{aligned}$$

Subtracting $F(u^n)$ from $F(u^{n+1})$ leads to

$$\begin{aligned} F(u^{n+1}) - F(u^n) &\approx f(\tau u^{n+1} + (1-\tau)u^n)(u^{n+1} - u^n) \\ (F(u^{n+1}), 1)_{\Omega} - (F(u^n), 1)_{\Omega} &\approx (f(\tau u^{n+1} + (1-\tau)u^n), u^{n+1} - u^n)_{\Omega} \end{aligned} \quad (3.40)$$

$$\begin{aligned} \int_0^1 ((F(u^{n+1}), 1)_{\Omega} - (F(u^n), 1)_{\Omega}) d\tau &\approx \int_0^1 (f(\tau u^{n+1} + (1-\tau)u^n), u^{n+1} - u^n)_{\Omega} d\tau \\ (F(u^{n+1}), 1)_{\Omega} - (F(u^n), 1)_{\Omega} &\approx \int_0^1 (f(\tau u^{n+1} + (1-\tau)u^n), u^{n+1} - u^n)_{\Omega} d\tau \end{aligned}$$

We note that $a_h(\mu(u^n); w^{n+1} + w^n, w^{n+1} + w^n) \geq 0$ similar to previous section. Using this identity and subtracting (3.38) from (3.39) and substituting the last equation in(3.40), we obtain

$$\begin{aligned} -\frac{\Delta t}{4} a_h(\mu(u^n); w^{n+1} + w^n, w^{n+1} + w^n) &\approx (F(u^{n+1}), 1)_{\Omega} + \frac{1}{2} a_h(\epsilon^2; u^{n+1}, u^{n+1}) \\ & - \left((F(u^n), 1)_{\Omega} + \frac{1}{2} a_h(\epsilon^2; u^n, u^n) \right) \\ & \leq 0 \end{aligned}$$

which implies that $\mathcal{E}_{DG}^h(u^{n+1}) \leq \mathcal{E}_{DG}^h(u^n)$. Hence, the AVF discretized scheme is unconditionally energy stable.

3.4 Numerical Results

In this section, we present a set of numerical examples that show the accuracy and the stability of our numerical approach. We first verify the accuracy of our numerical approach for CH equation with constant and degenerate mobility for both time integrators. Furthermore, the discrete energy dissipation and discrete mass conservation properties of CH equation is demonstrated. In all numerical examples, we have used quadratic elements for space discretization and average vector field method is used for time discretization.

3.4.1 Constant mobility function and double-well potential under Neumann boundary condition

We first carry out 2D CH equation with constant mobility function $\mu(u) = 1$ under homogenous Neumann boundary condition [20]. The CH equation in $\Omega = [-1, 1] \times [-1, 1]$ for $0 < t < 1$ with the exact solution

$$u(x, y, t) = e^{\cos(t)} \cos(\pi x) \cos(\pi y)$$

is considered. The source function g is computed from the left hand side by using the exact solution and $\epsilon = 0.1$. The initial condition is taken to be consistent with the exact solution. The L^2 error and the numerical order of accuracy using time steps $\Delta t = 0.5\Delta x$ at time $T = 1$ with linear and quadratic DG polynomials are presented in Table 3.1. We can see that both methods with \mathbb{P}^k elements give a $(k + 1)$ -th order of accuracy.

Table 3.1: Example 3.4.1: Accuracy test with constant mobility for backward Euler and AVF methods

			Backward Euler		Average Vector Field	
	Δx	DoF	L^2 -Error	Order	L^2 -Error	Order
\mathbb{P}^1	1/2	24	1.871e+000	-	3.347e+000	-
	1/4	96	7.320e-001	1.35	1.633e+000	1.04
	1/8	384	2.035e-001	1.85	4.810e-001	1.76
	1/16	1536	4.797e-002	2.09	1.079e-001	2.16
\mathbb{P}^2	1/2	48	4.880e-001	-	6.694e-001	-
	1/4	192	1.428e-001	1.77	2.685e-001	1.32
	1/8	768	1.968e-002	2.86	3.376e-002	2.99
	1/16	3072	2.256e-003	3.12	3.733e-003	3.18

3.4.2 Degenerate mobility function and double-well potential under periodic boundary condition

The next example is the CH equation in [40] with exact solution

$$u(x, y, t) = e^{-2t} \sin(x) \sin(y)$$

in the domain $\Omega = [0, 2\pi] \times [0, 2\pi]$ for $0 < t < 1$ under periodic boundary condition with degenerate mobility function $\mu(u) = 1 - u^2$ and double-well potential. The effective diffusivity is taken as $\epsilon = 1$.

The L^2 -error and the numerical order of accuracy at time $T = 1$ for backward Euler method and AVF method are presented in Table 3.2 with linear and quadratic polynomials. For the first order DG polynomials we use time steps $\Delta t = 0.0032\pi$ and quadratic DG polynomials $\Delta t = 0.00032\pi$ with AVF method. Time steps are taken as $\Delta t = 0.00032\pi$ for linear DG polynomials and $\Delta t = 0.000032\pi$ for quadratic DG polynomials with backward Euler method. Order reduction is observed in Table 3.2 for the first and second order DG polynomial which be due to the non-linearity of the degenerate mobility function. Both methods with \mathbb{P}^k elements give a $(k + 1)$ -th order of accuracy.

Table 3.2: Example 3.4.2: Accuracy test with degenerate mobility for backward Euler and AVF methods

			Backward Euler		Average Vector Field	
	Δx	DoF	L^2 -Error	Order	L^2 -Error	Order
\mathbb{P}^1	$\pi/2$	24	1.620e+000	-	2.054e+000	-
	$\pi/4$	96	4.690e-001	1.79	5.742e-001	1.84
	$\pi/8$	384	1.294e-001	1.86	1.566e-001	1.87
	$\pi/16$	1536	3.308e-002	1.97	5.478e-002	1.52
\mathbb{P}^2	$\pi/2$	48	4.181e-001	-	4.342e-001	-
	$\pi/4$	192	1.040e-001	2.01	1.136e-001	1.93
	$\pi/8$	768	4.240e-002	1.29	1.713e-002	2.73
	$\pi/16$	3072	6.007e-002	-0.50	4.895e-003	1.81

3.4.3 Constant mobility function and double-well function under Neumann boundary condition: spinodal decomposition and nucleation

We consider 2D CH equation with constant mobility $\mu(u) = 1$ and double-well energy function under homogenous Neumann boundary condition [37]. The computational domain is taken $\Omega = [0, 1] \times [0, 1]$ for $0 < t < 0.4$ with $\epsilon = 1 \times 10^{-5}$.

This problem represents the two main separation mechanisms; spinodal decomposition and nucleation. Both mechanisms in the CH equation are defined by the initial condition $u_0(x) = \bar{u} + r$ where \bar{u} is a constant and r is random number uniformly distributed on $[-0.005, 0.005]$.

When $\bar{u} = 0$, the spinodal decomposition is formed in Figure (3.1). First, the mixture separates from a randomly perturbed homogeneous state ($\bar{u} = 0$), and then a complicated striped pattern that coarsens over time is produced. If we let the simulation evolve, the stationary solution would be a fully separated flow with two rectangular patches.

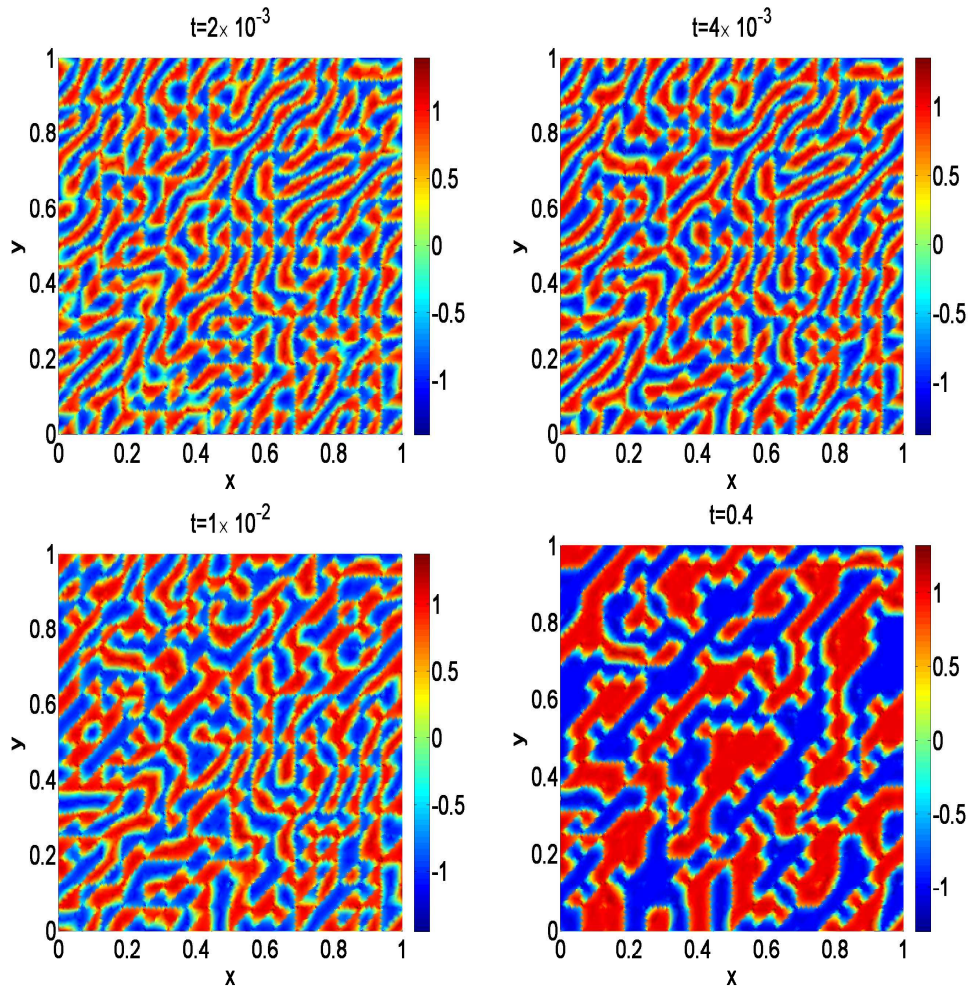


Figure 3.1: Example 3.4.3: Phase solution of 2D CH equation with constant mobility with $\Delta t = 1 \times 10^{-5}$ (spinodal decomposition)

While $\bar{u} \neq 0$, the nucleation is formed seen Figure (3.3). The simulation results are given for $\bar{u} = 0.4$. The other parameters are the same as in the previous one. In the nucleation mechanism, isolated nuclei come up from the mixture. Again, the spatial microstructure of the mixture coarsens over time.

In both cases the discrete energy dissipates and the mass is conserved (see Figure 3.2 and 3.4). Our results are similar to those in [37], where for spatial discretization local discontinuous Galerkin method and for time discretization implicit convex splitting are used.

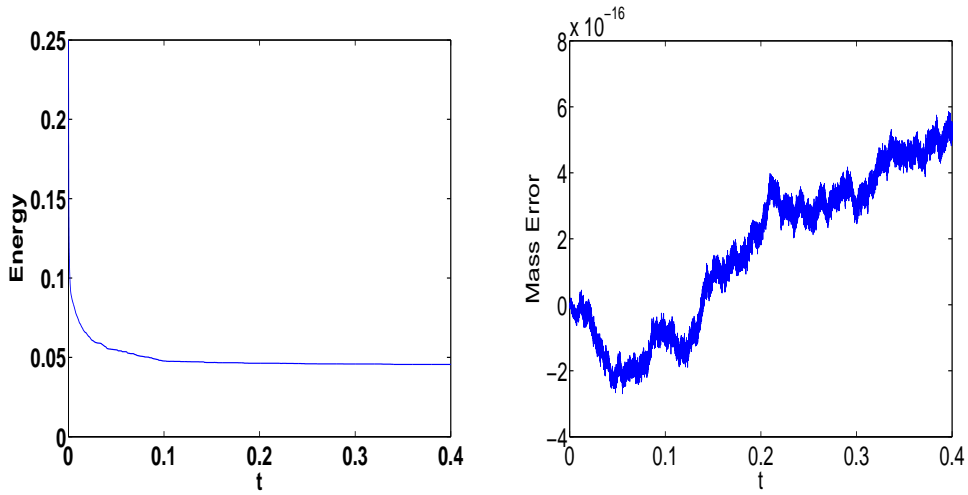


Figure 3.2: Example 3.4.3: Energy decrease and mass conservation of 2D CH equation with constant mobility with $\Delta t = 1 \times 10^{-5}$ (spinodal decomposition)

3.4.4 Constant mobility and logarithmic energy under Neumann Boundary Condition

2D CH equation with constant mobility function and logarithmic energy function $F(u) = 600(u \ln u + (1 - u) \ln(1 - u)) + 1800u(1 - u)\mu(u) = 1$ is considered under homogeneous Neumann boundary condition [40]. The diffusion constant is taken as $\epsilon = 1$. The initial condition is

$$u(x, 0) = \begin{cases} 0.71 & x \in \Omega_1 \\ 0.69 & x \in \Omega_2 \end{cases}$$

where the square domain $\Omega = (-0.5, 0.5) \times (-0.5, 0.5)$, $\Omega_1 = (-0.2, 0.2) \times (-0.2, 0.2)$, $\Omega_2 = \Omega - \Omega_1$.

The plus shaped region evolves into a circular region as shown in Figure 3.5. The evolution process is characterized by grain diffusion and coarsening. Also, energy decreases and mass is conserved as seen in Figure 3.6.

3.4.5 Degenerate mobility and logarithmic energy under Neumann boundary condition

We consider 2D CH equation with degenerate mobility function $\mu(u) = u(1 - u)$ under homogeneous Neumann boundary condition [40] with diffusion constant $\epsilon = 1$. The computational domain is $\Omega = [-0.5, 0.5] \times [-0.5, 0.5]$ for $0 < t < 0.2$. The logarithmic energy function $F(u) = 3000(u \ln u + (1 - u) \ln(1 - u)) + 9000u(1 - u)$ is given. The initial condition is a random variation of uniform state $u = 0.63$ with a change no larger than 0.05.

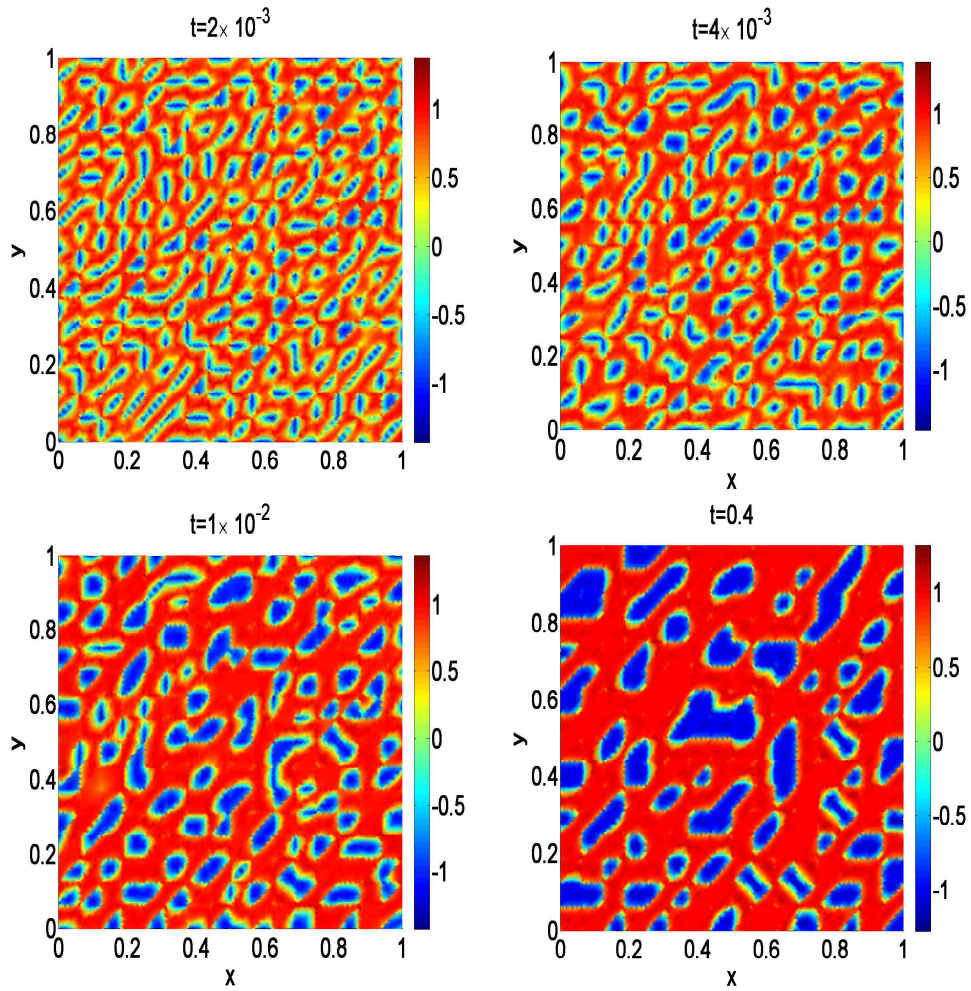


Figure 3.3: Example 3.4.3: Phase solution of 2D CH equation with constant mobility with $\Delta t = 1 \times 10^{-5}$ (nucleation)

Figure (3.7) shows the evolution of the concentration field. The two phases in the concentration evolution, the phase separation stage and the coarsening process stage, can be seen clearly. We can also see in Figure 3.8 that energy decrease and mass conservation is satisfied.

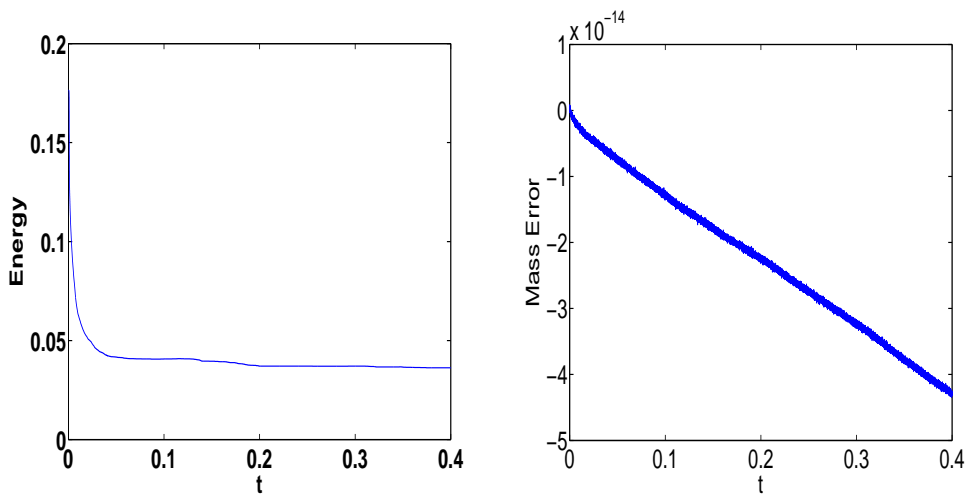


Figure 3.4: Example 3.4.3: Energy decrease and mass conservation of 2D CH equation with constant mobility with $\Delta t = 1 \times 10^{-5}$ (nucleation)

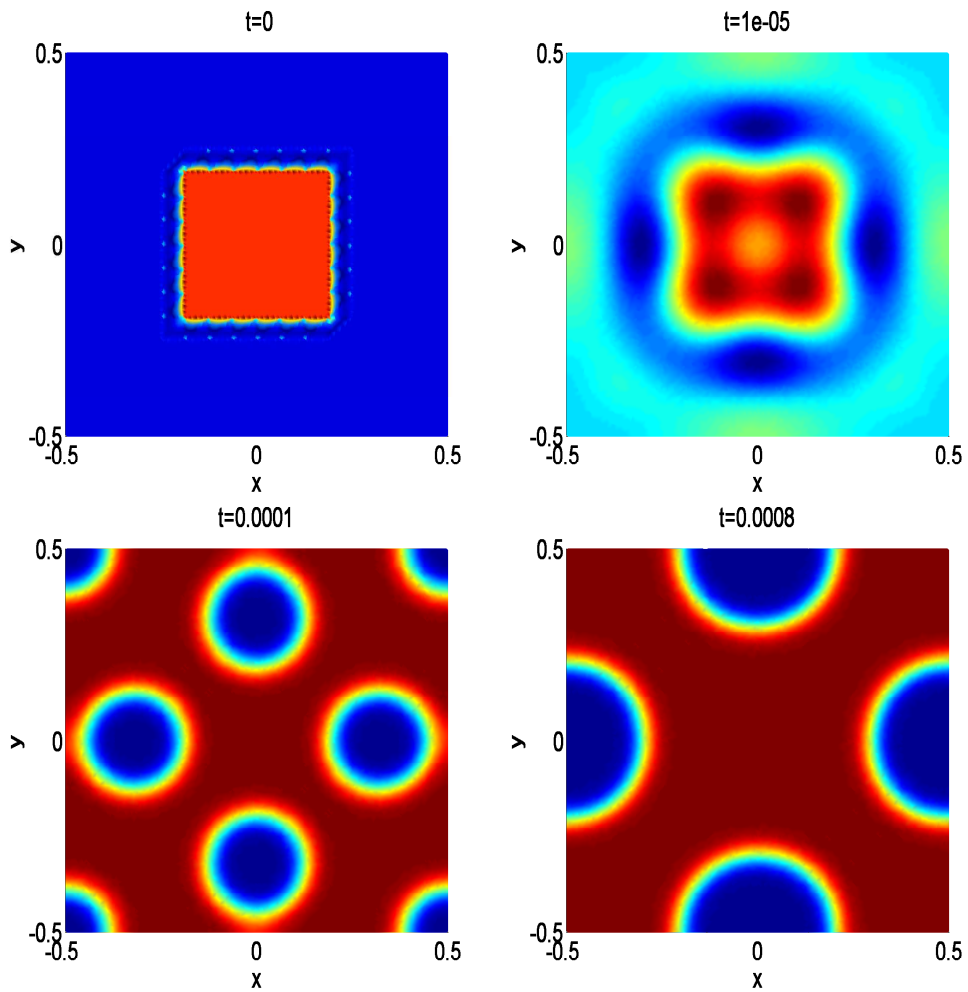


Figure 3.5: Example 3.4.4: Phase solution of 2D CH equation with constant mobility with $\Delta t = 1 \times 10^{-8}$

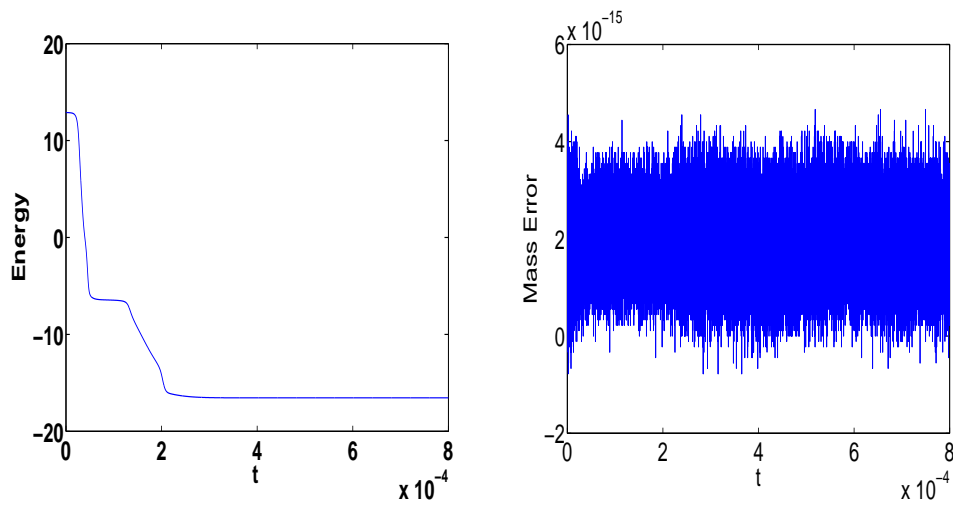


Figure 3.6: Example 3.4.4: Energy decrease and mass conservation of 2D CH equation with constant mobility with $\Delta t = 1 \times 10^{-8}$

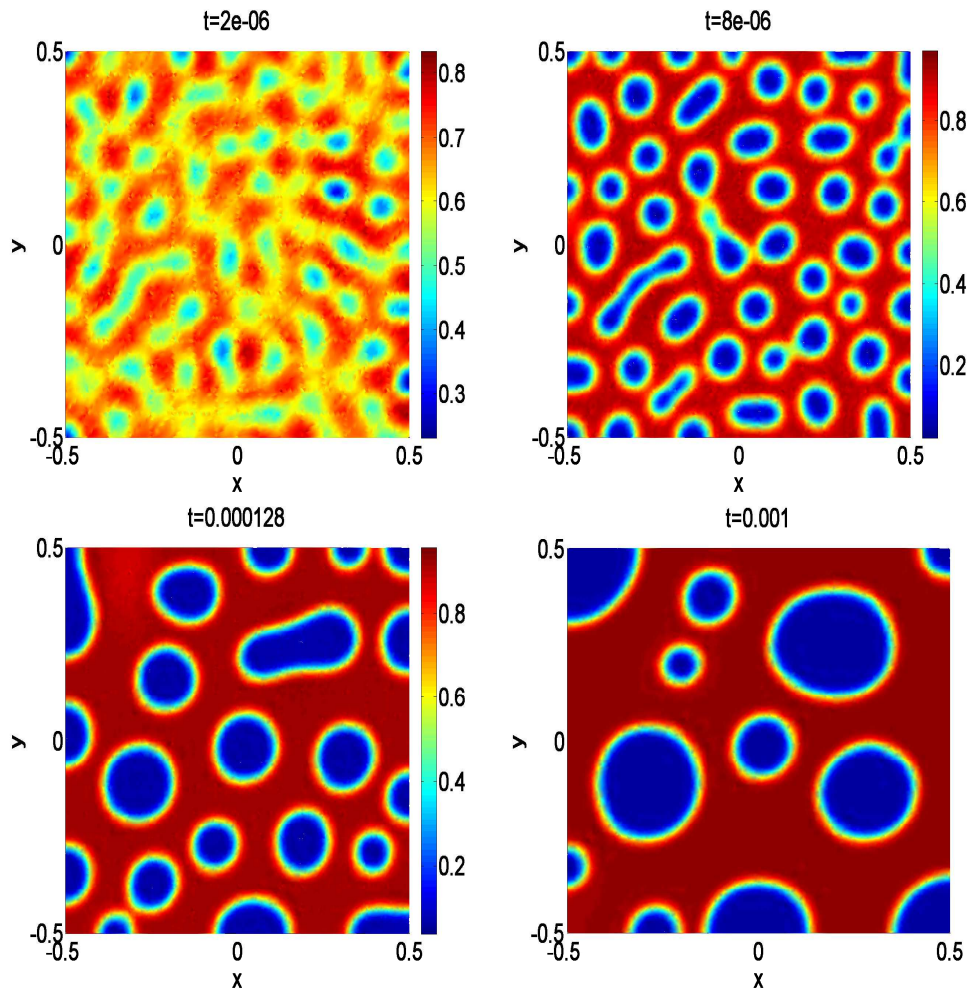


Figure 3.7: Example 3.4.5: Phase solution of 2D CH equation with degenerate mobility with $\Delta t = 1 \times 10^{-7}$

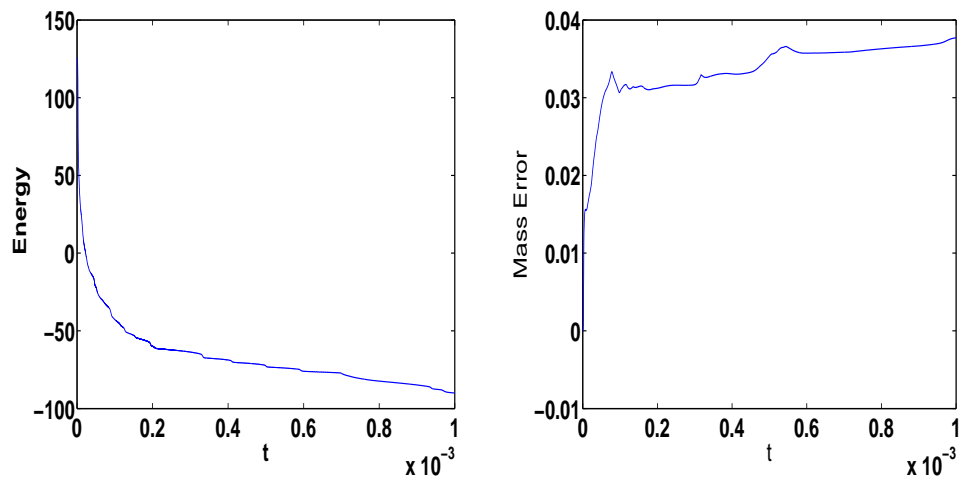


Figure 3.8: Example 3.4.5: Energy decrease and mass conservation of 2D CH equation with degenerate mobility with $\Delta t = 1 \times 10^{-7}$

CHAPTER 4

ADVECTIVE ALLEN-CAHN EQUATION

Interfacial dynamics has great importance in the modeling of multi phase flow. Recently, it has raised quite interest since it plays an important role in different scientific and industrial applications such as micro-structure evolution and grain growth in material science [21], binary fluids flow movement [59], and complex interfacial dynamics [44].

There have been various diffuse interface models for multi phase flow [49, 57]. In this study, we focus on a specific model of diffuse interface for two phase flow; Allen-Cahn model with advection. It is the most known dynamical model for diffuse interface dynamics associated with surface energies [57]. Actually, it models droplet breakup phenomenon of an incompressible material with another compressible fluid. It is an important model problem for studying the influence of flow field and surface tension on droplet breakup phenomena.

The AC model with advection is

$$\begin{aligned} \frac{\partial u}{\partial t} + \nabla \cdot (\mathbf{V}u) &= \epsilon \Delta u - \frac{1}{\epsilon} f(u), \quad \text{in } \Omega \times (0, T] \\ \frac{\partial u}{\partial n} &= 0 \quad \text{on } \partial\Omega \times (0, T] \end{aligned} \quad (4.1)$$

with an appropriate initial condition, $f(u) = F'(u) = 2u(1-u)(1-2u)$ double-well potential and prescribed velocity field $\mathbf{V} = (V_1, V_2)^T$. The velocity field is related to the Navier-Stokes equations since AC model with advection originally comes from the combination of AC dynamics and fluid mechanics [49, 57]. In most of the studies, it generally satisfies Navier-Stokes equations, thus the velocity field \mathbf{V} is divergent free. Here, our main interest is when $\nabla \cdot \mathbf{V} \neq 0$ in general, i.e. \mathbf{V} is not divergent free which is the less studied case. The flow is stated as expanding when $\nabla \cdot \mathbf{V} > 0$ and contracting when $\nabla \cdot \mathbf{V} < 0$.

It is known from the previous chapters, the original AC equation does not satisfy the mass conservation. For this reason, an additional term λ is often added to the equation such that by adding the term λu instead of λ to keep u localized, the mass conservative advective AC equation can be written as

$$\begin{aligned}\frac{\partial u}{\partial t} + \nabla \cdot (\mathbf{V}u) &= \epsilon \Delta u - \frac{1}{\epsilon} f(u) + \lambda u \quad \text{in } \Omega \times (0, T] \\ \frac{\partial u}{\partial n} &= 0 \quad \text{on } \partial\Omega \times (0, T]\end{aligned}\tag{4.2}$$

where λ is chosen so that $\int_{\Omega} u(\mathbf{x}, 0) d\Omega = M$, M is a constant which can also be computed as

$$\lambda = \frac{1}{\epsilon} \frac{\int_{\Omega} f(u)}{M},$$

and it is called as the advective non-local AC equation.

Problems with surface tension in two-phase fluids are known as multi-scale problems with two different time scales, the small surface tension, and the convection time scale, which results in computational stiffness. Most of the studies for surface tension in two phase fluids are based on the modeling aspect. Actually, there exists three main algorithms: the sharp interface algorithm method, the level-set algorithm method and the diffuse interface method [57]. The numerical simulations are illustrated using finite elements method in space and semi-implicit schemes or semi-implicit schemes with splitting in time [10, 56].

In this chapter, we focus on the numerical solution of advective AC equation. In the solution some unphysical oscillations occur at the interior layers due to convection and non-linear reaction leads to sharp fronts. Since the standard FEMs are known to produce strong oscillations around layers, we utilize the adaptive algorithms to tackle all the so-called unphysical oscillations and shock. The adaptivity does this by refining the mesh locally instead of refining the all mesh. By this way an accurate approximation can be found with less degrees of freedom (DoFs) and computational time. The major part of the adaptive algorithms is to estimate the local errors to refine the elements if their estimated local errors are large. A posteriori error estimation is the main tool to estimate the local errors which uses the approximate solution and the given problem data. Many of the studies on a posteriori error estimation are obtained by the weak formulation with respect to the energy norm [1, 8, 77]. Since the DG methods have the flexibility on adaptive meshes, there have been many studies on a posteriori error estimation using DG discretization. The first study for a posteriori error estimation using DG methods was proposed by Karakashian and Pascal in [47]. Then, Hoppe et al. [45] proposed the convergence analysis of a posteriori error estimation for SIPG method. A posteriori error estimation using DG discretization are also studied by Rivière et al. [64], Houston et al. [46] and Ern et al. [29], and references therein.

We introduce an adaptive strategy for the numerical solution of advective non-local AC equation (4.2). In the previous chapters, AC and CH equations are first discretized in space by the SIPG method and the resulting large systems of ODEs are integrated using implicit Euler and AVF methods. On the other hand, the advective non-local AC equation is discretized first in time by implicit Euler method which produces a sequence of semilinear elliptic equations, which is known as Rothe's method [26]. Then, the resulting equations are solved with an adaptive version of SIPG method using upwinding for the convective term. The adaptive strategy is based on a residual based

a posteriori error estimation. We prove the a posteriori error bounds with respect to the energy norm induced by the SIPG formulation of the system given in [74] for semi-linear diffusion-convection-reaction equations with divergent free velocity field. We have applied only space adaptivity because the solutions do not show strong variations with respect to time.

In this chapter, we first derive time discretization of advective AC equation to obtain a stationary problem in Section 4.1. Then, SIPG formulation is constructed in Section 4.2 for the fully discrete advective AC equation. A detailed explanation for space adaptive algorithm is presented in Section 4.3. In Section 4.4. we derive a posteriori error bound for stationary problem. Finally, a series of numerical examples are given in Section 4.5 to demonstrate the applicability of the method.

4.1 Time Discretization of Advective AC Equation

Since the solutions of advective AC equation do not change much with the evolution of time, we apply only space adaptivity. For this reason, we first derive semi-discrete formulation of the problem (4.2) using backward Euler method, which corresponds to Rothe's method [26]. For the semi-discrete scheme, we consider the uniform partition $0 = t_0 < t_1 < \dots < t_J = T$ of the time interval $[0, T]$ with time step-size $\Delta t = t_k - t_{k-1}$, $k = 1, 2, \dots, J$. Then, the semi-discrete problem, implicit Euler in time, reads as: given initial condition u_0 , set $u^0 = u_0$ and for $k = 1, 2, \dots, J$, find $u^k \approx u(t_k)$ satisfying the stationary problem

$$\frac{u^k - u^{k-1}}{\Delta t} - \epsilon \Delta u^k + \mathbf{V} \cdot \nabla u^k + (\nabla \cdot \mathbf{V})u^k - \lambda u^k + \frac{1}{\epsilon} f(u^k) = 0. \quad (4.3)$$

For each $k = 1, 2, \dots, J$, the system (4.3) can be written in the form of a semi-linear elliptic problem as

$$\alpha u^k - \epsilon \Delta u^k + \mathbf{V} \cdot \nabla u^k + r(u^k) = h(u^{k-1}), \quad (4.4)$$

where $\alpha = \left(\frac{1}{\Delta t} + \nabla \cdot \mathbf{V} - \lambda\right)$, $r(u) = \frac{1}{\epsilon} f(u)$, and $h(u) = \frac{1}{\Delta t} u$. The stationary semi-linear elliptic equation (4.4) are solved using SIPG method with an adaptive strategy.

We assume that the non-linear reaction term is bounded and locally Lipschitz continuous, i.e., satisfy for any $s, s_1, s_2 \geq 0$, $s, s_1, s_2 \in \mathbb{R}$ the following conditions

$$\begin{aligned} |r(s)| &\leq C, \quad C > 0 \\ \|r(s_1) - r(s_2)\|_{L^2(\Omega)} &\leq L \|s_1 - s_2\|_{L^2(\Omega)}, \quad L > 0. \end{aligned} \quad (4.5)$$

Moreover, we assume that there is a non-negative constant κ_0 satisfying

$$\alpha - \frac{1}{2} \nabla \cdot \mathbf{V}(x) \geq \kappa_0, \quad \|\nabla \cdot \mathbf{V} + \alpha\|_{L^\infty(\Omega)} \leq c^* \kappa_0, \quad (4.6)$$

for a positive constant c^* . In (4.6) the coercivity of the bilinear form a_h is satisfied by the first condition, and the latter is used to prove the reliability of our a posteriori error estimator [67].

4.2 Full Discretization of Advective AC Equation

In this section, we apply SIPG method using upwinding for the convective term [52, 62] to discretize the stationary problem (4.4). For discretization of the convection term, we first define the sets of inflow edges Γ_t^- and outflow edges Γ_t^+ for the boundary edges for $t \in [0, T]$ by

$$\Gamma_t^- = \{x \in \partial\Omega : \mathbf{V}(x, t) \cdot \mathbf{n}(x) < 0\}, \quad \Gamma_t^+ = \{x \in \partial\Omega : \mathbf{V}(x, t) \cdot \mathbf{n}(x) \geq 0\},$$

where \mathbf{n} is the unit outward normal to the boundary $\partial\Omega$. The set of inflow and outflow boundary edges of an element $E \in \mathcal{T}_h$ is defined in a similar way by

$$\partial E_t^- = \{x \in \partial E : \mathbf{V}(x, t) \cdot \mathbf{n}_E(x) < 0\}, \quad \partial E_t^+ = \{x \in \partial E : \mathbf{V}(x, t) \cdot \mathbf{n}_E \geq 0\}.$$

where \mathbf{n}_E is the unit outward normal vector to the element boundary ∂E . Moreover, for an interior edge ∂E , we denote the trace of a function u from inside the element E by u^{in} and from outside the element E by u^{out} .

The set of interior and boundary edges are denoted by E_h^0 and E_h^∂ , respectively, such that the frame of the mesh is the union $E_h = E_h^0 \cup E_h^\partial$. The initial mesh is specified by \mathcal{T}_h^0 and then a mesh \mathcal{T}_h^k is associated to each time step $k \geq 1$ which is obtained by locally refining or coarsening the mesh \mathcal{T}_h^{k-1} . We also assign the finite element space $V_h^k = V_h(\mathcal{T}_h^k)$ to each mesh \mathcal{T}_h^k . Then, applying the SIPG construction given in Chapter 2 the fully-discrete problem reads as: for $t = 0$, set $u_h(0) \in V_h(\mathcal{T}_h^0)$ as the projection (orthogonal L^2 -projection) of u_0 onto $V_h(\mathcal{T}_h^0)$; for $k = 1, 2, \dots, J$, find $u_h^k \in V_h(\mathcal{T}_h^k)$ such that for all $v_h^k \in V_h(\mathcal{T}_h^k)$

$$a_h(t^k; u_h^k, v_h^k) + b_h(t^k; u_h^k, v_h^k) = I_h(t^k; v_h^k), \quad (4.7)$$

$$\begin{aligned} a_h(t^k; u_h^k, v_h^k) &= \sum_{E \in \mathcal{T}_h} \int_E \epsilon \nabla u_h^k \cdot \nabla v_h^k dx + \sum_{E \in \mathcal{T}_h} \int_E (\mathbf{V} \cdot \nabla u_h^k + \alpha u_h^k) v_h^k dx \\ &+ \sum_{E \in \mathcal{T}_h} \int_{\partial E_t^- \setminus \partial\Omega} \mathbf{V} \cdot \mathbf{n}_E ((u_h^{out})^k - (u_h^{in})^k) v_h^k ds \\ &- \sum_{E \in \mathcal{T}_h} \int_{\partial E_t^- \cap \Gamma_t^-} \mathbf{V} \cdot \mathbf{n}_E (u_h^{in})^k v_h^k ds + \sum_{e \in E_h} \frac{\sigma \epsilon}{h_e} \int_e [u_h^k] \cdot [v_h^k] ds \\ &- \sum_{e \in E_h} \int_e (\{\epsilon \nabla v_h^k\} \cdot [u_h^k] - \{\epsilon \nabla u_h^k\} \cdot [v_h^k]) ds, \end{aligned} \quad (4.8)$$

$$b_h(t^k; u_h^k, v_h^k) = \sum_{E \in \mathcal{T}_h} \int_K r(u_h^k) v_h^k dx, \quad (4.10)$$

$$I_h(t^k; v_h^k) = \sum_{E \in \mathcal{T}_h} \int_K h(u^{k-1}) v_h^k dx. \quad (4.11)$$

4.3 The adaptive algorithm

In this section, an adaptive procedure (in space) is presented for advective non-local AC equation (4.2) which is similar to the one [74]. Following the steps of the adaptive algorithm given in Figure 4.1, for each time step, we solve the fully discrete stationary system (4.7) of the advective non-local AC equation (4.2) adaptively through the residual-based a posteriori error estimator.

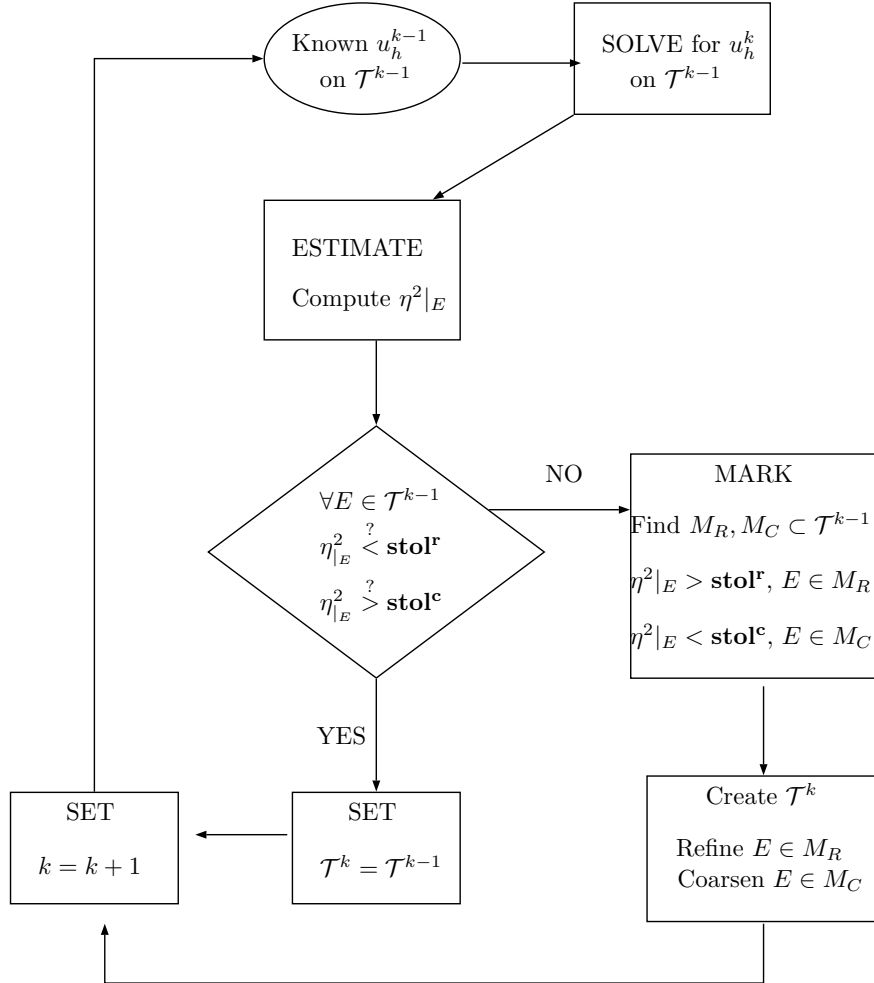


Figure 4.1: Adaptive algorithm chart on a single step $(t_{k-1}, t_k]$

In the adaptive algorithm, the first step SOLVE corresponds to numerical solution of SIPG discretized system (4.7) for the unknown u_h^k on the given triangulation \mathcal{T}_h^{k-1} . The ESTIMATE step constitutes the crucial part of the adaptive procedure. This step provides information to mark the elements to refine/coarsen. We prescribe two tolerances stol^r and stol^c related to the refinement and coarsening, respectively. A residual based error estimator is used to mark the elements, which is a modification of the error estimator given in [67] for non-stationary diffusion-convection-reaction equation with non-linear reaction mechanism [74]. For this, the non-linear reaction term is inserted in the a posteriori error indicator as local contributions to the cell residuals and not to

the interior/boundary edge residuals [78, Chp. 5.1.4]. For convenience, we ignore the superscript k and we let u_h be the solution to the elliptic problem (4.7) at an arbitrary time step. Then, the local error indicators η_E^2 for each element $E \in \mathcal{T}_h^{k-1}$ is given as

$$\eta_E^2 = \eta_{R_E}^2 + \eta_{E_E^0}^2 + \eta_{E_E^N}^2, \quad (4.12)$$

where η_{R_E} stands for the cell residual

$$\eta_{R_E}^2 = \rho_E^2 \|h(u_h) - \alpha u_h + \epsilon \Delta u_h - \mathbf{V} \cdot \nabla u_h - r(u_h)\|_{L^2(E)}^2,$$

while, $\eta_{E_E^0}$ and $\eta_{E_E^N}$ denote the edge residuals coming from the jump of the numerical solution on the interior and Neumann boundary edges, respectively

$$\begin{aligned} \eta_{E_E^0}^2 &= \sum_{e \in \partial E \cap E_h^0} \left(\frac{1}{2} \epsilon^{-\frac{1}{2}} \rho_e \|[\epsilon \nabla u_h]\|_{L^2(e)}^2 + \frac{1}{2} \left(\frac{\epsilon \sigma}{h_e} + \kappa_0 h_e + \frac{h_e}{\epsilon} \right) \| [u_h] \|_{L^2(e)}^2 \right), \\ \eta_{E_E^N}^2 &= \sum_{e \in \partial E \cap E_h^0} \epsilon^{-\frac{1}{2}} \rho_e \| \epsilon \nabla u_h \cdot \mathbf{n} \|_{L^2(e)}^2. \end{aligned}$$

On an element E , we set the weights ρ_E and ρ_e as

$$\rho_E = \min\{h_E \epsilon^{-\frac{1}{2}}, \kappa_0^{-\frac{1}{2}}\}, \quad \rho_e = \min\{h_e \epsilon^{-\frac{1}{2}}, \kappa_0^{-\frac{1}{2}}\},$$

for $\kappa_0 \neq 0$. When $\kappa_0 = 0$, we take $\rho_E = h_E \epsilon^{-\frac{1}{2}}$ and $\rho_e = h_e \epsilon^{-\frac{1}{2}}$. Then, our a posteriori error indicator is given by

$$\eta = \left(\sum_{E \in \mathcal{T}_h^{k-1}} \eta_E^2 \right)^{1/2}. \quad (4.13)$$

Also, we introduce the data approximation error

$$\Theta = \left(\sum_{E \in \mathcal{T}_h^{k-1}} \Theta_E^2(f) \right)^{1/2},$$

where

$$\Theta_E^2(f) = \rho_E^2 (\|h(u) - h(u_h)\|_{L^2(E)}^2 + \|(\mathbf{V} - \mathbf{V}_h) \cdot \nabla u_h\|_{L^2(E)}^2 + \|(\alpha - \alpha_h)u_h\|_{L^2(E)}^2).$$

In the step MARK, we form the sets M_R and M_C of the elements to be refined and coarsened, respectively, given by

$$\begin{aligned} M_R &= \{E \in \mathcal{T}_h^{k-1} : \eta^2|_E > \mathbf{stol}^r\}, \\ M_C &= \{E \in \mathcal{T}_h^{k-1} : \eta^2|_E < \mathbf{stol}^c\}, \end{aligned}$$

where the error indicator η is introduced in (4.12).

Finally, we create the new mesh \mathcal{T}_h^k by refining the elements $E \in M_R$ using the newest vertex bisection method [19], and by coarsening the elements $E \in M_C$. Numerical studies show the capability of the error indicator to find the layers properly.

4.4 A posteriori error estimation

We utilize the energy norm and the semi-norm to present the reliability and efficiency of a posteriori error estimator. The energy norm is given by

$$|||v|||^2 = \sum_{E \in \mathcal{T}_h} (\|\epsilon \nabla v\|_{L^2(E)}^2 + \kappa_0 \|v\|_{L^2(E)}^2) + \sum_{e \in E_h^0} \frac{\epsilon \sigma}{h_e} \|[v]\|_{L^2(e)}^2, \quad (4.14)$$

and the semi-norm is

$$|v|_C^2 = |\mathbf{V}v|_*^2 + \sum_{e \in E_h^0} (\kappa_0 h_e + \frac{h_e}{\epsilon}) \|[v]\|_{L^2(e)}^2, \quad (4.15)$$

with

$$|q|_* = \sup_{u \in H_0^1(\Omega) \setminus \{0\}} \frac{\int_{\Omega} q \cdot \nabla u dx}{|||u|||}.$$

The terms $|\mathbf{V}v|_*^2$ and $\frac{h_e}{\epsilon} \|[v]\|_{L^2(e)}^2$ in the semi-norm are used to bound the convective part. The other term $\kappa_0 h_e \|[v]\|_{L^2(e)}^2$ is used to bound the linear reaction part of the discrete system. To bound the non-linear reaction part, the boundedness property (2a) [Chp. 5.1.1-4, [78]] is used.

Theorem 4.1. *For any time-step $k = 1, 2, \dots, J$, let u and u_h be the solutions to the continuous problem (4.4) and the discrete SIPG problem (4.7) respectively. Also, assume that the assumptions (4.5) and (4.6) hold. Then, we have the a posteriori error bounds*

$$|||u - u_h||| + |u - u_h|_C \lesssim \eta + \Theta \quad (\text{reliability}), \quad (4.16)$$

$$\eta \lesssim |||u - u_h||| + |u - u_h|_C + \Theta \quad (\text{efficiency}). \quad (4.17)$$

4.4.1 Proof of a Posteriori Error Bounds

For the proof of a posteriori error estimate, we follow [74] which is for stationary diffusion-convection-reaction equation with a nonlinear reaction mechanism. We use the DG norm defined by

$$\|v\|_{DG}^2 = |||v|||^2 + |v|_c^2 \quad (4.18)$$

with the definitions (4.14) and (4.15). Also, the symbols \lesssim and \gtrsim represents the bounds that are eligible up to positive constants independent of the local mesh size h , the diffusion coefficient ϵ and the penalty parameter σ .

Since the spatial error $\|u^s - u_h^s\|_{DG}$ is not well-defined due to $u^s \in H_0^1(\Omega)$ and $u_h^s \in V_h(\mathcal{T}_h) \not\subset H_0^1(\Omega)$, we first split the stationary SIPG solution u_h^s as

$$u_h^s = u_h^c + u_h^r$$

where $u_h^c \in H_0^1(\Omega) \cap V_h(\mathcal{T}_h)$ is the conforming part of the solution and $u_h^r \in V_h(\mathcal{T}_h)$ is the remainder term. By this way, we get $u_h^s \in H_0^1(\Omega) + V_h(\mathcal{T}_h)$, and

$$\|u^s - u_h^s\|_{DG} \leq \|u^s - u_h^c\|_{DG} + \|u_h^r\|_{DG}$$

holds from the triangular inequality. Note that all the terms on the right hand side become well-defined norms, and now we can find bounds for them. First, the following auxiliary forms are utilized:

$$D_h(t; u, v) = \sum_{E \in \mathcal{T}_h} \int_E (\epsilon \nabla u \cdot \nabla v + (\alpha - \nabla \cdot \mathbf{V})uv) dx, \quad (4.19)$$

$$\begin{aligned} O_h(t; u, v) &= - \sum_{E \in \mathcal{T}_h} \int_E \mathbf{V}u \cdot \nabla v dx + \sum_{E \in \mathcal{T}_h} \int_{\partial E^+ \cap \Gamma^+} \mathbf{V} \cdot \mathbf{n} u v ds, \\ &+ \sum_{E \in \mathcal{T}_h} \int_{\partial E^+ \setminus \partial \Omega} \mathbf{V} \cdot \mathbf{n} u (v - v^{out}) ds \end{aligned} \quad (4.20)$$

$$K_h(t; u, v) = - \sum_{e \in E_h} \int_e (\{\epsilon \nabla v_h\} \cdot [u_h] - \{\epsilon \nabla u_h\} \cdot [v_h]) ds,$$

$$J_h(t; u, v) = \sum_{e \in E_h^0} \frac{\sigma \epsilon}{h_e} \int_e [u] \cdot [v] ds. \quad (4.21)$$

Then, for a specific $t \in [0, T]$ the bilinear form $\tilde{a}_h(t; u, v)$ fulfills,

$$\tilde{a}_h(t; u, v) = D_h(t; u, v) + O_h(t; u, v) + J_h(t; u, v)$$

which is well-defined on $H_0^1(\Omega) + V_h(\mathcal{T}_h)$ and satisfies the coercivity property [Lemma 4.1, [67]]

$$\tilde{a}_h(t; u, v) \geq \|u\|^2, \quad u \in H_0^1(\Omega).$$

Furthermore, the SIPG bilinear form $a_h(t; u, v)$ in (4.7) satisfies

$$a_h(t; u, v) = \tilde{a}_h(t; u, v) + K(t; u, v), \quad \forall u, v \in V_h(\mathcal{T}_h), \quad (4.22)$$

$$a_h(t; u, v) = \tilde{a}_h(t; u, v), \quad \forall u, v \in H_0^1(\Omega). \quad (4.23)$$

Also, the auxiliary forms are continuous [Lemma 4.2, [67]]:

$$|D_h(t; u, v)| \lesssim \|u\| \|v\|, \quad u, v \in H_0^1(\Omega) + V_h(\mathcal{T}_h), \quad (4.24)$$

$$|O_h(t; u, v)| \lesssim |\mathbf{V}u|_* \|v\|, \quad u \in H_0^1(\Omega) + V_h(\mathcal{T}_h), v \in H_0^1(\Omega), \quad (4.25)$$

$$|J_h(t; u, v)| \lesssim \|u\| \|v\|, \quad u, v \in H_0^1(\Omega) + V_h(\mathcal{T}_h), \quad (4.26)$$

and for $u \in V_h(\mathcal{T}_h)$, $v \in V_h(\mathcal{T}_h) \cap H_0^1(\Omega)$ [Lemma 4.3, [67]]

$$|K_h(t; u, v)| \lesssim \sigma^{-1/2} \left(\sum_{e \in E_h^0} \frac{\sigma \epsilon}{h_e} \| [u] \|_{L^2(e)} \right)^{1/2} \|v\|. \quad (4.27)$$

Moreover, using the boundedness assumption of non-linear term given in (4.5), we get for non-linear form $b_h(t; u, v)$ for a specific time t

$$|b_h(t; u, v)| \lesssim |||v|||, \quad u, v \in H_0^1(\Omega) + V_h(\mathcal{T}_h). \quad (4.28)$$

Then, some auxiliary results and conditions used in the proofs are given.

Lemma 4.2. *The inf-sup condition in [Lemma 4.4, [67]] gives*

$$|||u||| + |\mathbf{V}u|_* \lesssim \sup_{v \in H_0^1(\Omega) \setminus \{0\}} \frac{\tilde{a}_h(t; u, v)}{|||v|||}. \quad (4.29)$$

for all $u \in H_0^1(\Omega)$.

Definition 4.1. For any $u \in V_h(\mathcal{T}_h)$, the following inequalities hold

$$\sum_{E \in \mathcal{T}_h} \|u - A_h u\|_{L^2(E)}^2 \lesssim \sum_{e \in E_h^0} \int_e h_e |u|^2 ds, \quad (4.30)$$

$$\sum_{E \in \mathcal{T}_h} \|\nabla(u - A_h u)\|_{L^2(E)}^2 \lesssim \sum_{e \in E_h^0} \int_e \frac{1}{h_e} |u|^2 ds. \quad (4.31)$$

where $A_h : V_h(\mathcal{T}_h) \mapsto V_h^c$ is the approximation operator with $V_h^c = V_h(\mathcal{T}_h) \cap H_0^1(\Omega)$ being the conforming subspace of $V_h(\mathcal{T}_h)$.

Lemma 4.3. *For any $u \in H_0^1(\Omega)$, the interpolation operator is defined as*

$$I_h : H_0^1(\Omega) \mapsto \{w \in C(\bar{\Omega}) : w|_E \in \mathbb{P}_1(E), \forall K \in \mathcal{T}, w = 0 \text{ on } \Gamma\}$$

and it satisfies

$$|||I_h u||| \lesssim |||u|||, \quad (4.32)$$

$$\left(\sum_{E \in \mathcal{T}} \rho_E^{-2} \|u - I_h u\|_{L^2(E)}^2 \right)^{1/2} \lesssim |||u|||, \quad (4.33)$$

$$\left(\sum_{e \in E_h^0} \epsilon^{1/2} \rho_e^{-1} \|u - I_h u\|_{L^2(E)}^2 \right)^{1/2} \lesssim |||u|||. \quad (4.34)$$

Now, consider the splitting of the stationary solution $u_h^s = u_h^c + u_h^r$ as $u_h^c = A_h u_h^s \in H_0^1(\Omega) \cap V_h(\mathcal{T}_h)$ with A_h is the approximation operator and $u_h^r = u_h^s - u_h^c \in V_h$.

Lemma 4.4 (Lemma 4.4, [67]). *The bound for the remainder term holds*

$$\|u_h^r\| \lesssim \eta \quad (4.35)$$

where η is the a posteriori error estimator given in (4.13).

Lemma 4.5. For a given $t \in (0, T]$ and for any $v \in H_0^1(\Omega)$, we have

$$\int_{\Omega} h(u_h^s)(v - I_h v) dx - \tilde{a}_h(u_h^s)(v - I_h v) - b_h(t; u_h^s, v - I_h v) \lesssim (\eta + \Theta) \|v\| \quad (4.36)$$

where I_h is the interpolation operator.

Proof. Let

$$T = \int_{\Omega} h(t; u_h^s, v - I_h v) dx - \tilde{a}_h(t; u_h^s, v - I_h v) - b_h(t; u_h^s, v - I_h v).$$

Applying integration by parts gives

$$\begin{aligned} T &= \sum_{E \in \mathcal{T}_h} \int_E (h(u_h^s) + \epsilon \Delta u_h^s - \mathbf{V} \cdot \nabla u_h^s - r(u_h^s))(v - I_h v) dx \\ &\quad - \sum_{E \in \mathcal{T}_h} \int_{\partial E} \epsilon \nabla u_h^s \cdot \mathbf{n} (v - I_h v) ds \\ &\quad + \sum_{E \in \mathcal{T}_h} \int_{\partial E^- \setminus \partial \Omega} \mathbf{V} \cdot \mathbf{n} (u_h^s - u_h^{s, out}) (v - I_h v) ds \\ &= T_1 + T_2 + T_3. \end{aligned}$$

Addition and subtraction of the data approximation terms into the term T_1 yields

$$\begin{aligned} T_1 &= \sum_{E \in \mathcal{T}_h} \int_E (h(u_h^s) + \epsilon \Delta u_h^s - \mathbf{V}_h \cdot \nabla u_h^s - r(u_h^s))(v - I_h v) dx \\ &\quad + \sum_{E \in \mathcal{T}_h} \int_E ((h(u) - h(u_h)) - (\mathbf{V} - \mathbf{V}_h) \cdot \nabla u_h^s)(v - I_h v) dx. \end{aligned}$$

Using the Cauchy-Schwarz inequality and interpolation operator identity (4.33)

$$\begin{aligned} T_1 &\lesssim \left(\sum_{E \in \mathcal{T}_h} \eta_{R_E}^2 \right)^{1/2} \left(\sum_{E \in \mathcal{T}_h} \rho_E^{-2} \|v - I_h v\|_{L^2(E)}^2 \right)^{1/2} \\ &\quad + \left(\sum_{E \in \mathcal{T}_h} \Theta_E^2 \right)^{1/2} \left(\sum_{E \in \mathcal{T}_h} \rho_E^{-2} \|v - I_h v\|_{L^2(E)}^2 \right)^{1/2} \\ &\lesssim \left(\sum_{E \in \mathcal{T}_h} (\eta_{R_E}^2 + \Theta_E^2) \right)^{1/2} \|v\|. \end{aligned}$$

For the terms T_2 and T_3 , we have [Lemma 4.8, [67]]

$$T_2 \lesssim \left(\sum_{E \in \mathcal{T}_h} \eta_{E_E}^2 \right)^{1/2} \|v\|$$

$$T_3 \lesssim \left(\sum_{E \in \mathcal{T}_h} \eta_{J_E}^2 \right)^{1/2} |||v|||.$$

□

Lemma 4.6. For a given $t \in (0, T]$, the bound of the conforming part of the error satisfies

$$\|u^s - u_h^c\|_{DG} \lesssim \eta + \Theta. \quad (4.37)$$

Proof. Since $u^s - u_h^c \in H_0^1(\Omega)$, we have $|u^s - u_h^c|_C = |\mathbf{V}(u^s - u_h^c)|_*$. Then, from the inf-sup condition (4.29)

$$\|u^s - u_h^c\|_{DG} = |||u^s - u_h^c||| + |u^s - u_h^c|_C \lesssim \sup_{v \in H_0^1(\Omega) \setminus \{0\}} \frac{\tilde{a}_h(t; u^s - u_h^c, v)}{|||v|||}.$$

So, we need to bound the term $a_h(t; u^s - u_h^c, v)$. Using that $u^s - u_h^c \in H_0^1(\Omega)$, we have

$$\begin{aligned} \tilde{a}_h(t; u^s - u_h^c, v) &= \tilde{a}_h(t; u^s, v) - \tilde{a}_h(t; u_h^c, v) \\ &= \int_{\Omega} h(u^s)v dx - b_h(t; u^s, v) - \tilde{a}_h(t; u_h^c, v) \\ &= \int_{\Omega} h(u^s)v dx - b_h(t; u^s, v) - D_h(t; u_h^c, v) - J_h(t; u_h^c, v) - O_h(t; u_h^c, v) \\ &= \int_{\Omega} h(u^s)v dx - b_h(t; u_h^s, v) + b_h(t; u_h^s, v) - b_h(t; u^s, v) \\ &\quad - \tilde{a}_h(t; u_h^s, v) + D_h(t; u_h^r, v) + J_h(t; u_h^r, v) + O_h(t; u_h^r, v). \end{aligned}$$

We also have from the SIPG scheme

$$\int_{\Omega} h(u^s)I_h v dx = \tilde{a}_h(t; u_h^s, I_h v) + K_h(t; u_h^s, I_h v) + b_h(t; u_h^s, I_h v)$$

Hence, we obtain

$$\tilde{a}(t; u^s - u_h^c, v) = T_1 + T_2 + T_3 + T_4$$

$$\begin{aligned} T_1 &= \int_{\Omega} h(u_h^s)(v - I_h v) dx - \tilde{a}_h(t; u_h^s, v - I_h v) - b_h(t; u_h^s, v - I_h v) \\ T_2 &= D_h(t; u_h^r, v) + J_h(t; u_h^r, v) + O_h(t; u_h^r, v) \\ T_3 &= K_h(t; u_h^s, I_h v) \\ T_4 &= b_h(t; u_h^s, v) - b_h(t; u^s, v) \end{aligned}$$

From the inequality (4.36), we have

$$T_1 \lesssim (\eta + \Theta) |||v|||$$

The continuity results (4.24-4.26) and the bound to remainder term (4.35) yields

$$T_2 \lesssim (|||u_h^r||| + |\vec{\beta}u_h^r|_*) |||v||| \leq \eta |||v|||$$

Moreover, using the identities (4.27) and (4.32), we get

$$T_3 \lesssim \sigma^{-1/2} \left(\sum_{E \in \mathcal{T}} \eta_{J_E}^2 \right)^{1/2} |||I_h v||| \lesssim \sigma^{-1/2} \left(\sum_{E \in \mathcal{T}} \eta_{J_E}^2 \right)^{1/2} |||v|||.$$

Finally, using Cauchy-Schwarz inequality and the boundedness property (4.28), we get

$$\begin{aligned} T_4 &= b_h(t; u_h^s, v) - b_h(t; u^s, v) = \int_{\Omega} r(u_h^s) v dx - \int_{\Omega} r(u^s) v dx \\ &\leq C_1 \|v\|_{L^2(\Omega)} - C_2 \|v\|_{L^2(\Omega)} \\ &\lesssim |||v|||. \end{aligned}$$

which finishes the proof. \square

Now, we can give the proof of Theorem 4.1.

Proof. Combining the bounds (4.35) and (4.37) to the remainder and the conforming parts of the error, respectively, we obtain

$$\begin{aligned} \|u^s - u_h^s\|_{DG} &\leq \|u^s - u_h^c\|_{DG} + \|u_h^r\|_{DG} \\ &\leq \eta + \Theta + \eta \\ &\lesssim \eta + \Theta \end{aligned}$$

\square

The proof of the efficiency is similar to Theorem 3.3 in [67]. We only use the boundedness property (4.5) of the non-linear reaction term to bound the terms occurring in the procedure in [67].

4.5 Numerical Results

In this section, we present several numerical examples for advective non-local AC equation under homogenous Neumann boundary conditions for one and two dimensional problems. For the 1D problems, our aim is to show the droplet breakup phenomena, where space adaptivity is not needed. For 2D problems we demonstrate the effectiveness of the adaptive SIPG method to recapture sharp layers in convection dominated cases.

4.5.1 1D advective non-local AC equation

The advective AC equation does not satisfy the droplet breakup under certain situations. We present a set of 1D numerical examples under what conditions the droplet

breakup is formed by focusing on the dynamics of the solutions when the strength of the velocity field changes.

We first consider 1D advective non-local AC equation [56] in the domain $\Omega = [-5, 5]$ for $0 < t < 0.2$ with the initial condition

$$u(x, 0) = \begin{cases} 1; & -0.3 \leq x \leq 0.3 \\ 0; & \text{otherwise.} \end{cases}$$

This test example was solved in [56] by taking the diffusion constant $\epsilon = 0.01$ with the linear finite elements in space and semi-implicit splitting scheme in time for mesh sizes $\Delta x = 0.005$ and time steps $\Delta t = 0.001$. The velocity field is taken as $\mathbf{V} = V_0 x$. We performed simulations with coarser mesh sizes $\Delta x = 0.1$ and with the same time steps $\Delta t = 0.001$. For different values of V_0 , we obtain different results. As V_0 increases, two different types of solutions appear. When $V_0 = 3$ is small as in Figure 4.2, the solution decreases and settles into a non-constant steady state depicting a single droplet. Also, mass conservation is seen in Figure 4.3, right. If $V_0 = 10$ which is large in Figure 4.4, the solution decays to a small constant value. Mass is again conserved as shown in Figure 4.5, right. These two examples reveal that a typical advective AC equation that does not show droplet breakup phenomena.

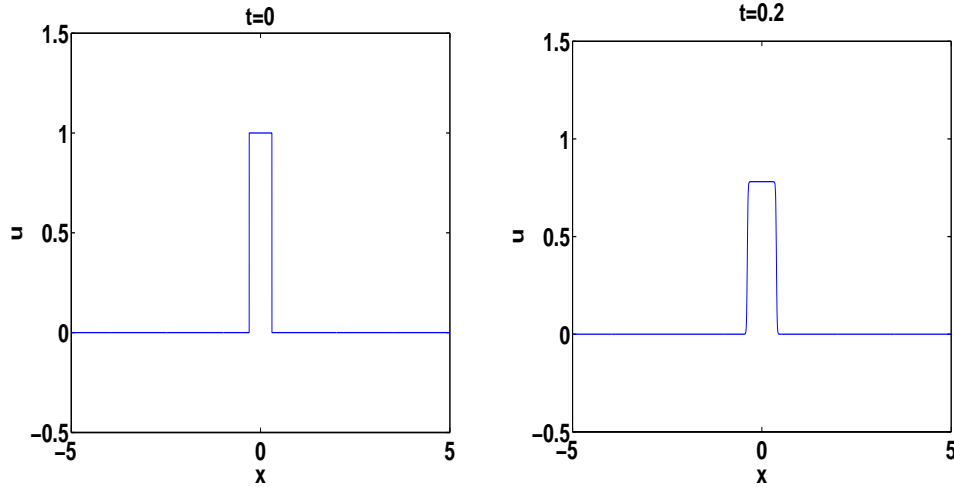


Figure 4.2: Example 4.5.1: Solutions at initial and final times with $V_0 = 3$

4.5.2 1D advective non-local AC equation: non-monotone initial condition

We again consider 1D advective non-local AC equation [56] in the domain $\Omega = [-5, 5]$ for $0 < t < 0.45$ with the diffusion constant $\epsilon = 0.01$ which is solved again by linear finite elements in space and semi-implicit splitting scheme in time with mesh sizes $\Delta x = 0.005$ and time steps $\Delta t = 0.001$, respectively. The velocity field is taken as $\mathbf{V} = 5x$. The non-monotone initial condition is given by

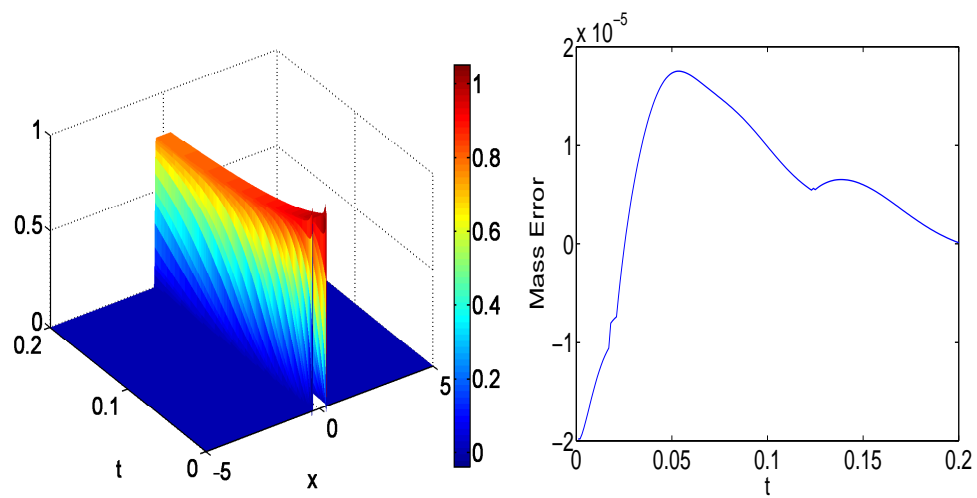


Figure 4.3: Example 4.5.1: Solution profile (left) and mass error (right) with $V_0 = 3$

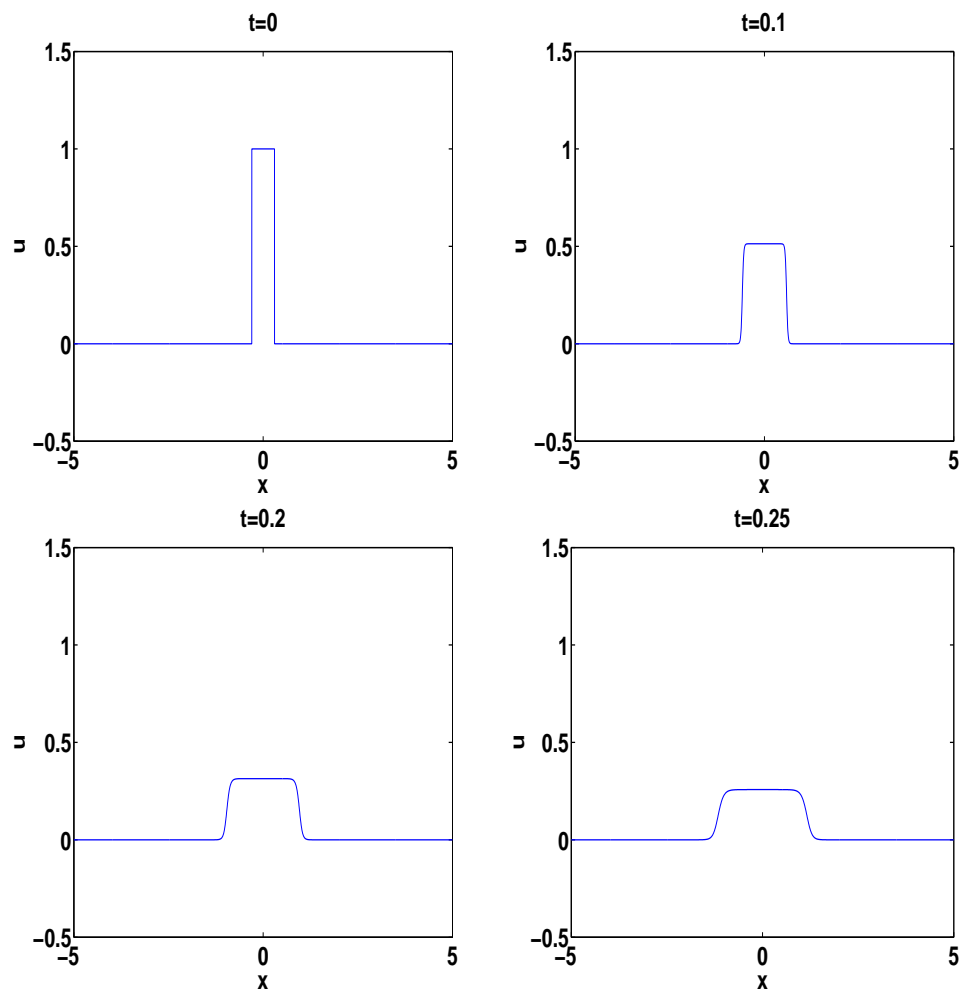


Figure 4.4: Example 4.5.1: Solutions with $V_0 = 10$

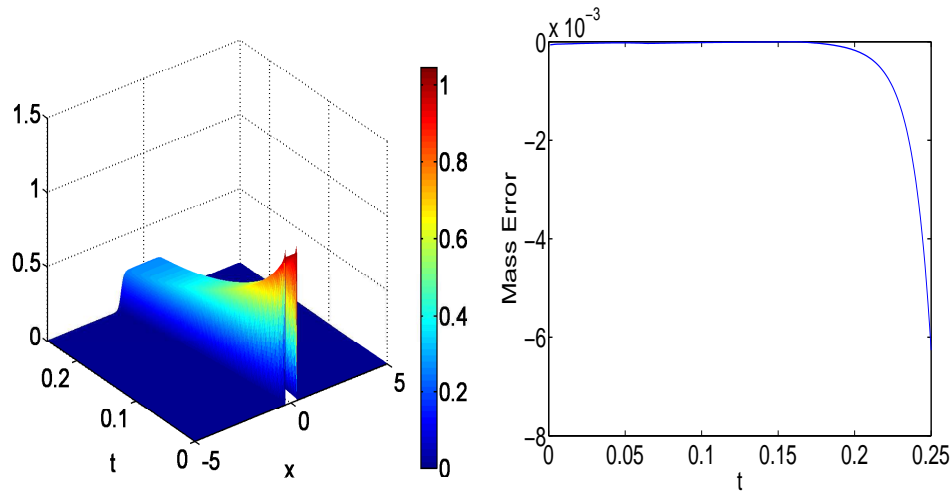


Figure 4.5: Example 4.5.1: Solution profile (left) and mass error (right) with $V_0 = 10$

$$u(x, 0) = \begin{cases} 1; & [-0.5, 0.01) \cup (0.01, 0.5] \\ 0.99; & [-0.01, 0.01] \\ 0; & \text{otherwise} \end{cases}$$

We have used the same coarse mesh sizes Δx and the same time steps Δt as in the previous example. When the initial value is non-monotone, as shown in Figure 4.6, the solutions take a different form. Even a small concavity at the origin leads to a completely different evolution. The solution shows a breakup. Also, mass conservation is satisfied in Figure 4.7, right.

4.5.3 2D advective non-local AC equation: expanding flow

For 2D problems, we consider the expanding velocity field and a shear flow [56]. For the expanding case, the velocity field is prescribed as

$$\mathbf{V} = (V_0x, V_0y),$$

and for shear flow

$$\mathbf{V} = (0, -V_0x).$$

We first test the expanding flow case. We work on the domain $\Omega = [-1, 1] \times [-1, 1]$ for $0 < t < 0.06$ with the diffusion constant $\epsilon = 0.01$ and $V_0 = 10$. The initial condition is

$$u(x, 0) = \begin{cases} 1; & x^2 + y^2 \leq 0.3 \\ 0; & \text{otherwise} \end{cases}$$

We first solve by uniform mesh using linear DG elements with mesh sizes $\Delta x = \Delta y = 1/32$ and the time step size is $\Delta t = 1 \times 10^{-3}$. Similar to 1D case, advective AC

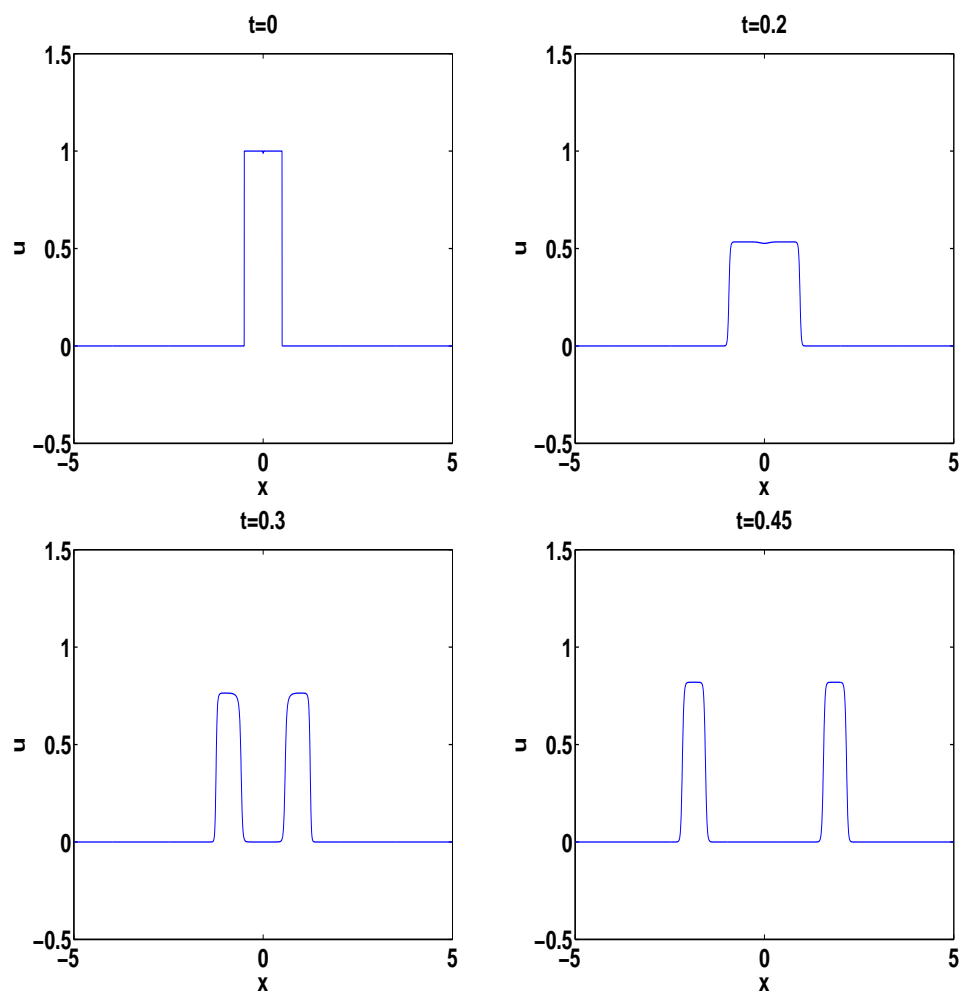


Figure 4.6: Example 4.5.2: Solutions with non-monotone initial condition

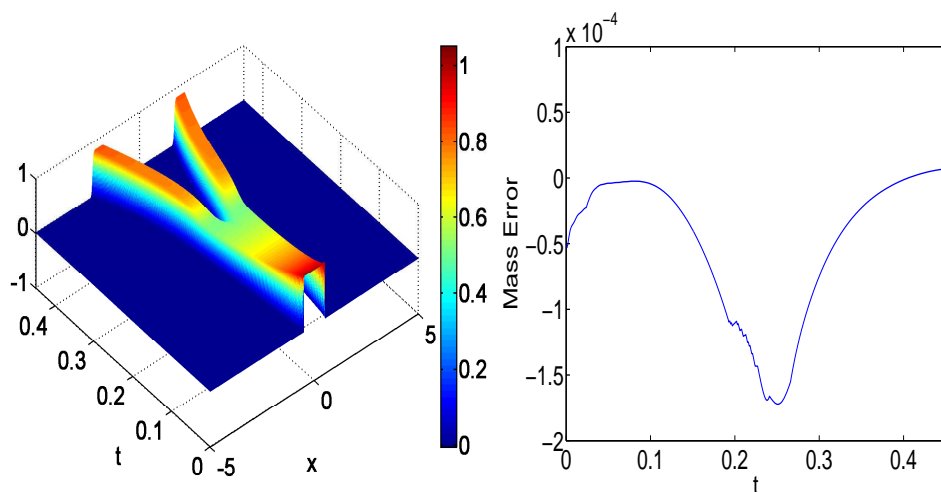


Figure 4.7: Example 4.5.2: Solution profile (left) and mass error (right)

does not have droplet breakup as shown in Figure 4.8, top. Mass conservation is also satisfied as shown in Figure 4.8, bottom. However, the solutions show some unphysical oscillations (see Figure 4.10, left). We have applied the space adaptive algorithm with the prescribed tolerances $\text{stol}^r = 1 \times 10^{-3}$, $\text{stol}^c = 1 \times 10^{-6}$ and uniform time step size $\Delta t = 1 \times 10^{-3}$. The adaptive mesh at time $T = 0.06$ is shown in Figure 4.9, left. It can be clearly seen in Figure 4.9, right, that refinement/coarsening of the adaptive algorithm works well and spurious oscillations disappear in Figure 4.10, right.

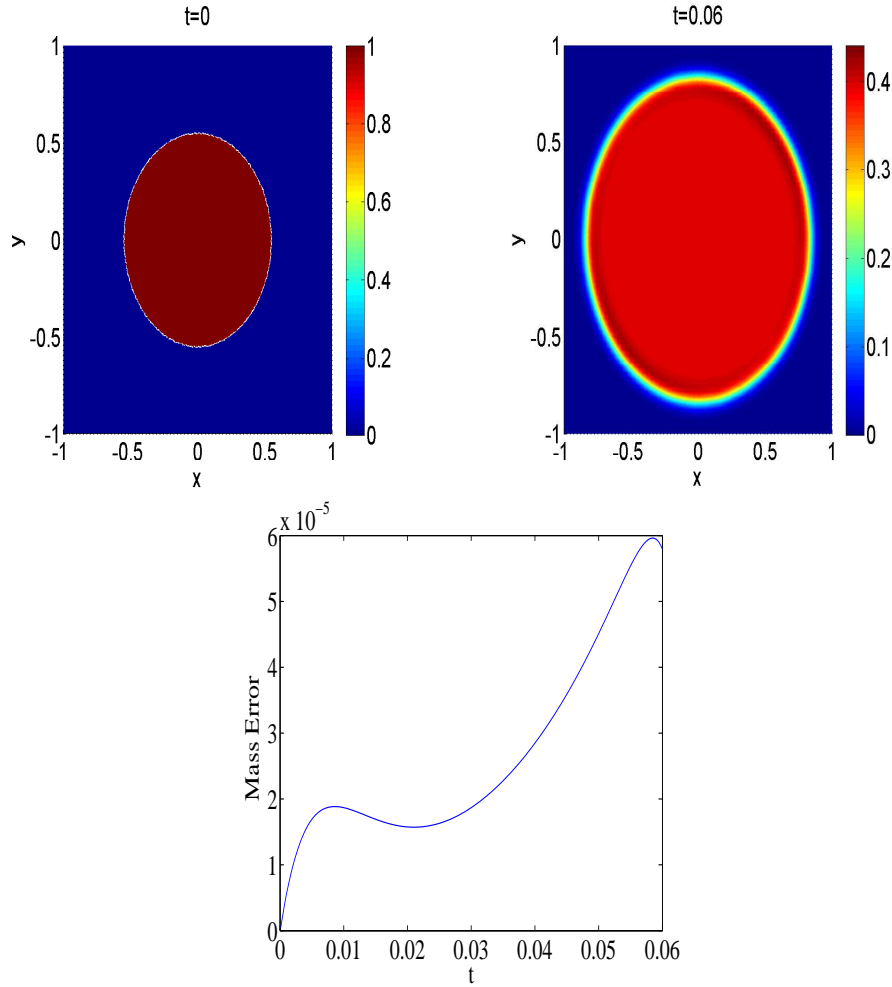


Figure 4.8: Example 4.5.3: Uniform solutions at initial and final times (top) for expanding flow and mass error plot (bottom)

Then, we consider the same problem with the square initial data

$$u(x, 0) = \begin{cases} 1; & -0.3 \leq x, y \leq 0.3 \\ 0; & \text{otherwise} \end{cases}$$

The uniform and adaptive solutions at final time $t = 0.06$ are given in Figure 4.11, top, which shows the effectiveness of our adaptive algorithm. It can be seen from Figure 4.11, bottom right, that initially the mesh is refined, afterward the mesh is coarsened non-monotonically around the internal layer.

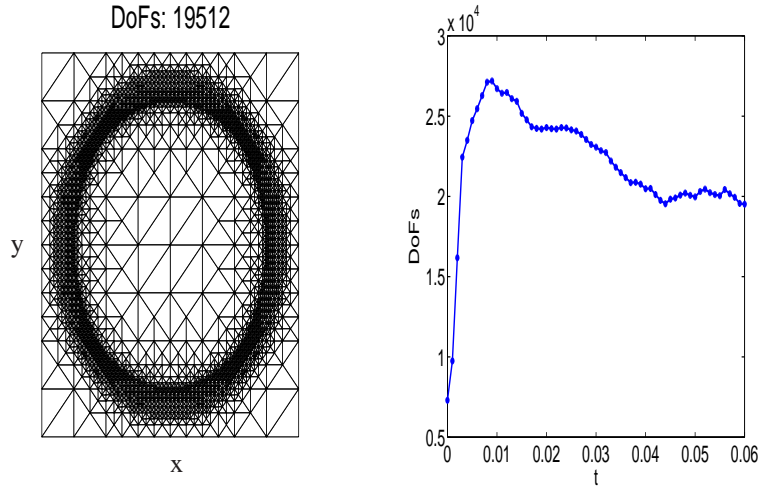


Figure 4.9: Example 4.5.3: Adaptive mesh at final time $t = 0.06$ (left) and evolutions of DoFs (right) for expanding flow

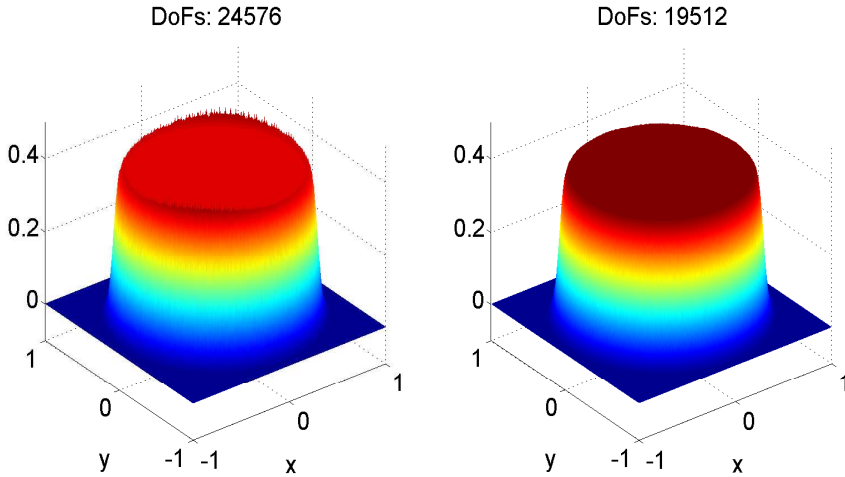


Figure 4.10: Example 4.5.3: Uniform (left) and adaptive (right) solutions at final time $t = 0.06$ for expanding flow

4.5.4 2D advective non-local AC equation: sheer flow

Now, we test the sheering flow case. We consider 2D advective non-local AC equation [56] in the domain $\Omega = [-1, 1] \times [-1, 1]$ for $0 < t < 0.06$ with diffusion constant $\epsilon = 0.01$ and $v_0 = 100$. The initial condition is

$$u(x, 0) = \begin{cases} 1; & -0.1 \leq x, y \leq 0.1 \\ 0; & \text{otherwise} \end{cases}$$

We solve using linear DG elements on uniform mesh with mesh sizes $\Delta x = \Delta y = 1/32$ and time step size is taken as $\Delta t = 1 \times 10^{-3}$. It can be easily seen in Figure 4.12, top, that advective AC does not have droplet breakup. The mass conservation

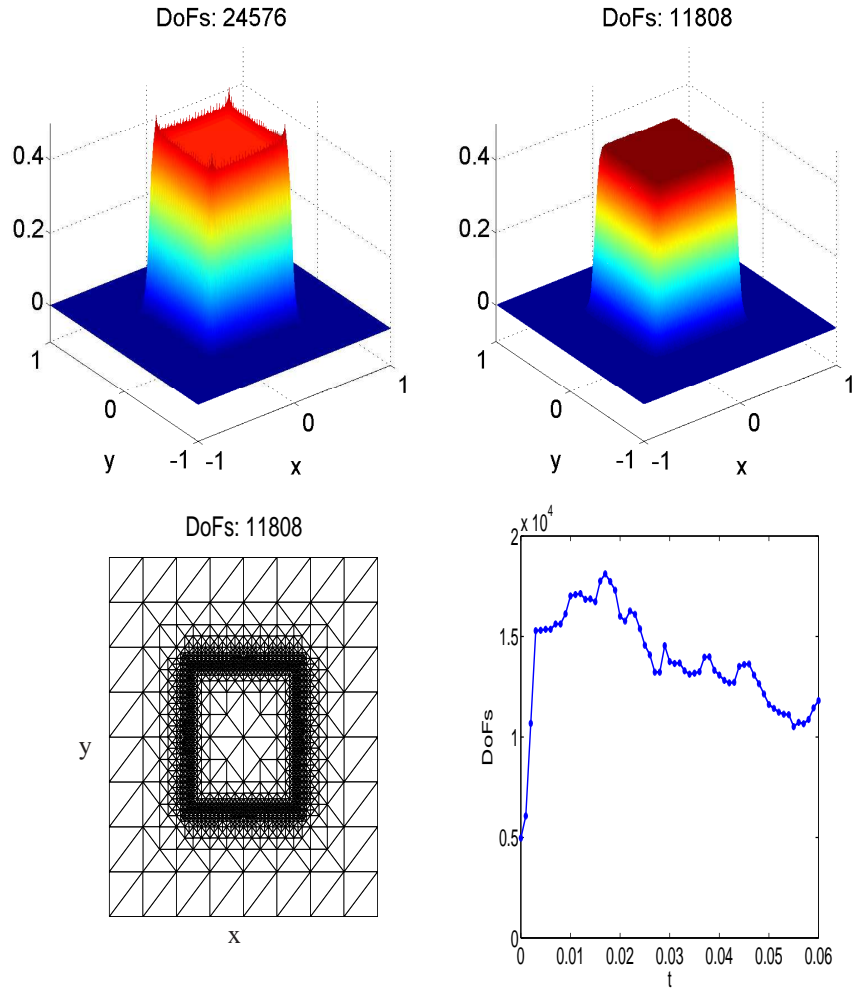


Figure 4.11: Example 4.5.3: (Top) Uniform (left) and adaptive (right) solutions at final time $t = 0.06$, (Bottom) adaptive mesh (left) at final time $t = 0.06$ and evolution of DoFs (right) for expanding flow with square initial data

is satisfied which is seen in Figure 4.12, bottom. However, there have been internal layers in the solution. We have applied space adaptivity algorithm to handle these unphysical oscillations with tolerances $\text{stol}^r = 1 \times 10^{-3}$, $\text{stol}^c = 1 \times 10^{-6}$ and time step size $\Delta t = 1 \times 10^{-3}$, as well. The adaptive mesh at time $T = 0.06$ is given in Figure 4.13, left. In Figure 4.14, it is shown that all the oscillations are damped out by adaptive algorithm using less DoFs compared to the uniform one. When we take smaller diffusion parameter as $\epsilon = 0.001$ and the other parameters are the same, the accuracy of the adaptive algorithm can be seen clearly in Figure 4.15. In contrast to the expanding flow, the grids are refined monotonically around the internal layer (Figure 4.13, right).

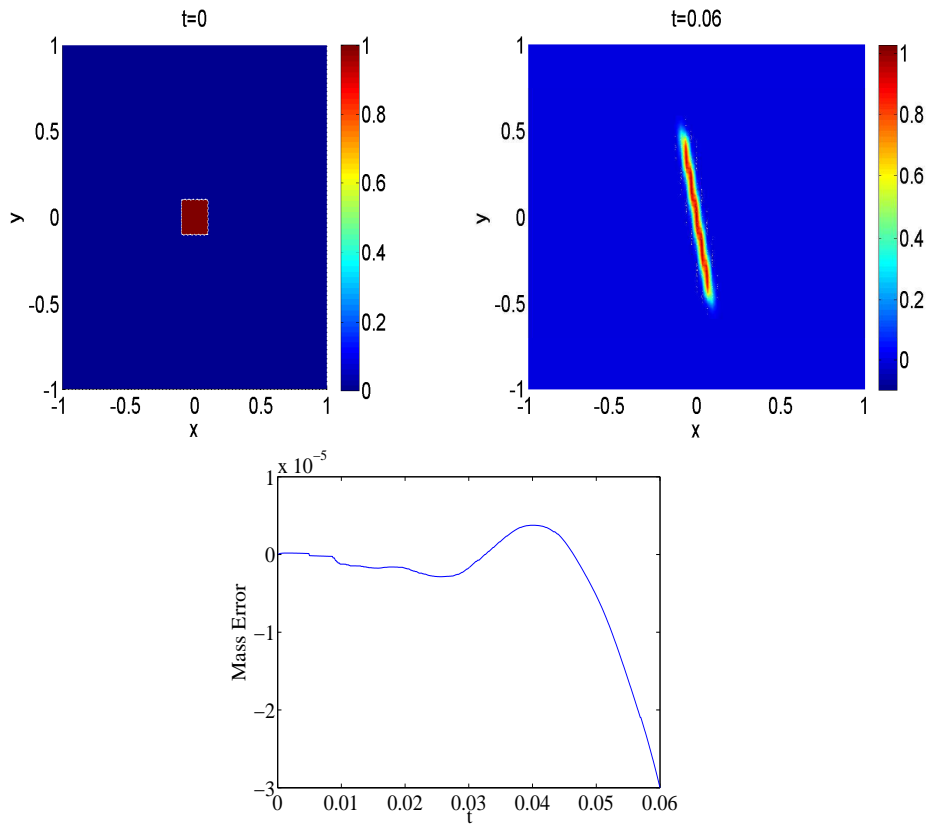


Figure 4.12: Example 4.5.4: Uniform solutions at initial and final times (top) and mass error plot (bottom) for shear flow with $\epsilon = 0.01$

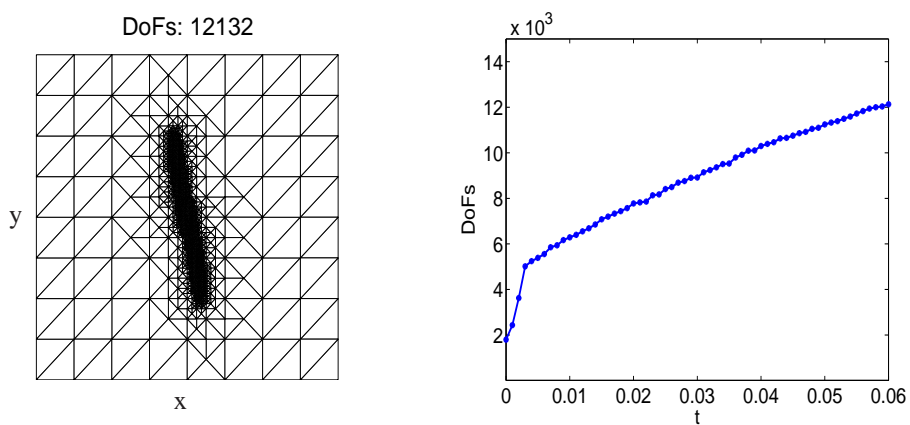


Figure 4.13: Example 4.5.4: Adaptive mesh at final time $t = 0.06$ (left) and evolution of DoFs (right) for shear flow with $\epsilon = 0.01$

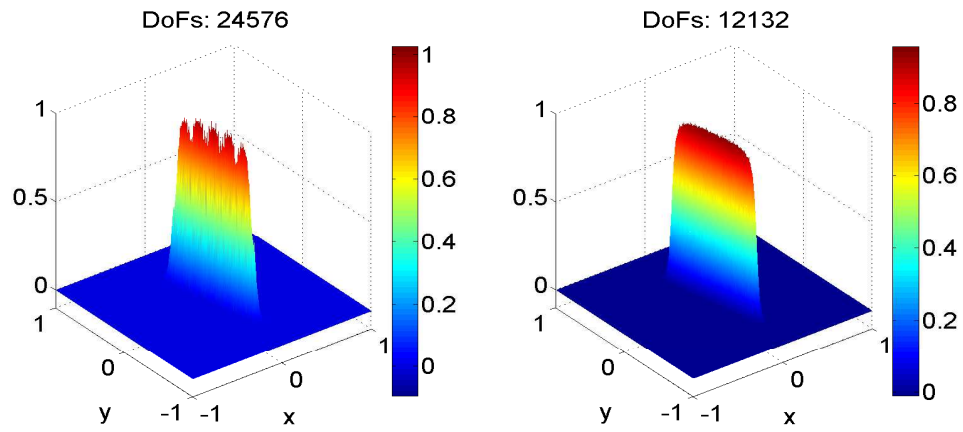


Figure 4.14: Example 4.5.4: Uniform (left) and adaptive (right) solutions at final time $t = 0.06$ for shear flow with $\epsilon = 0.01$

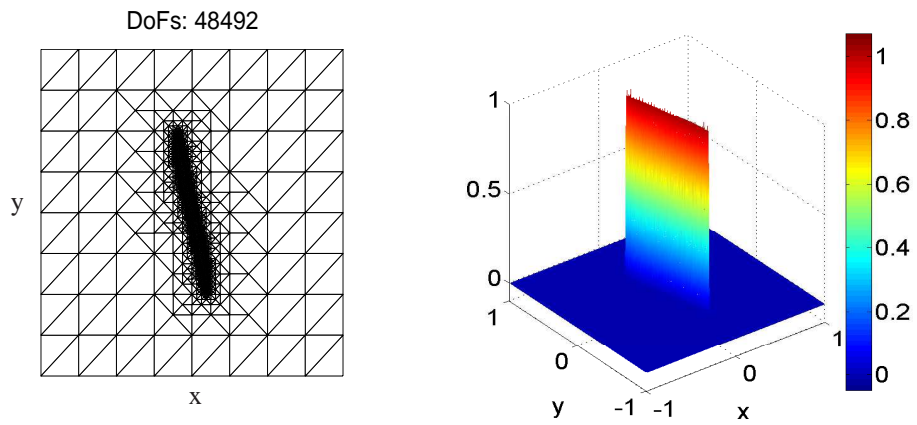


Figure 4.15: Example 4.5.4: Adaptive mesh (left) and adaptive solution (right) at final time $t = 0.06$ for shear flow with $\epsilon = 0.001$

CHAPTER 5

CONCLUSION

In this thesis, we have studied AC and CH equations modeling the phase separation in material sciences. Both equations are considered for a general class of problems with constant and degenerate mobility, convex double-well and non-convex logarithmic free energy functions. AC and CH equations have gradient flow structure with the energy decreasing property. We have applied the SIPG method, a type of discontinuous Galerkin methods, as an effective space discretization technique for both models. The SIPG method is combined with the energy stable time integrators implicit Euler and AVF methods in order to capture the gradient flow structure of AC and CH equations. We gave the proofs of energy decreasing property of the fully discrete solutions for both equations. Numerical results demonstrate the convenience of time integrators with the structure of both equation. The presence of the effective diffusivity ϵ leads to multiple time scale of the dynamics of both equation. This is handled by the SIPG space discretization being an alternate to the well-known stabilized continuous Galerkin methods such as streamline upwind Petrov-Galerkin (SUPG) method. The nonlinear terms were accurately integrated using standard Newton method arising from the discrete system of stationary equations. The energy decreasing property of implicit Euler and AVF methods for both AC and CH equations in very general form is confirmed by several numerical examples.

We have also considered advective AC equation modeling the droplet breakup phenomenon of an incompressible material with another compressible fluid. The AC and CH equations are first discretized in space by the SIPG method and the resulting large systems of ODEs are integrated using the implicit Euler and AVF methods which corresponds to method of lines. On the other hand, the advective AC equation is discretized first in time by implicit Euler method which produces a sequence of semilinear elliptic equations, which is known as Rothe's method. At each time step, a space adaptive version of the SIPG method is used to discretize the semilinear elliptic equations. Using this space adaptive version of the SIPG method, we have shown that the internal layers are resolved accurately for convection dominated problems as an alternate to the shock/discontinuity capturing techniques in the literature. The adaptivity tool is based on the residual-based a posteriori error estimation. Then, we have also proven the a posteriori error bounds for stationary semilinear elliptic equations at each time step. Numerical results demonstrate that the space adaptive algorithm resolves well the multiscale dynamics of the advective AC equation for expanding and contracting velocity fields.

Extension of the methods to more realistic three dimensional AC and CH equations, advective AC equation might be the major topic of a future work. Also the development of an efficient time–space adaptive method would be considered in future studies to resolve the multiscale dynamics of AC and CH equations and advective AC equation. Since the formation of the steady state solutions takes a long time which makes the computation expensive, a model order reduction technique could be also considered for a future work.

As a further study, numerical solution of Navier Stokes AC and CH equations might also be considered as different versions of advective AC equation.

REFERENCES

- [1] M. Ainsworth and J. T. Oden, *A posteriori error estimation in finite element analysis*, Wiley-Interscience, 1997.
- [2] M. S. Allen and J. W. Cahn, A microscopic theory for antiphase boundary motion and its application to antiphase domain coarsening, *Acta Metallurgica*, 27(6), pp. 1085–1095, 1979.
- [3] A. C. Aristotelous, O. A. Karakashian, and S. M. Wise, Adaptive, second-order in time, primitive-variable discontinuous galerkin schemes for a Cahn–Hilliard equation with a mass source, *IMA Journal of Numerical Analysis*, 2014.
- [4] D. Arnold, F. Brezzi, B. Cockburn, and L. Marini, Unified analysis of discontinuous Galerkin methods for elliptic problems, *SIAM J. Numer. Anal.*, 39, pp. 1749–1779, 2002.
- [5] D. N. Arnold, An interior penalty finite element method with discontinuous elements, *SIAM J. Numer. Anal.*, 19, pp. 724–760, 1982.
- [6] B. Ayuso and L. D. Marini, Discontinuous Galerkin methods for advection-diffusion-reaction problems, *SIAM J. Numer. Anal.*, 47, pp. 1391–1420, 2009.
- [7] I. Babuška, , and M. Zlámal, Nonconforming elements in the finite element method with penalty, *SIAM J. Numer. Anal.*, 10, pp. 45–59, 1973.
- [8] I. Babuška and T. Strouboulis, *The finite element method and its reliability*, Numerical mathematics and scientific computation, Clarendon Press, 2001.
- [9] J. W. Barrett and J. F. Blowey, Finite element approximation of the Cahn-Hilliard equation with concentration dependent mobility, *Mathematics of Computation*, 68(226), pp. 487–517, 1999.
- [10] J. W. Barrett, J. F. Blowey, and H. Garcke, Finite element approximation of a fourth order nonlinear degenerate parabolic equation, *Numerische Mathematik*, 80(4), pp. 525–556, 1998.
- [11] J. W. Barrett, J. F. Blowey, and H. Garcke, Finite element approximation of the Cahn-Hilliard equation with degenerate mobility, *SIAM Journal on Numerical Analysis*, 37(1), pp. 286–318, 2000.
- [12] S. Bartels and R. Müller, Error control for the approximation of Allen-Cahn and Cahn-Hilliard equations with a logarithmic potential, *Numerische Mathematik*, 119(3), pp. 409–435, 2011.

- [13] F. Bassi and S. Rebay, A high order accurate discontinuous finite element method for the numerical solution of the compressible Navier-Stokes equations, *J. Comput. Phys.*, 131, pp. 267–279, 1997.
- [14] C. E. Baumann and J. T. Oden, A discontinuous hp finite element method for convection-diffusion problems, *Comput. Methods Appl. Mech. Engrg.*, 175, pp. 311–341, 1999.
- [15] F. Brezzi, G. Manzini, D. Marini, P. Pietra, and A. Russo, Discontinuous Galerkin approximations for elliptic problems, *Numer. Methods Partial Differential Equations*, 16, pp. 365–378, 2000.
- [16] J. W. Cahn and J. E. Hilliard, Free energy of a nonuniform system. i. interfacial free energy, *The Journal of Chemical Physics*, 28(2), pp. 258–267, 1958.
- [17] E. Celledoni, V. Grimm, R. McLachlan, D. McLaren, D. O’Neale, B. Owren, and G. Quispel, Preserving energy resp. dissipation in numerical {PDEs} using the “average vector field” method, *Journal of Computational Physics*, 231(20), pp. 6770 – 6789, 2012.
- [18] K.-Y. Chen, *Numerical Studies on the Allen-Cahn and Cahn-Hilliard Equations*, Master’s thesis, National Chiao Tung University, Hsinchu, Taiwan, Republic of China, July 2007.
- [19] L. Chen, *iFEM: an innovative finite element methods package in MATLAB*, Technical report, Department of Mathematics, University of California, Irvine, 2008.
- [20] L. Chen and C. Xu, A time splitting space spectral element method for the Cahn-Hilliard equation, *East Asian Journal on Applied Mathematics*, 3(4), pp. 333–351, 2013.
- [21] L.-Q. Chen, Phase-field models for microstructure evolution, *Annual review of materials research*, 32(1), pp. 113–140, 2002.
- [22] J.-W. Choi, H. G. Lee, D. Jeong, and J. Kim, An unconditionally gradient stable numerical method for solving the Allen–Cahn equation, *Physica A: Statistical Mechanics and its Applications*, 388(9), pp. 1791 – 1803, 2009.
- [23] A. Christlieb, J. Jones, B. W. K. Promislow, and M. Willoughby, High accuracy solutions to energy gradient flows from material science models, *Journal of Computational Physics*, 257, pp. 193–215, 2014.
- [24] B. Cockburn and C. W. Shu, The local discontinuous Galerkin method for time-dependent convection-diffusion systems, *SIAM J. Numer. Anal.*, 35, pp. 2440–2463, 1999.
- [25] D. Cohen and E. Hairer, Linear energy-preserving integrators for poisson systems, *BIT Numerical Mathematics*, 51(1), pp. 91–101, 2011.
- [26] P. Deuffhard and M. Weiser, *Adaptive Numerical Solution of PDEs*, De Gruyter Textbook, Walter de Gruyter, 2012.

- [27] J. Douglas and T. Dupont, Interior penalty procedures for elliptic and parabolic Galerkin methods, in R. Glowinski and J. L. Lions, editors, *Computing Methods in Applied Sciences*, volume 58 of *Lecture Notes in Phys*, pp. 207–216, Springer Berlin Heidelberg, 1976.
- [28] C. Elliott and H. Garcke, On the Cahn-Hilliard equation with degenerate mobility, *SIAM Journal on Mathematical Analysis*, 27(2), pp. 404–423, 1996.
- [29] A. Ern, A. F. Stephansen, and M. Vohralík, Guaranteed and robust discontinuous Galerkin a posteriori error estimates for convection-diffusion-reaction problems, *Journal of Computational and Applied Mathematics*, 234, pp. 114–130, 2010.
- [30] D. Estep and R. Freund, Using Krylov-subspace iterations in discontinuous Galerkin methods for nonlinear reaction-diffusion systems, in B. Cockburn, G. Karniadakis, and C.-W. Shu, editors, *Discontinuous Galerkin Methods*, volume 11 of *Lecture Notes in Computational Science and Engineering*, pp. 327–335, Springer Berlin Heidelberg, 2000.
- [31] X. Feng and Y. Li, Analysis of interior penalty discontinuous Galerkin methods for the Allen-Cahn equation and the mean curvature flow, arXiv:1310.7504v2 [math.NA], 2014.
- [32] X. Feng and A. Prohl, Numerical analysis of the Allen-Cahn equation and approximation for mean curvature flows, *Numerische Mathematik*, 94(1), pp. 33–65, 2003.
- [33] X. Feng, H. Song, T. Tang, and J. Yang, Nonlinear stability of the implicit–explicit methods for the Allen-Cahn equation, *Inverse Problems and Imaging*, 7(3), pp. 679–695, 2013.
- [34] X. Feng, T. Tang, and J. Yang, Stabilized Crank-Nicolson/Adams-Bashforth schemes for phase field models, *East Asian J. Appl. Math*, 3, pp. 59–80, 2013.
- [35] X. Feng and H. Wu, A posteriori error estimates and an adaptive finite element method for Allen-Cahn equation and mean curvature flow, *Journal of Scientific Computing*, 24, pp. 121–146, 2005.
- [36] H. Gómez, V. Calo, and Y. Bazilevs, Isogeometric analysis of the Cahn–Hilliard phase-field model, *Computer Methods in Applied Mechanics and Engineering*, 197(49–50), pp. 4333–4352, 2008.
- [37] H. Gomez, A. Reali, and G. Sangalli, Accurate, efficient, and (iso)geometrically flexible collocation methods for phase-field models, *Journal of Computational Physics*, 262(0), pp. 153 – 171, 2014.
- [38] J. Gopalakrishnan and G. Kanschat, A multilevel discontinuous Galerkin method, *Numer. Math*, 95, pp. 527–550, 2003.
- [39] R. Guo, L. Ji, and Y. Xu, Numerical simulation and error estimates for the local discontinuous Galerkin method of the Allen-Cahn equation, 2013, available at <http://home.ustc.edu.cn/guoguo88/>.

- [40] R. Guo and Y. Xu, Efficient solvers of discontinuous Galerkin discretization for the Cahn-Hilliard equations, *Journal of Scientific Computing*, 58(2), pp. 380–408, 2014.
- [41] E. Hairer, Energy-preserving variant of collocation methods, *Journal of Numerical Analysis, Industrial and Applied Mathematics*, 5, pp. 73–84, 2010.
- [42] E. Hairer and G. Wanner, *Solving Ordinary Differential Equations II: Stiff and Differential–Algebraic Problems*, Springer Series in Computational Mathematics:Berlin, Springer, 1996.
- [43] Y. He, Y. Liu, and T. Tang, On large time-stepping methods for the Cahn-Hilliard equation, *Applied Numerical Mathematics*, 57(5), pp. 616–628, 2007.
- [44] P. C. Hohenberg and B. I. Halperin, Theory of dynamic critical phenomena, *Reviews of Modern Physics*, 49(3), p. 435, 1977.
- [45] R. H. W. Hoppe, G. Kanschat, and T. Warburton, Convergence analysis of an adaptive interior penalty discontinuous Galerkin method, *SIAM Journal on Numerical Analysis*, 47, pp. 534–550, 2008.
- [46] P. Houston, C. Schwab, and E. Süli, Discontinuous hp-finite element methods for advection-diffusion-reaction problems, *SIAM J. Numer. Anal.*, 39, pp. 2133–2163, 2002.
- [47] O. A. Karakashian and F. Pascal, Convergence of adaptive discontinuous Galerkin approximations of second-order elliptic problems, *SIAM Journal on Numerical Analysis*, 45, pp. 641–665, 2007.
- [48] D. Kay, V. Styles, and E. Süli, Discontinuous Galerkin finite element approximation of the Cahn-Hilliard equation with convection, *SIAM Journal on Numerical Analysis*, 47(4), pp. 2660–2685, 2009.
- [49] M. S. Khan, *Phase Field Methods for Multi-Phase Flow Simulations*, Ph.D. thesis, Technische Universität Dortmund, Institut für Angewandte Mathematik (LS III), Dortmund., 2009.
- [50] Y. Khan, I. Ali, S. Islam, and W. Q. Biao, A microscopic theory for antiphase boundary motion and its application to antiphase domain coarsening, *International Journal of Numerical Methods for Heat-Mass Flow*, 23, pp. 558–597, 2013.
- [51] J. Kim, A numerical method for the Cahn-Hilliard equation with a variable mobility, *Communications in Nonlinear Science and Numerical Simulation*, 12(8), pp. 1560 – 1571, 2007.
- [52] P. Lesaint and P. A. Raviart, On a finite element for solving the neutron transport equation, mathematical aspects of finite elements in partial differential equations, *Math. Res. Center, Univ. of Wisconsin-Madison, Academic Press, New York*, pp. 89–123, 1974.
- [53] Y. Li, D. Jeong, J. Shin, and J. Kim, A conservative numerical method for the Cahn-Hilliard equation with dirichlet boundary conditions in complex domains, *Computers & Mathematics with Applications*, 65(1), pp. 102 – 115, 2013.

- [54] Y. Li, H. G. Lee, D. Jeong, and J. Kim, An unconditionally stable hybrid numerical method for solving the Allen–Cahn equation, *Computers & Mathematics with Applications*, 60(6), pp. 1591 – 1606, 2010.
- [55] F. Liu and J. Shen, Stabilized semi-implicit spectral deferred correction methods for Allen-Cahn and Cahn-Hilliard equations, *Mathematical Methods in the Applied Sciences*, 2013.
- [56] W. Liu, *Two Dynamical System Models on Real-World Scenarios: a Swarming Control Model and a Surface Tension Model*, Ph.D. thesis, University of California, Los Angeles, 2011.
- [57] W. Liu, A. Bertozzi, and T. Kolokolnikov, Diffuse interface surface tension models in an expanding flow, *Comm. Math. Sci*, 10(1), pp. 387–418, 2012.
- [58] J. Lowengrub, H. Frieboes, F. Jin, Y.-L. Chuang, X. Li, P. Macklin, S. Wise, and V. Cristini, Nonlinear modelling of cancer: bridging the gap between cells and tumours, *Nonlinearity*, 23, pp. R1–R91, 2010.
- [59] S. Osher and J. A. Sethian, Fronts propagating with curvature-dependent speed: algorithms based on Hamilton-Jacobi formulations, *Journal of computational physics*, 79(1), pp. 12–49, 1988.
- [60] M. Peletier, *Energies, gradient flows, and large deviations: a modelling point of view*, 2005.
- [61] J. Peraire and P. O. Persson, The compact discontinuous Galerkin (CDG) method for elliptic problems, *SIAM J. Sci. Comput.*, 30, pp. 1806–1824, 2008.
- [62] W. H. Reed and T. R. Hill, Triangular mesh methods for the neutron transport equation, Technical Report LA-UR-73-479, Los Alamos Scientific Laboratory, Los Alamos, NM, 1973.
- [63] B. Rivière, *Discontinuous Galerkin methods for solving elliptic and parabolic equations, Theory and implementation*, SIAM, 2008.
- [64] B. Rivière and M. F. Wheeler, A posteriori error estimates for a discontinuous Galerkin method applied to elliptic problems, *Computers Math. with Applications*, 46, pp. 141–163, 2003.
- [65] B. Rivière, M. F. Wheeler, and V. Girault, Improved energy estimates for interior penalty, constrained and discontinuous Galerkin methods for elliptic problems, *Comput. Geosci.*, 3, pp. 337–360, 1999.
- [66] F. Schieweck, A stable discontinuous Galerkin-Petrov time discretization of higher order, *Journal of Numerical Mathematics*, 18, pp. 25–27, 2010.
- [67] D. Schötzau and L. Zhu, A robust a-posteriori error estimator for discontinuous Galerkin methods for convection-diffusion equations, *Applied Numerical Mathematics*, 59, pp. 2236–2255, 2009.
- [68] J. Shen, T. Tang, and J. Yang, On the maximum principle preserving schemes for the generalized Allen-Cahn equation, 2014.

- [69] J. Shen and X. Yang, Numerical approximations of Allen-Cahn and Cahn-Hilliard equations, *Discrete Continuous Dynamical. Syst. A*, 28, pp. 1669–1691, 2010.
- [70] P. Solin, K. Segeth, and I. Dolezel, *Higher-Order Finite Element Methods*, Chapman & Hall/CRC Press, 2003.
- [71] L. Song, G.-M. Gie, and M.-C. Shiue, Interior penalty discontinuous Galerkin methods with implicit time-integration techniques for nonlinear parabolic equations, *Numerical Methods for Partial Differential Equations*, 29(4), pp. 1341–1366, 2013.
- [72] G. Tierra and F. Guillén-González, Numerical methods for solving the Cahn–Hilliard equation and its applicability to related energy-based models, *Archives of Computational Methods in Engineering*, pp. 1–21, 2014.
- [73] M. Tokman, J. Loffeld, and P. Tranquilli, New adaptive exponential propagation iterative methods of Runge-Kutta type EPIRK, *SIAM J. Sci. Comput.*, 34(5), pp. A2650–A2669, 2012.
- [74] M. Uzunca, B. Karasözen, and M. Manguoğlu, Adaptive discontinuous Galerkin methods for non-linear diffusion-convection-reaction equations, *Computers and Chemical Engineering*, 68, pp. 24–37, 2014.
- [75] K. van der Zee, T. Oden, S. Prudhomme, and A. Hawkins-Daarud, Goal-oriented error estimation for Cahn-Hilliard models of binary phase transition, *Numerical Methods for Partial Differential Equations*, 27(1), pp. 160–196, 2011.
- [76] K. Vemaganti, Discontinuous Galerkin methods for periodic boundary value problems, *Numerical Methods for Partial Differential Equations*, 23(3), pp. 587–596, 2007.
- [77] R. Verfürth, Robust a posteriori error estimates for stationary convection-diffusion equations, *SIAM Journal on Numerical Analysis*, 43, pp. 1766–1782, 2005.
- [78] R. Verfürth, *A posteriori Error Estimation Techniques for Finite Element Methods*, Oxford University Press, 2013.
- [79] G. Wells, E. Kuhl, and K. Garikipati, A discontinuous Galerkin method for the Cahn-Hilliard equation, *Journal of Computational Physics*, 218, pp. 860–877, 2006.
- [80] M. F. Wheeler, An elliptic collocation-finite element method with interior penalties, *SIAM J. Numer. Anal.*, 15, pp. 152–161, 1978.
- [81] M. Willoughby, *High-Order Time-Adaptive Numerical Methods for the Allen-Cahn and Cahn-Hilliard Equations*, Master’s thesis, The University of British Columbia, Vancouver, December 2011.
- [82] X. Wu, G. van Zwieten, and K. van der Zee, Stabilized second-order convex splitting schemes for Cahn-Hilliard models with application to diffuse-interface tumor-growth models, *International Journal for Numerical Methods in Biomedical Engineering*, 30(2), pp. 180–203, 2014.

- [83] Y. Xia, Y. Xu, and C.-W. Shu, Local discontinuous Galerkin methods for the Cahn-Hilliard type equations, *Journal of Computational Physics*, 227(1), pp. 472–491, 2007.
- [84] J. Zhu, L.-Q. Chen, J. Shen, and V. Tikare, Coarsening kinetics from a variable-mobility Cahn-Hilliard equation: Application of a semi-implicit Fourier spectral method, *Phys. Rev. E*, 60, pp. 3564–3572, 1999.

z

CURRICULUM VITAE

PERSONAL INFORMATION

Surname, Name: Sariaydın Filibelioglu, Ayşe
Nationality: Turkish
Date and Place of Birth: 01.10.1982, Kaman
Marital Status: Married
Phone: +90 312 2105610
Fax: +90 312 2102987

EDUCATION

Degree	Institution	Year of Graduation
M.S.	Scientific Computing, IAM, METU	2009
B.S.	Department of Mathematics, Kırıkkale University	2006
High School	Mehmet Akif Ersoy Anatolian High School	2000

AWARDS

- 2012 METU Graduate Courses Performance Award (The most successful student in the PhD Program of the Dept. of Scientific Computing in 2010-2011 Academic Year)

LANGUAGE SKILLS

Turkish(native), English(fluently), German(basic)

COMPUTER SKILLS

Proficient in MATLAB, LATEX

PROFESSIONAL EXPERIENCE

Year	Place	Enrollment
2007–Present	Institute of Applied Mathematics, METU	Research Assistant

PUBLICATIONS

Papers submitted to international journals

- A. Sariaydın Filibelioglu, M. Uzunca, B. Karasözen, *Energy Stable Discontinuous Galerkin Finite Element Method for the Allen–Cahn Equation*, 2015.
- B. Karasözen, A. Sariaydın Filibelioglu, M. Uzunca, *Energy Stable Interior Point Discontinuous Galerkin Finite Element Method for Cahn–Hilliard Equation*, 2015.
- B. Karasözen, A. Sariaydın Filibelioglu, M. Uzunca, *Adaptive Discontinuous Galerkin Method for Advective Allen–Cahn Equation*, 2015.

Presentations in International Scientific Meetings

- B. Karasözen, A. Sariaydın Filibelioglu, M. Uzunca, *Adaptive Discontinuous Galerkin Finite Element Method for Non-Local Allen-Cahn Equation*, European Conference on Numerical Mathematics and Advanced Applications (ENUMATH) 2015, 14-18 Eylül 2015, Ankara, Turkey.
- A. Sariaydın, M. Uzunca, B. Karasözen, *Symmetric Interior Penalty Galerkin (SIPG) Method with Average Vector Field Method (AVF) for Cahn–Hilliard System with Degenerate Mobility*, 26th Biennial Numerical Analysis, 23 – 26 Haziran 2015, Glasgow, UK.
- A. Sariaydın, M. Uzunca, B. Karasözen, *Adaptive Discontinuous Galerkin Finite Element Methods for advective Allen-Cahn equation*, Advanced Computational Methods in Engineering 2014, 23 – 28 Haziran 2014, Ghent, Belgium.
- A. Sariaydın, M. Uzunca, B. Karasözen, *Structure Preserving Discontinuous Galerkin Methods in Space and Time for Allen-Cahn Equation*, SciCADE 2013 International Conference on Scientific Computation and Differential Equations, 16-20 Eylül 2013, Valladolid, Spain.

Presentations in National Scientific Meetings

- A. Sariaydın, *Advective Allen-Cahn Denklemi için Uyarlanabilir Sürekli Olmayan Galerkin Sonlu Elemanlar Yöntemleri*, 27. Ulusal Matematik Sempozyumu 23-26 Ağustos, Yeditepe Üniversitesi, ISTANBUL.